Non-Magmatic Glasses

Maria Rita Cicconi, John Mccloy, Daniel R. Neuville

Chapter 23

Non-magmatic glasses

Cicconi Maria Rita[1], McCloy John S.[2], Neuville Daniel R.[1]

1 University of Paris, Institut de Physique du Globe de Paris, Èquipe Géomatériaux, 1, rue Jussieu F-75005 Paris, France

cicconi@ipgp.fr

neuville@ipgp.fr

2 School of Mechanical & Materials Engineering, Washington State University, PO Box 642920, Pullman, WA 99164-2920, USA

john.mccloy@wsu.edu

Overview

On Earth, natural glasses are typically produced by rapid cooling of melts, and as in the case of minerals and rocks, natural glasses can provide key information on the evolution of the Earth. However, natural glasses are products not solely terrestrial and different formation mechanisms give rise to a variety of natural amorphous materials. In this chapter, we provide an overview of the different natural glasses of non-magmatic origin, and on their formation mechanisms. Here we focus on natural glasses formed by mechanisms other than magmatic activity. Included are metamorphic and glasses from highly energetic events (shock metamorphism). The study of these materials has strong repercussions on planetary surface processes, paleogeography/paleoecology and even on the origin of life.

Outline:

Introduction

1. The composition and origin of natural glasses

- Brief description of the most common natural amorphous materials and of the different mechanisms of formation.

2 Metamorphism

- 2.1 Pyrometamorphic glasses
- 2.2 Pseudotachylites

3. Glasses from highly energetic events (shock metamorphism)

- 3.1 - Impactites
  - 3.1.1 – Distal ejecta
    - Tektite and microtektites
    - **Enigmatic Impact glasses**
  - 3.1.2 – Proximal impactite - suevite
- 3.2 fulgurite
  - Case study: fulgurite.
- 3.3 trinitite

4. Glass properties

Acronyms & Glossary

Hypervelocity impacts = Impacts, involving impacting bodies that are traveling at speed (generally greater than a few km/s) higher enough to generate shock waves upon impact.
K-Pg = Cretaceous–Paleogene (K–Pg) boundary (~66 million years ago)
KT = Cretaceous-Tertiary boundary (former name for K-Pg)
Lechatelierite = shock-fused SiO_2 glass
LDG = Libyan Desert Glass
m-T = microtektites; Small distal ejecta with diameter less than 1 mm.
MN = Muong Nong-Type tektites
PDFs = Planar deformation features; microscopic parallel, isotropic features in minerals that originate from elevated shock metamorphism.
SF = tektite/impact glass strewn fields
TAS = Total-Alkalis versus Silica diagram
Tektites = millimeter- to centimeter-scale, glassy particles of ballistically transported impact melt, formed by the impact of an extraterrestrial projectile.
Tg = Glass Transition temperature
YD = Younger Dryas is a geological period from ~ 12,900 to ~ 11,700 BP
YDB = Younger Dryas boundary
XAS = X-ray Absorption Spectroscopy

INTRODUCTION

Natural glasses have accompanied human civilization and have always aroused human curiosity. Overtime, mankind tried, first of all, to understand the origin and the properties of these materials, and then, they have tried to recreate and improve, the natural occurring specimens. That is what brought us into the "Glass Age", and nowadays, we cannot think of a life without glasses. Indeed, from rudimental weapons, decorative objects, or storage bottles, currently glasses are more high-tech materials used for example for high-speed communications, or in smart-windows. Many smart materials have been developed from the observations done on natural ones, but besides the material technology, are the natural sciences (*s.l.* incorporating life and physical sciences) that have gained the highest contribution from the study of natural amorphous materials. They have been used to explain why and when natural phenomena occurred, and to obtain a general understanding of natural phenomena. For example, in geosciences, knowledge about past events (geologically speaking) either on Earth or other terrestrial planets is often derived by the study of magmatic and non-magmatic glasses. Besides geosciences and engineering, the study of natural aluminosilicate glasses has been a key topic in the framework of waste managements, especially for evaluation of the long-term stability of nuclear waste form glasses (Chapman *et al.* 1984; Ewing 1979). Natural glasses may remain stable for very long periods (more than 1 Ma) in various geological settings and climatic conditions, in contrast to many manmade glasses from the Middle Age. Hence, natural glasses are used as analogues for extrapolation of short-term laboratory data (hours to years) to the long time periods (hundred to thousand years).

The aim of this chapter is to review natural glasses formed by mechanisms other than magmatic activity, and after a brief description of the most common natural amorphous materials and of the different mechanisms of formation, we report some examples on

metamorphic glasses, and on glasses from highly energetic events. At the end we report an overview of the properties of these natural amorphous materials.

In the last decades, several reviews, for specific natural glasses, have been published and the readers are referred to these exhaustive papers [*e.g.* Eby *et al.* 2010; Glass 1990; Glass & Simonson 2013; Koeberl 1997; Pasek *et al.* 2012]. More recent general reviews on different natural glasses are provided in Cicconi & Neuville 2019; Heide & Heide 2011; McCloy 2019.

1. The composition and origin of natural glasses

Natural glasses have different origins and chemical compositions, though, their chemical variability match the differentiations found in many common types of volcanic rocks. An overview of the enormous variability of natural glasses occurring on Earth and on Lunar soil can be appreciated in the TAS diagram (total alkali vs. silica; **Figure 1**). These amorphous materials have SiO_2 contents between ~33-99 wt.%, and alkali contents ranging between 0 and 15 wt.%, thus covering many common types of volcanic rocks. Despite the fact that these glasses are differentiated chemically as many common volcanic rocks, most of the times, non-magmatic glasses experienced extreme conditions of formations, far away from those of common igneous materials. Indeed, most of the glasses considered in this chapter have cooling rates orders of magnitude higher than volcanic terrestrial (or lunar) glasses, and/or have been subject to extremely elevated peak pressures. For instance, cooling rates may range from extremely high values, as in fulgurite formation (~10^{10} ºC/min) and submarine basaltic eruptions (10^{7} º/min), to moderate values in tektites 10^{4} -10^{-2} °/min, to very slow rates in massive obsidian flows 10^{-2} – 10^{-4} °/min (Potuzak *et al.* 2008; Rietmeijer *et al.* 1999; Switzer & Melson 1972; Weeks *et al.* 1984; Wilding *et al.* 1996b, 1996a). Out of curiosity, water, which

is considered to be a very weak glass former, requires cooling rates faster than 10E6 °/min to form an amorphous solid.

Before describing non-magmatic glasses, we would like to provide an overview of all amorphous materials found on Earth (and on other terrestrial planets), and of the various mechanisms of formation. The most known natural amorphous materials are of magmatic origin and include basaltic glasses and obsidians. Basaltic glasses have an average composition of about (wt.%) 50-54% SiO_2, 12-17% Al_2O_3, 8-12% FeO_{tot}, 2-4% alkali (K_2O + Na_2O), 15-20% alkali-earth (CaO + MgO) (Cicconi & Neuville 2019 and references therein) and their low viscosity favors crystallization (devitrification). Volcanic glasses produced upon rapid cooling of basaltic melts are called sideromelane, but they also occur as volcanic ash, fibers and teardrops (*i.e.* Pele's Hair and Pele's Tears) and more rarely form solidified foam – reticulite (Cicconi & Neuville 2019). Obsidian glass was first described by Pliny The Elder's Natural History with the name of "*obsiana*", so called because its similarity to a very dark stone found in Ethiopia by Obsius. This glass has accompanied and influenced human evolution since prehistoric times, and nowadays, it still enters the popular culture, even if with more fanciful name (*i.e.* dragonglass, after the fantasy drama television series Game of Thrones). Obsidians are generally subalkalic rhyolitic with an average composition of about (wt.%) 72-77% SiO_2, 10-15% Al_2O_3, 1-2% FeO_{tot}, 7-10% alkali (K_2O + Na_2O), 0.5-2% alkali-earth (CaO + MgO) (Cicconi & Neuville 2019 and references therein). The glass-forming processes of obsidian melts are strongly influenced by the content, size and shape of microlites (Castro *et al.* 2002), and by the contents of volatile components (such as water, fluorine and chlorine, sulphur and carbon oxides (Carmichael 1979; Heide & Heide 2011), and small variations in volatile contents can cause important changes in the flow dynamics of obsidian melts.

Other natural amorphous materials are formed by metamorphic processes. For instance, the so-called pyrometamorphic glasses form due to burning of fossil fuels such as coal and natural gas or other organic material (McCloy 2019 and references therein). The term pyrometamorphism, which defines a type of contact metamorphism, was originally proposed in 1912 by Brauns (Grapes 2010 and references therein) to describe a high-temperature/ low pressure metamorphism observed in schist xenoliths in trachyte and phonolite magma of the East Eifel area (Germany). The terms buchite is used to define those partially or completely melted materials as a consequence of pyrometamorphism.

Glasses from highly energetic events are formed in a completely different way, and with a completely different timescale than magmatic and metamorphic ones. For instance, impact glasses formation is related to the collision of an extraterrestrial body on the surface of the Earth. Thus, they derive from shock metamorphism of existing silicate rocks and sediments. Impacts or airbursts (shock melting caused by a cosmic object exploding in the atmosphere) can be either natural or artificial, and both provide shock markers due to the extreme high temperatures and pressures. Among natural glasses that experienced extremely high temperatures in a very short time there are also the fulgurites, formed following lightning strike.

Finally, biomineralization processes can produce amorphous materials. These are considered eco-friendly and thus they have captured the attention either of organic-/inorganic-chemists or materials scientists. Several siliceous marine organisms exhibit discontinuous, three-dimensional frameworks of short chains of SiO_4 tetrahedra, bonded with apical hydroxyls. The low-temperature hydrated variety of silica, opal (SiO_2*nH_2O), is a biomineral, and displays different arrangements of amorphous SiO_2, water, and cristobalite, and/or tridymite (Cicconi & Neuville 2019). Depending on the arrangements, it is possible to distinguish three opal types: i) opal-C (cristobalite); ii) opal-CT (cristobalite and tridymite); iii) opal-A (X-ray-amorphous opal). The latter can be further divided in opal-AN (*e.g.*, hyalite) and

opal-AG with an amorphous silica gel structure. In a "maturation process" (Ostwald ripening) opals are transformed as follows (Skinner & Jahren 2003 and references therein): Opal-AG → Opal-CT → Opal-C → microcrystalline quartz.

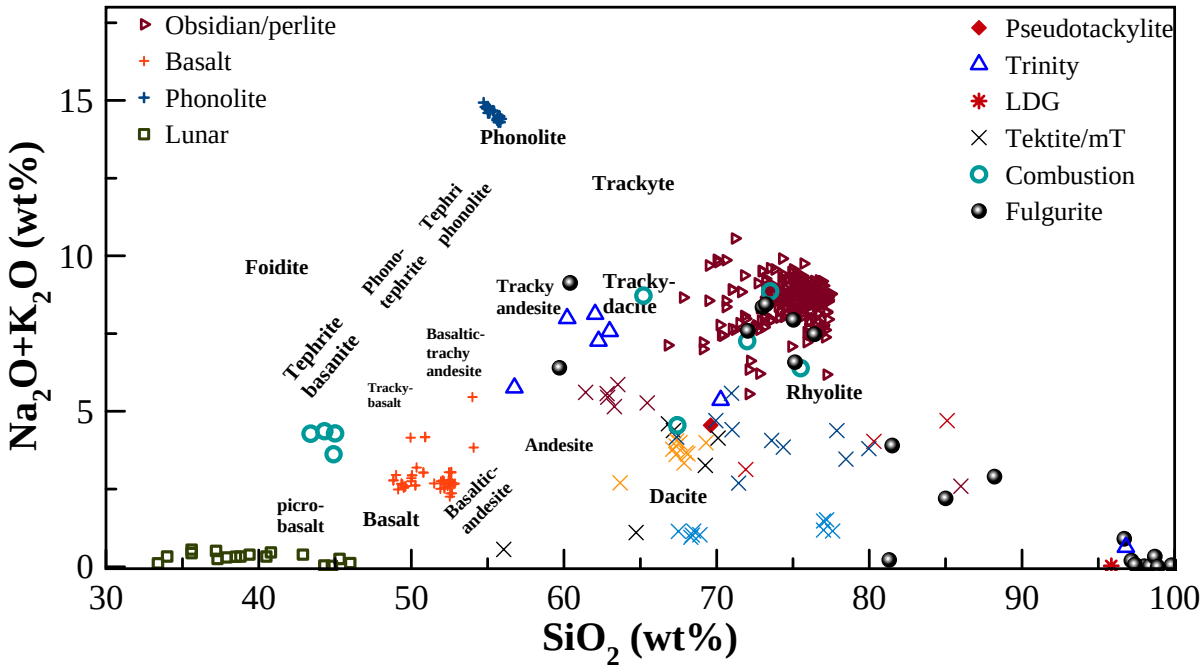

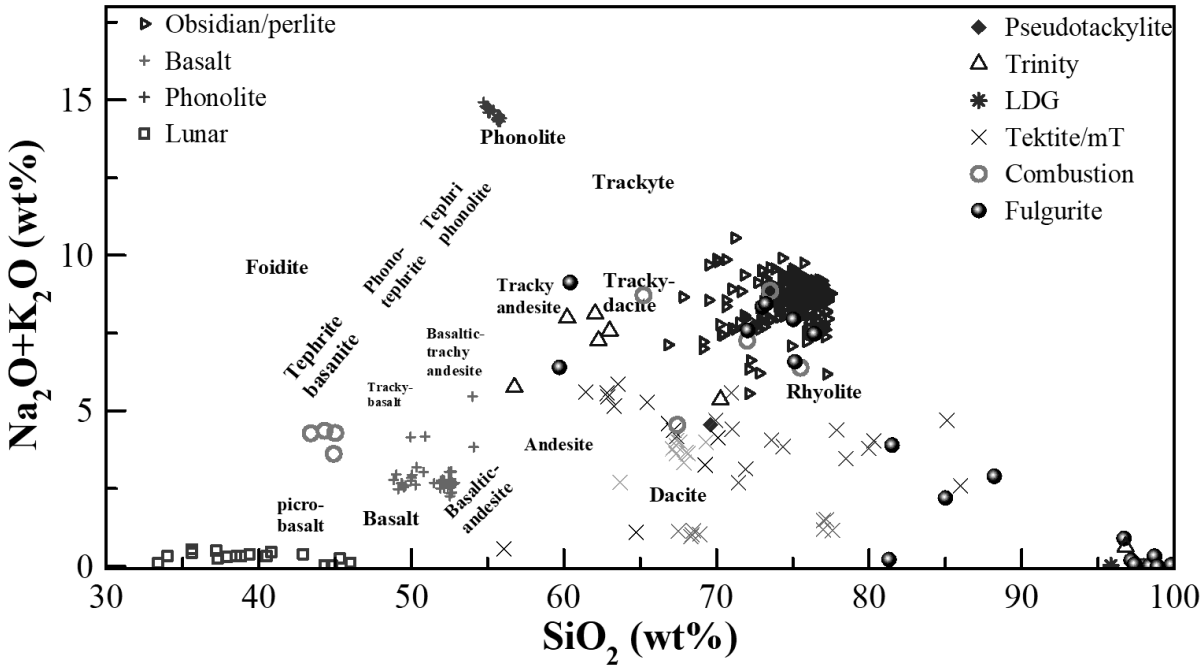

Figure 1 – SiO_2 *vs.* total alkali (wt%) diagram for several natural non-magmatic glasses described in this chapter. Glasses deriving from magmatic processes are reported for comparison. Data compilation from Cicconi & Neuville 2019. LDG = Libyan Desert Glass; mT = microtektites.

2. Metamorphic glasses

2.1 Pyrometamorphic glasses

2.1.1 General features of pyrometamorphism

Pyrometamorphic glasses are in important class of amorphous materials summarized by (Grapes 2010). The term 'pyrometamorphism' was originally used by (Brauns 1912) to describe changes in contact zones (*i.e.*, aureoles) between magma intrusions and country rock, where high temperature and atmospheric pressure result in particular mineralogical and morphological changes. These high temperature changes are often observed in xenoliths within later igneous rocks, near shallow magmatic intrusions, and within tuffs and breccias. Brauns assumed that pyrometamorphism must create melting in the heat-affected rocks and vitrification on cooling. Other terms have been introduced but have fallen out of favor, such as optalic metamorphism, emphasizing the transient, quickly dissipated heat such as used when 'baking a brick.' Pyrometamorphized rocks tend to lose all volatiles, and melts recrystallize with anhydrous mineral assemblages. Some characteristic evidences of such processes include bleaching of carbonate rocks, reddening of iron-containing rocks, fusion of mineral grains, hardening, and similar morphological and chemical changes similar to those observed in earthenware ceramic and clay brick-making processes. Heat for pyrometamorphic transformations need not come from contact magmatic heat, but also from other sources, such as combustion of coal beds and organic-rich sediments or even lightning. The Subcommission on the Systematics of Metamorphic Rocks (SCMR) of the International Union of Geological Sciences (IUGS) categorizes these effects as subvariants of contact metamorphism, namely 'burning/combustion metamorphism' and 'lightning metamorphism,' *i.e.*, fulgurites (Callegari & Pertsev 2007).

While contact and lightning metamorphism are highly localized, high temperature changes in rock due to coal bedding combustion can be regionally extensive. Well documented examples in the USA occur in the Grimes Canyon area, Monterey Formation, California

(Bentor *et al.* 1981); the Powder River Basin, Wyoming (Cosca *et al.* 1989; Herring & Modreski 1986); and various coal-bearing areas of Montana and Colorado (Rogers 1918). The phenomenon of combustion metamorphism has been found to be quite common (Bentor *et al.* 1981; Grapes 2010), including examples in China (de Boer *et al.* 2001), Mongolia (Peretyazhko *et al.* 2018), India, Russia (*e.g.*, Chelyabinsk brown coal basin) (Sokol *et al.* 1998), Iran, Jordan (Khoury *et al.* 2015), Israel (Ron & Kolodny 1992; Sokol *et al.* 2014), Czechia, Germany, England, Italy (Melluso *et al.* 2004), Mali (Svensen *et al.* 2003), Canada (Canil *et al.* 2018; Mathews & Bustin 1984), New Zealand, and Australia.

Some terms are commonly used for pyrometamorphic rocks as follows. Hornfels forms where clay-rich rocks contact a hot igneous body, and partially or completely recrystallize after in-situ melting, resulting in baked and hardened silicate + oxide systems. Clinker originally referred to altered or burned coal, but now refers generally to burnt brick-like rock which 'rings' ('clinks') when struck. Note that clinker is also the high-temperature processed calcium aluminosilicate used as the reactive precursor for Portland cement. These same 'clinker' minerals, *e.g.*, belite sulfoaluminate, have been found in Israel in natural pyrometamorphic contexts (Sokol *et al.* 2014). Buchite, in contrast to hornfels, is largely vitrified from high heat applied to sandstones or pelites, resulting in hard, fused, and glassy material; the term is not restricted to coal fire lithologies, so in that case should be referred to as 'buchite clinker.' Finally, paralava resembles artificial slag or basalt, is generally vesicular and aphanitic, sometimes shows evidence of flow, and formed from burning and melting of sedimentary rocks (shale, sandstone, marl) by proximal combusting coal seams. The distinction among these is based on both protolith and peak temperature, which can be ~ 400 to >1600 °C locally, resulting in a continuum from baked/burnt rock to fused-grained rock (clinker) to partially melted buchite, to wholly melted and partially devitrified rock (paralava), often all in the same area. Terminology is not uniform employed, and in certain localities clinker is still be called 'scoria'

224 despite the different volcanic origin assumed from that term. Use of the terms 'buchite' and
225 'paralava' imply the observable presence of glass resulting from a quenched rock melt (Grapes
226 2010).
227
228 2.1.2 Coal fires and spontaneous combustion
229 Coals in the Western USA, known to spontaneous combust, are typically lignite or sub-
230 bituminous grade (Rogers, 1917). Spontaneous combustion occurs due to a complex process
231 involving absorption of oxygen, such as through cracks, and oxidation of unsaturated
232 hydrocarbons. The main exothermic reaction is that of carbon reacting with oxygen gas to form
233 CO_2 (Grapes 2010). These early reactions take place at temperatures as low as 80 °C, but this
234 oxidation further generates heat until about 200 °C, where autogenous oxidation occurs,
235 followed by ignition at 350-400 °C. Fine dust lignite, however, which has typically absorbed a
236 large amount of oxygen, can ignite at temperatures as low as 150 °C (Rogers 1918). Moisture
237 is said to exacerbate this effect, with escaping hydrogen-containing gases also playing a role.
238 Other factors influencing the combustion reaction include coal factors such as rank and pyrite
239 content, reaction factors such as particle size and temperature, and macroscopic factors such as
240 air flow, overbedding rock type, and thermal conduction (Grapes 2010). Often areas can burn
241 in the absence of additional oxygen, producing highly reducing conditions and the creation of
242 coal ash with evidence of metallic iron (de Boer *et al.* 2001; Grapes 2010).
243 Combustion of coal beds has been observed in modern times on the coast of Dorset,
244 England; in the 'Smoking Hills' of Canada (Mathews & Bustin 1984); and at the 'Burning
245 Mountain' (Mt. Wingen) in New South Wales, Australia (Bentor *et al.* 1981). The Smoking
246 Hills are thought to have been burning for at least 150 years, while the Burning Mountain has
247 been combusting for at least 15,000 years. The Posidonia shales in Germany, though not

currently combusting, are thought to have been active in the Middle Ages (Bentor *et al.* 1981). Many other examples are known (Kuenzer & Stracher 2012).

Examples of modern creation of pyrometamorphic materials are known from burning of a wide range of fossil fuels, from spontaneous combustion but also other natural or anthropogenic ignition (Kuenzer & Stracher 2012). Combustion in coal mining 'spoil heaps' has resulted in recent pyrometamorphic processes in Russia (Chelyabinsk) (Sokol *et al.* 1998) and Italy (Ricetto) (Capitanio *et al.* 2004; Stoppa *et al.* 2005) (**Figure 2**). One of the interesting features of the assemblage in Russia is the presence of pure glassy carbon, known as shungite. Additionally, minerals have been observed which were crystallized from the gas phase in cracks, including pure oxide, sulfide, silicate, and carbide single crystals.

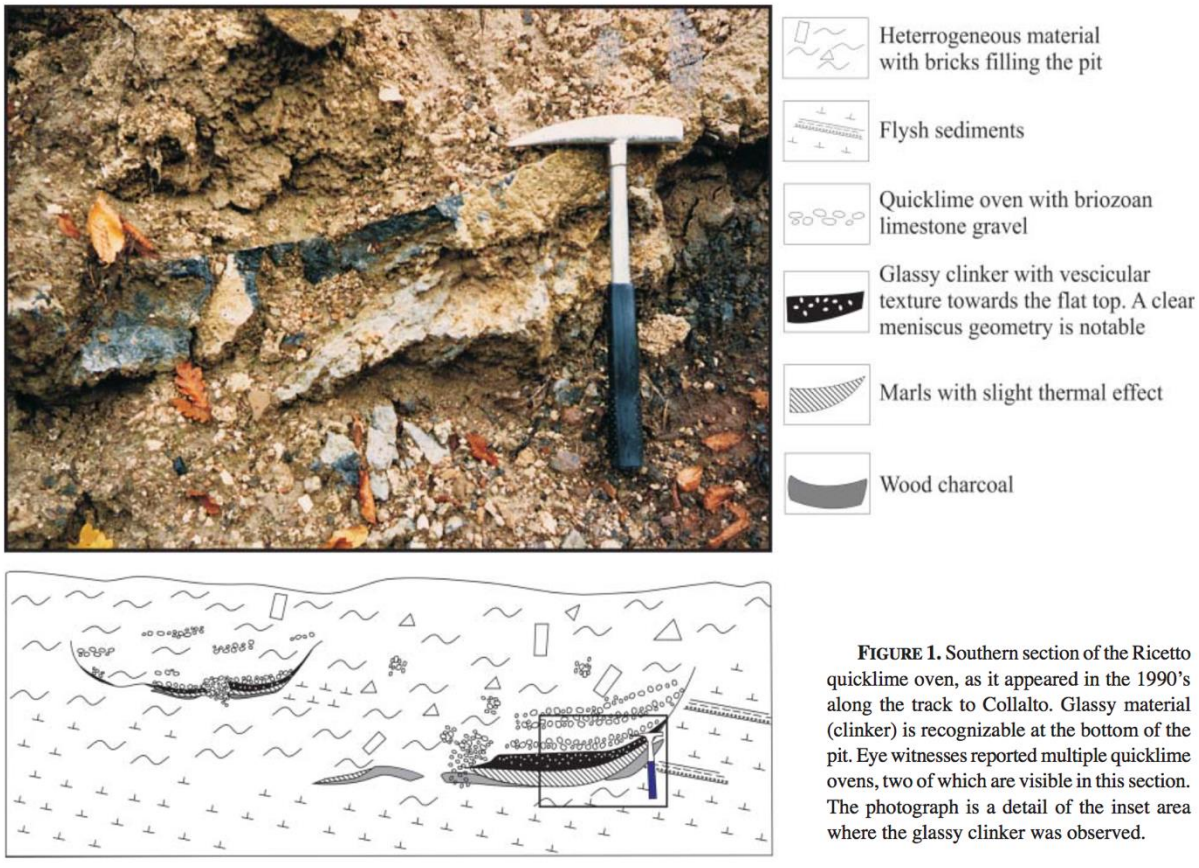

FIGURE 1. Southern section of the Ricetto quicklime oven, as it appeared in the 1990's along the track to Collalto. Glassy material (clinker) is recognizable at the bottom of the pit. Eye witnesses reported multiple quicklime ovens, two of which are visible in this section. The photograph is a detail of the inset area where the glassy clinker was observed.

Figure 2: pyrometamorphic material at Ricetto (Italy). Image from Stoppa *et al.* 2005 Figure1_Stoppa2005_AM90_1919. MSA copyright.

2.1.3 Other processes fueling pyrometamorphism

It should be noted that pyrometamorphic rocks and glasses can be produced by high temperature burning using any fuel, not just coal. Many examples have been described where the fuel was biomass or organic material covered by sediment. This organic material can be deposited naturally, and subsequently be covered to ignite and burn in the subsurface under dry conditions, such as examples in Chile (Roperch *et al.* 2017) and Africa (Melson & Potts 2002; Svensen *et al.* 2003). Alternatively, organic deposits can be a result of human activity, such as archaeologically observed middens (Thy *et al.* 1995) or modern-day haystacks (Baker & Baker 1964), the burning of which produces glassy material.

Organic gases can be fuels for rock burning as well. One of the most studied areas of pyrometamorphic rocks, the Dead Sea region in Israel, has been interpreted as having a pyrometamorphic origin, from a mud volcano and associated methane and hydrocarbon gas combustion (Sokol *et al.* 2010). Gas seeps and their associated 'eternal flames' from spontaneous combustion have played important roles in human history, especially in religious and mythological traditions. For example, the methane seeps known as Chimera in southwest Turkey was the site of the first Olympic fire in the ancient Greek world, and the site of a temple of Hephaestus (Vulcan) the god of fire and metallurgy (Etiope 2015; Hosgormez *et al.* 2008), and it still burns today. All kerogens of various grades, from bitumen to oil, are potential sources of fuel for creation of pyrometamorphic rocks and glass.

Pyrometamorphic melts are also known to be produced from oilfield fire. Characteristic glasses, known as tengizites after the Tengiz oildfield in Kazakhstan, formed in this inferno (Kokh *et al.* 2016). Tengizites, essentially a type of paralava/slag, contain 59-69 wt.% SiO_2, 7.3 - 9.7 wt.% Al_2O_3, 12.8 - 17.9 wt.% CaO, 2.0 - 3.7 wt.% MgO, 2.0 - 3.0 wt.% Na_2O, 1.3 - 1.9 wt.% K_2O, < 0.3 wt.% H_2O and < 0.4 wt.% total volatiles, as a result of melting sand and clayey silt along with biogenic calcite (Kokh *et al.* 2016). The associated buchite at the site is known as mesolite, consisting of partially melted and highly altered sediment, and compared to

tengizite has lower SiO_2, higher Al_2O_3, MgO, K_2O, TiO_2, and total volatiles, but lower FeO/Fe_2O_3 ratio.

One detailed example

Compositions of pyrometamorphic glasses vary drastically depending on the local chemical environment derived from the protolith, extent of melting, mixing of the melt, and subsequent crystallization. For example, most Western US coal-bearing regions are interbedded with predominantly shale and sandstone (Rogers 1918). The famous example Grimes Canyon in California consists of protoliths of mudstone containing clays, detrital quartz and feldspar, opal, apatite, biogenic carbonates (calcite and dolomite), and gypsum, while also being bituminous, containing more than 10% carbon (Bentor *et al.* 1981). Some diatomites, shales, and phosphorites also were locally metamorphized; phosphorite contains predominantly detrital apatite, which melts at 1650 °C (Bentor 1984). Some constituents elevated in the metamorphized rocks such as sulfate, and in other cases chloride, likely came from groundwater introduction during the combustion process (Bentor *et al.* 1981; Rogers 1918).

Bentor (1984) distinguishes between combustion 'glasses' and 'crystalline slags' for these materials, depending on the peak melting temperature achieved. 'Glasses' result from low temperature melts ≤ 1000 °C, are enriched in Na, K, Al, and Si, and maintain high viscosity in the small volume seams between unmelted rock, thus preventing crystallization. 'Crystalline slags' melted at ≥ 1100 °C, dissolving even apatite crystals and other refractory minerals, resulting in a lower viscosity, more basalt-like melt, which underwent extensive crystallization on cooling (hence 'slag'). These 'slags' are essentially synonymous with paralavas. There is strong evidence of silicate/phosphate liquid immiscibility from the lower temperature silicate melt and higher temperature phosphorite melt in these cases (Bentor 1984; Bentor *et al.* 1981; Capitanio 2005; Peretyazhko *et al.* 2018).

Two samples of Grimes Canyon were investigated by X-ray diffraction. Not all phases could be accurately identified by XRD, but diffraction indicated the majority was amorphous glass (50-75%), with large fractions of feldspar (12-25%), apatite (6-7%), calcite (3-4%), pyroxene (1-9%), and tridymite (1-4%). The lighter portions of the banded material contained more carbonate and phosphate crystalline phases. These phases are broadly consistent with those observed in Bentor et al. (1981). In Wyoming Powder River Basin paralavas, phenocrysts of olivine, cordierite, and spinel (magnetite-hercynite-ulvospinel) are also common, along with many unusual minerals and mineral associations (Cosca *et al.* 1989). In the Apennine region in Italy, pyrometamorphic outcrops include wollastonite and melilite, likely from protoliths of mixed marly sediments of carbonates and shales (Melluso *et al.* 2004).

In summary, pyrometamorphic glasses and rocks are highly variable due to the varying temperatures, mineral protoliths, and local environmental conditions, resulting in equally variable disequilibrium melting, volatilization, mixing, and crystallization (Canil *et al.* 2018; Peretyazhko *et al.* 2018; Sokol *et al.* 1998).

2.2 Pseudotachylite or frictionites

Pseudotachylite is a generic name for friction melts, and usually, in the geological terminology, pseudotachylites are classified as fault rocks (Killick 2003) even if the genesis could be quite broad. In agreement with Heide & Heide (2011), we classify these glasses as metamorphic ones, and in turn, among those glasses that originated from pre-existing rocks and display marked modifications due to changes in the pressure-temperature conditions.

Friction melts (and especially those with a pumice texture) were firstly associated exclusively to volcanic origin or to impact events. The term itself was introduced to describe the abundant dark glassy veins in Vrederfort (South Africa), the largest impact structure on

Earth. Nowadays, pseudotachylites are associated to large impact structures, earthquake-generated layers (veins), and very large rock avalanches (*e.g.* Reimold & Gibson 2005; Spray 2010). Indeed, the exclusive volcanic or impact-associated origin hypotheses have been both ruled out from the study of pumiceous rocks from Ötz Valley (Köfels landslide, see De Blasio & Medici 2017; Erismann *et al.* 1977), and since then, several studies focused on fault related friction melts that form by co-seismic friction (fault pseudotachylite) or avalanches.

The typical generic definition provided for pseudotachylite is: "dense rock produced in the compression and shear associated with intense fault movements, involving extreme mylonitization or partial melting," (Bates & Jackson 1987). Thus, the term "pseudotachylite" should be used to describe rocks that present unambiguous evidence of high temperatures. Because sometime this name is used regardless the origin of the glass, it is recommended to point out the differences between impact-related and fault-related pseudotachylites, such as the thickness of the material, or their formation history (Kenkmann *et al.* 2000; Reimold & Gibson 2005). The mechanisms o formation of (impact)-pseudotachylites in large impact structure are described in Reimold & Gibson 2005 In the following we will briefly describe pseudotachylites associated to very large landslides or formed along a fault plane during seismic deformation.

Fault pseudotachylite usually are veins of a few millimeters to a few centimeters in width that are related to large magnitude seismic events and located mostly in the upper crust (Ferré *et al.* 2005). Large seismic events can induce to a local increase of the temperature and to the melting of the host rocks along the fault plane, resulting in the creation of amorphous (cryptocrystalline) veins in response to frictional fusion. Depending on the maximum temperature achieved during seismic slip, the mineral phases present in the host rocks will be either melted or preserved as relict grains in the glassy matrix (Spray 1992). The chemical composition of the fault pseudotachylites is often slightly more mafic than the host rock, but the glass chemistry is dependent on bulk composition, mineral assemblage, and texture of the

host rocks (Di Toro *et al.* 2005; Maddock 1992). The study of the microlites and of the compositions of the glass matrix can be used to determine the temperature regimes associated to the seismic events. For example, artificial pseudotachylites have been produced by direct high-speed friction experiments (*e.g.* Kenkmann *et al.* 2000; Lin & Shimamoto 1998; Spray 1987) and the estimated melt temperatures of natural and experimental pseudotachylites are in the range of 750–1400 °C (Lin & Shimamoto 1998). Heide & Heide 2011 report melting temperatures of 1700 °C because of the presence of lechatelierite inclusions in frictionite melts. Nestola *et al.* (2010) report the occurrence of hexagonal $CaAl_2Si_2O_8$ (dmisteinbergite) in a fault pseudotachylite from the Gole Larghe Fault (Adamello, Italy), a polymorph that is formed at high temperatures (1200-1400 ºC) by rapid cooling. The constrain of the temperature regimes during seismic events is considered very important in order to better understand fault processes and to infer earthquake source parameters.

Friction melts can be generated as well during very large landslides (Erismann *et al.* 1977; Legros *et al.* 2000; Weidinger *et al.* 2014). Well-studied landslides-derived pseudotachylites are in Köfels (Austria) and Himalaya (Nepal). The latter is a giant rockslides (dislocation of ~170 m) that caused the formation of a homogeneous glassy layer with thickness between 1 - 3 cm (Masch & Preuss 1977). Masch & Preuss 1977 report a detailed study of both events and they observed that glass matrix is chemically heterogeneous with schlieren, bubbles, and relicts from the parent rock materials (partial to almost complete melting of host rocks of granitic to granodioritic composition). Moreover, they report the occurrence of glasses with pure quartz, plagioclase and alkali-feldspar compositions. Weidinger *et al.* (2014) report a review of several basal deposits of giant rockslides and defined that very short (<10 s) giant moving rockslides could produce friction-induce partial melting with basal temperatures > 1500 ºC (in anhydrous conditions).

2. Glasses from highly energetic events

We will describe amorphous materials deriving from highly energetic events, either natural or artificial. First of all, glasses produced by natural events, such as tektites and impact spherules, will be taken into account. Then, we are going to describe some enigmatic natural glasses that are almost certainly of impact origin (accepted or assumed) but that are not found in stratigraphic contexts. Notable examples of such glasses are Libyan Desert Glass, Darwin Glass, and Dakhleh Glass. Finally, we are going to describe other glasses, resulting from a rapid "shock" event, the fulgurites. At the end, we will consider also a glass, not strictly natural, but that can be considered as an analogues of impact glasses: the atomic glass - trinitite.

2.1 Impactites

Impact processes are able to greatly influence the evolution of planets. Just looking at the Moon, we can recognize with bare eye that the surface is heavily affected by impact cratering. Besides our satellite, planets such as Mercury, Mars and many satellites in the Solar System have circular depressions that testify the occurrence of numerous impacts, with only a few exceptions, including Earth, where the topography has been remodeled by active geological processes. The first impact crater directly witnessed on Earth (the so-called Carancas event) is very recent. It occurred near the southern shore of Lake Titicaca in Peru on September 2007, where the impact of a stony meteorite produced a 13.5 m crater (Tancredi *et al.* 2009).

The recognition of impact cratering as a fundamental process in the evolution of a planet has occurred as well rather recently, with the discovery of small spherules worldwide distributed in the Cretaceous- Paleogene K-Pg layer (formally known as KT, Cretaceous-Tertiary), first detected in Gubbio, Italy by Alvarez and coauthors (1980). These spherules and the associated layer contain chemical and physical evidences for a major impact that caused the mass extinction event at the K-Pg boundary. In 1991, a 170-180 km diameter crater was

identified on the Yucatan peninsula as the impact site (Chicxulub crater) of a 10 to 15 km asteroid that induced the cataclysmic event responsible for the formation of the K-Pg worldwide ejecta horizons and caused the end-Cretaceous mass extinction, around 65 Ma ago.

As might be expected, impacts have caused catastrophic effects on clime and landscape, however, they do not produce just destruction and extinction. Indeed, there are also beneficial effects associated to such events, such as the economic significance of impact deposits (*i.e.* Sudbury, Canada; Vredefort, South Africa), or the associated hydrothermal systems created (Osinski & Pierazzo 2012; Pierazzo & Melosh 2012).

The impact of a large object (>50 m for a stony object), moving at a great speed (> 11 km s^{-1}; French 1998), with the surface will create an impact crater after a very short sequence of complex events, which can be summarized into three main stages: contact and compression, excavation and modifications (Melosh 2011). The generic term impactite refers to the large variety of materials (rocks, melts) formed by hypervelocity impact(s) of a large extraterrestrial body. A series of distinct materials is generated by the forces of a hypervelocity impact, starting with a shock wave (compression stage) and followed by decompression from peak shock pressures, with associated heat generation and material transport (excavation stage) Reimold & Jourdan 2012. The post-shock heat causes the solid-state deformation and/or melting of the target crustal rock and even its vaporization, and the original material is entirely altered by the extreme heat and pressure regimes. Simulation of impact processes have established that the timescale of crater formation is extremely short, compared to many other geological processes, and are in the order of seconds to minutes for craters ranging from 1 to 100 km, thus impactites will present very distinctive characteristics (French 1998; Stöffler *et al.* 2018; Stöffler & Grieve 2007). Impactite is the commonly used (and misused) word for all shocked, melted or vaporized materials as a consequence of a hypervelocity impact, and because of the confusion, a study

group proposed a classification and a nomenclature of these materials, based on geological setting, texture, composition, and degree of shock metamorphism (Stöffler *et al.* 2018; Stöffler & Grieve 2007). The first grouping is based on the location of the materials, thus "proximal impactites" is used for materials found in the proximity of the impact crater, whereas the term "distal impactites" refers to materials that do not occur directly in or around a source crater (*i.e.* distal ejecta). Further sub classifications have been applied to proximal impactites, and according to Stöffler & Grieve 2007, proximal can be further divided into three subgroups: shocked rocks, impact melt-rocks and impact breccias; depending on the peak pressure and the post-shock temperatures, both minerals and original rocks texture will present shock effects that allow to identify progressive stages of shock metamorphisms. For instance, by increasing shock pressure there are i) Planar Fractures (PFs) and Planar Deformation Features (PDFs) in minerals such as quartz, zircon and feldspars; ii) high-pressure quartz polymorphs (coesite, stishovite); iii) diaplectic mineral glasses (produced without fusion); iv) fused mineral glasses (produced with fusion), and v) melts (see **Figure 3** from Reimold & Jourdan 2012). For example, quartz grains exposed to shock compression develop planar microstructures depending on the pressure range: PFs for pressure range of 5 - 8 GPa, and PDFs over the pressure range of 5-10 GPa to ~ 35 GPa. Shock-induced deformation in zircon grains have been reported as well, indicating shock pressures higher than 20 GPa (*L. Ferrière and G. R. Osinski – impact cratering book, chapter 8*). Impact diamonds have been reported as well in many impact sites. The transition from carbon (graphite) to diamond and lonsdaleite is around 13-15 GPa, with temperature in the range of 1300–2000 K (French 1998; Pratesi 2009).

Figure 3 clearly shows that the pressure conditions for normal crustal metamorphism (regional, contact) differs completely from shock metamorphism, resulting in the production of characteristic features and materials. In normal crustal metamorphism the range of temperature and pressure is around ≤ 1000 ºC and 1 - 3 GPa, respectively, and rocks and mineral

transformations occur in very long times (>10^5 years), thus approaching equilibrium (French 1998). On the contrary, shock metamorphism is an instantaneous process, with peak pressures that reach > 100 GPa, and temperatures much higher than 3000 ºC. Because of the rapid process, quenched amorphous and crystalline metastable phases are characteristic. For a detailed description of all shocked materials, readers are referred to the comprehensive work of Stöffler & Langenhorst 1994 and to Osinski *et al.* 2012).

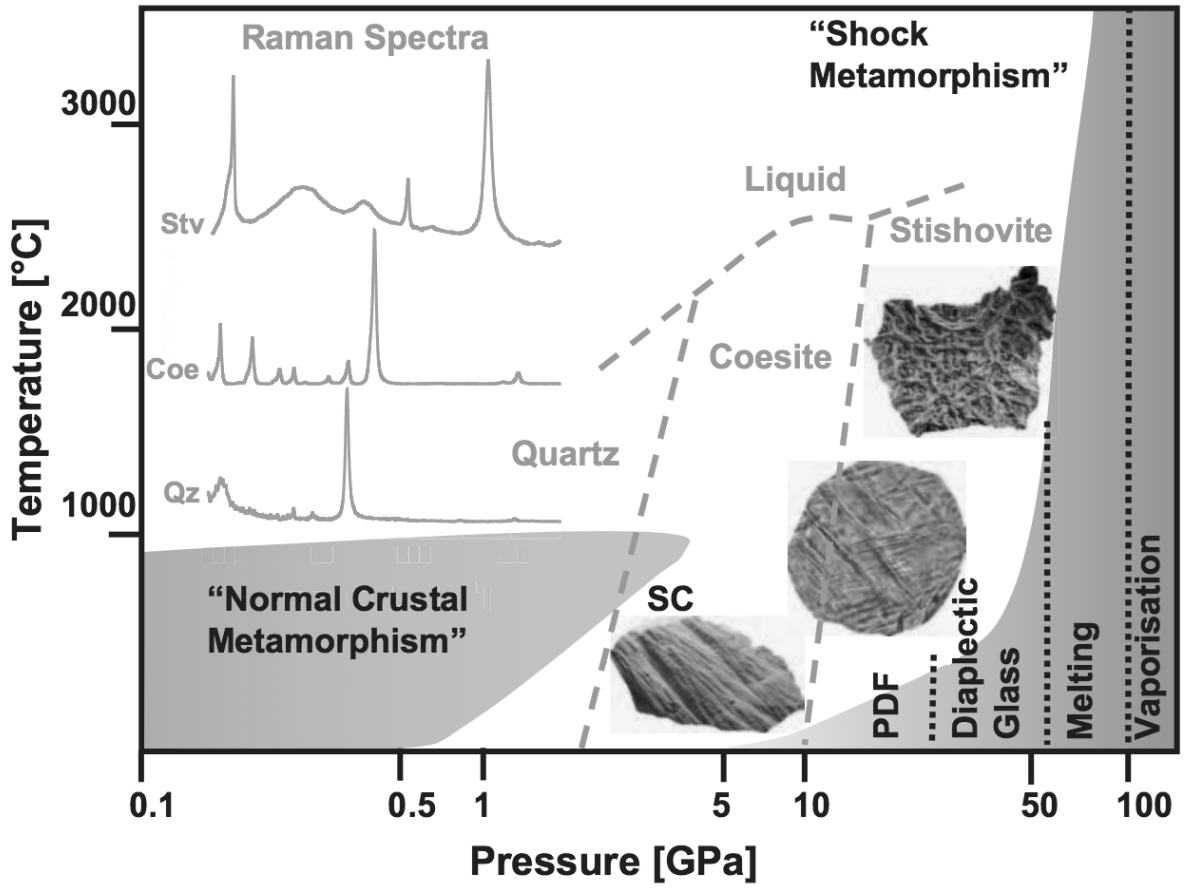

Figure 3 - Pressure (*P*)–temperature (*T*) diagram, for normal and shock metamorphisms. Figure from Reimold & Jourdan 2012; COPYRIGHT MSA

In the following, we will mainly discuss the most homogeneous glasses created by hypervelocity impact events, *i.e.* the distal ejecta tektites, but we will also provide a brief overview of some other distal ejecta and proximal glasses. To distinguish proximal impact glasses, volcanic glasses and distal ejecta tektites, Koeberl 2013 provides some characteristics that are distinctive of the distal ejecta, and enable their recognition. Tektites are:

i) amorphous and fairly homogeneous (no crystallites);

ii) contain lechatelierite (amorphous SiO_2);

iii) occur within definite areas, called strewn-fields (SF) and are associated to a single source impact crater;

iv) do not occur directly in or around a source crater (they are distal ejecta).

Moreover, tektites are strongly depleted in water (0.002 to 0.02 wt.%, at least an order of magnitude lower than the H_2O content of volcanic glasses) and are highly reduced (almost all iron occurs as Fe^{2+}) (Beran & Koeberl 1997; Fudali *et al.* 1987; Giuli *et al.* 2010a, 2013a, 2014a; Giuli 2017; Koeberl 1994, 2013; Melosh & Artemieva 2004; Rossano *et al.* 1999).

3.1.1 Distal Ejecta

As a consequence of a hypervelocity impact, the uppermost (200 m) surficial target rock is melted and ejected. A small portion of this molten ejected material will fly far away from the source crater and are called distal ejecta (according to Montanari & Koeberl 2000, ~ 90 % of the ejecta are proximal *i.e.* deposited within five crater radii from the impact site). The flying melts are quickly quenched to form fairly homogeneous amorphous materials with typical shapes (*e.g.* splash forms) like spheres, teardrops, disc-shaped form, and are known as tektites. A partial crystallization of primary microlites/crystallites (*e.g.* clinopyroxene or Ni-rich spinel) upon cooling could occur and the material formed is called microkrystite (Glass & Simonson 2013 and references therein).

Distal ejecta deposits (or air-fall beds) are deposited far away from the source crater and can be divided in two types: i) tektites and microtektites, and ii) spherule beds (Osinski *et al.* 2012). A more enigmatic kind of distal ejecta found on Earth consists of glassy materials, not volcanic in origin, but not having spherical shapes and not classified as tektites. Example of these enigmatic glasses are Libyan Desert Glass, and Darwin glass (Glass & Simonson 2013).

505 The reasons behind the formation of spherules and tektites remains poorly understood, and no
506 solid model or evidence has been found to explain why just a few impacts form large amounts
507 of high-speed ejected glasses and why only a few provides tektites (Howard 2011). Thus, tektite
508 formation must require specific impact conditions (see below).

509 On Earth, impact craters are not easily found (190 confirmed impact structure as of July
510 2019; Earth Impact Database 2019) because their morphology has been altered by hydrothermal
511 and chemical alteration, and by tectonic processes. Thus, most of the impact craters occurred
512 on Earth have been destroyed or covered. For instance, the Chicxulub impact structure is
513 located beneath ~ 1 km of sediment below and half offshore the Yucatan Peninsula, and until
514 1991, year of the discovery, the only proof of a connection between end-Cretaceous mass
515 extinction (K–Pg boundary layer) and a possible cataclysmic impact, was the worldwide
516 occurrence of distal ejecta horizons. Hence, sometimes, distal ejecta are the only remaining
517 witnesses of large impact events, and they provide important information regarding planetary
518 processes when found in the stratigraphic record. The importance of air-fall beds has been
519 compared to the study of volcaniclastic layers (Glass 2016).

520 When dealing with distal ejecta, or in general, with glass spherules, the most important
521 point is to gather enough evidences to rule out the volcanic origin. These evidences are usually
522 called ‘impact markers’ and includes chemical, isotopic, and mineralogical marks that indicate
523 the involvement of a cosmic body. Example of markers that indicate an extraterrestrial
524 contribution are the elevated content of siderophile elements (Ir, platinum group elements,
525 PGE), the occurrence of shocked minerals a/o Ni-rich spinels a/o impact diamonds, and atypical
526 isotope ratios. The complete list of the well-established or new ‘impact markers’ is beyond the
527 scope of this chapter, and the readers are referred to the exhaustive contribution of (Goderis *et*
528 *al.* 2012).
529

Tektites and microtektites

Tektites are small, typically dark, glassy objects that have been transported through the atmosphere hundreds to thousands of kilometers from the impact site, and are found only in certain areas of the Earth's surface, called tektite strewn fields (SF). Tektites are generally chemically homogeneous, Si-rich glasses of various sizes (usually > 1 cm), with typical aerodynamic shapes and very characteristic surface features (Figure 4). Microtektites are microscopic tektites, with diameter < 0.1 cm, largely found in deep-sea sediments.

Tektites can be further subdivided in three types, depending on their forms: Muong Nong-Type (or layered), ablated/flanged tektites (or aerodynamically shaped tektites), and the most common ones, the splash forms (or normal tektites). The morphology of the most common tektites varies between spherical, dumbbell-shaped, and teardrops (Figure 4) as a result of rapid rotation of the molten flying material.

Figure 4 - Australasian tektites with various shapes; dumbbell, teardrop and fragments. Dumbbells are formed by rapid rotation of melt droplets ejected into the atmosphere. When the rotation is high enough, the dumbbell is broken to form teardrops.

Muong Nong-Type tektites (MN - named after a region in Laos) are unusually large tektites (up to several tens of centimeters in size) and with layered structures. Koeberl 1992a

549 observed that Muong Nong-Type tektites are enriched in volatile elements (the halogens, Cu,
550 Zn, Ga, As, Se, Pb), and have higher water contents compared to splash-forms and ablated
551 tektites. Moreover, MN tektites present chemical heterogeneity (darker and lighter layers), and
552 may contain relict mineral grains (*e.g.* corundum, quartz, chromite and cristobalite) and very
553 large bubbles (Glass & Simonson 2013). Despite the differences with other tektites, still MN-
554 Type tektites have an average chemical composition (major element chemistry) and age
555 matching those of common tektites. Moreover, MN-Type tektites strongly differ from volcanic
556 glasses because of the presence of shocked mineral inclusions, for differences both in major
557 and trace element contents (*e.g.* REE patterns), lower water content, and highly reduced iron
558 (Koeberl 1992a). The presence of relict mineral grains, and the relatively higher water amount
559 in Muong Nong-Type tektites suggest that these glasses have experienced the lowest
560 temperatures of all tektites (Koeberl 1992a). For instance, the presence of volatiles (halogens,
561 Zn) and the vesicularity of lechatelierite particles seem to indicate lower formation
562 temperatures (Montanari & Koeber 2000). Is assumed that Muong Nong-type tektites have been
563 deposited closer to the source crater and based on ^{10}Be data they should derive from a greater
564 depth in the target deposits than were most of the other tektites (Ma *et al.* 2004). The layered
565 structure of these tektites, with their chemical heterogeneities, and the presence of relict mineral
566 grains, may serve to better constrain tektite conditions of formation, because they supposedly
567 represent the major link between target rocks and tektites (Montanari & Koeber 2000).

568 To date, of the four known tektite strewn-fields, all but one have been linked to source
569 craters, based on geographic location, geochemical evidences, and composition (Koeberl 2013
570 and references therein). The oldest strewn field known is the North American (NA) one of 35.3
571 Ma age (± 0.1) associated with the 85 Km diameter Chesapeake Bay (USA) impact structure
572 and includes Bediasites, Georgianites, Barbados and Cuba tektites. The central European (CE)
573 or moldavite strewn field of 14.8 Ma age (± 0.2; Schmieder *et al.* 2018) is associated with the

574 Nördlinger Ries impact structure of about 24 km in diameter (Nördlinger Ries, Bavaria, D).
575 There is another impact crater, the Steinheim crater, ~ 3.8 km in diameter, located about 42
576 kilometers west-southwest from the center of Nördlinger Ries. These two craters are believed
577 to have formed nearly simultaneously by the impact of a binary asteroid (Stöffler *et al.* 2002).
578 Moldavites are found mainly within a 200–450 km ranges from the Ries crater, in Czech
579 Republic (Bohemia, Moravia), Austria and Germany. Recently, a sub-strewn field in Poland
580 has been reported as well (Brachaniec *et al.* 2014.), circa 485 km from the Ries crater.
581 Moldavites have a unique green color and have strong surface sculpture deriving from erosion.
582 Stöffler et al. 2002, and more recently Artemieva et al. 2013, modeled the formation of the CE
583 strewn field, suggesting a 1.1-1.5 km stony meteorite impactor hitting the target surface with
584 an angle of 30º, at 15-18 km/s. The Ivory Coast (IC) tektite strewn field is associated with the
585 1.07 Ma old Bosumtwi crater (10.5-11 km diameter, Ghana, Africa) (Koeberl *et al.* 2007). The
586 Bosumtwi crater is the youngest well-preserved impact structure known, and it is almost
587 completely filled by a lake (Lake Bosumtwi). The youngest strewn-field, of 803±3 ka (Lee &
588 Wei 2000), is the Australasian one, for which no source crater has been identified so far.
589 Tektites of the Australasian strewn field (AA) include australites, thailandites, indochinites,
590 philippinites and javanites. The AA strewn field is very extensive and finding of microtektites
591 on land and oceans (microtektite-bearing deep sea cores) have improved the determination of
592 the AA geographic distribution, which is inhomogeneous (**Figure 5**) and spread from the
593 southeastern region of Asia down to Australia and Tasmania. Recently, smaller tektites
594 (microtektites) that were found in four different sites in northern Victoria Land Transantarctic
595 Mountains (TAM, Antarctica) have been related to AA and there are clear evidences Folco *et*
596 *al.* 2008, 2009, 2010, 2011; Giuli *et al.* 2014a) that these samples represent a major
597 southeastward extension of the Australasian strewn field. Thus, the AA strewn field covers
598 more than 10% of the Earth's surface, and even if no source crater has been identified yet,

several authors suggest its location somewhere in the Indochina region (Folco *et al.* 2016). Besides these four well-known tektite strewn fields, recently, other two have been proposed, one from central American (Belize glasses), and the second from Uruguay (uruguaites) (Ferrière *et al.* 2017; Giuli *et al.* 2014b; Povenmire *et al.* 2011; Povenmire & Cornec 2015; Senftle *et al.* 2000).

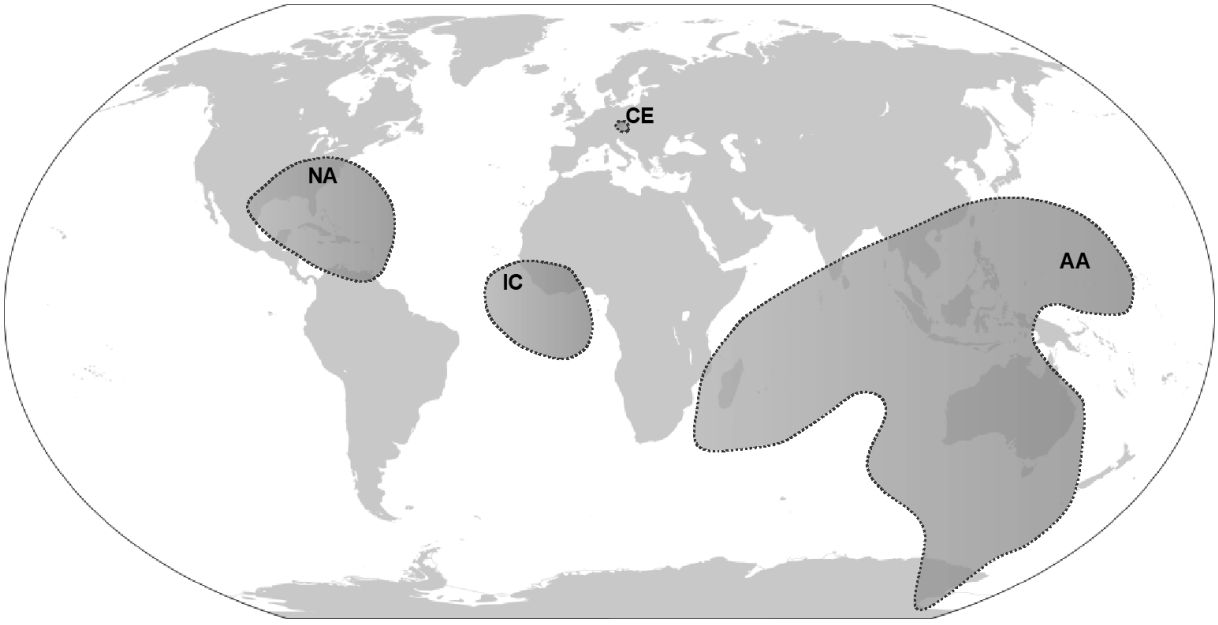

Figure 5: Approximate location and extension of the four strewn fields: NA (North American), IC (Ivory Coast), CE (Central Europe) and AA (Australasian). The known source craters are Chesapeake Bay (NA), Ries (CE) and Bosumtwi crater (IC). Redrawn after Folco et al. 2011, 2016; Glass 2016.

The chemical composition of tektites is fairly homogeneous within the same strewn-field, and also among the four strewn-fields the chemistry of all distal ejecta shows that these glasses are aluminosilicates with high SiO_2 contents and alkalis depleted (see Table 1).

Tektites are usually black/dark green, except moldavites that have a characteristic lighter green color, and do not contain microlites or relict minerals, but they contain vesicles, mostly spherical, or elongated as evidence of glass flow. **Figure 6** shows the light transmitted optical image of an australasian tektite. Flow lines and small vesicles are clearly visible. Bubbles are very frequent in tektites, and many studies have been done in order to determine the

composition, the content and pressure of the trapped gases. These data are very important because they provide information on the nature of the atmosphere during formation (quenching). Oxygen, C-based (CO, CO_2, CH_4) and noble gases have been identified in different proportions, and sometimes even contradictory results have been presented, mainly because of the extraction methods used. Early studies reported the presence of CO_2, CO, H_2, SO_2, CH_4, N_2, and O_2 with total gas contents ranging between 0.23 and 0.82 cm^3/g (Ottemann 1966 and references therein). Gentner & Zähringer (1959) and Zähringer & Gentner (1963) studied noble gases in several tektites and found heavy noble gases (Ar: Kr: Xe) ratios very similar to that of the Earth's atmosphere, thus confirming the terrestrial origin of these specimens. Moreover, the established contents of argon (Ar40) was fundamental to determine the age of tektites across the AA strewn fields and to confirm that the different specimens were of the same age, and in turn, of the same origin. A recent review by Zak et al (2012) lists all studies concerning C-based gases in tektites (excluding noble-gases). More recent studies on gas ratios, and noble gas isotopic ratios confirmed that gases have terrestrial atmosphere origin, with a typical enrichment of lighter noble gases (He, Ne) compared to the heavy ones (Ar, Kr, Xe) (*e.g.* Jessberger & Gentner 1972; Matsubara & Matsuda 1991; Matsuda *et al.* 1996; Müller & Gentner 1968; O'Keefe *et al.* 1962). Moreover, the estimated bubbles internal pressures are very low (<< 1atm) thus suggesting that vesicles formation must result from internal gas pressure during tektite cooling, that happened in an atmosphere under low pressures (at high altitude). For instance, Matsuda et al. (Matsuda *et al.* 1996) reported a bubble pressure of ~ 10^{-4} atm, and a solidification of the molten ejecta that should have occurred high in the stratosphere at altitudes above 20-40 km, in agreement with earlier observations (Rost 1964).

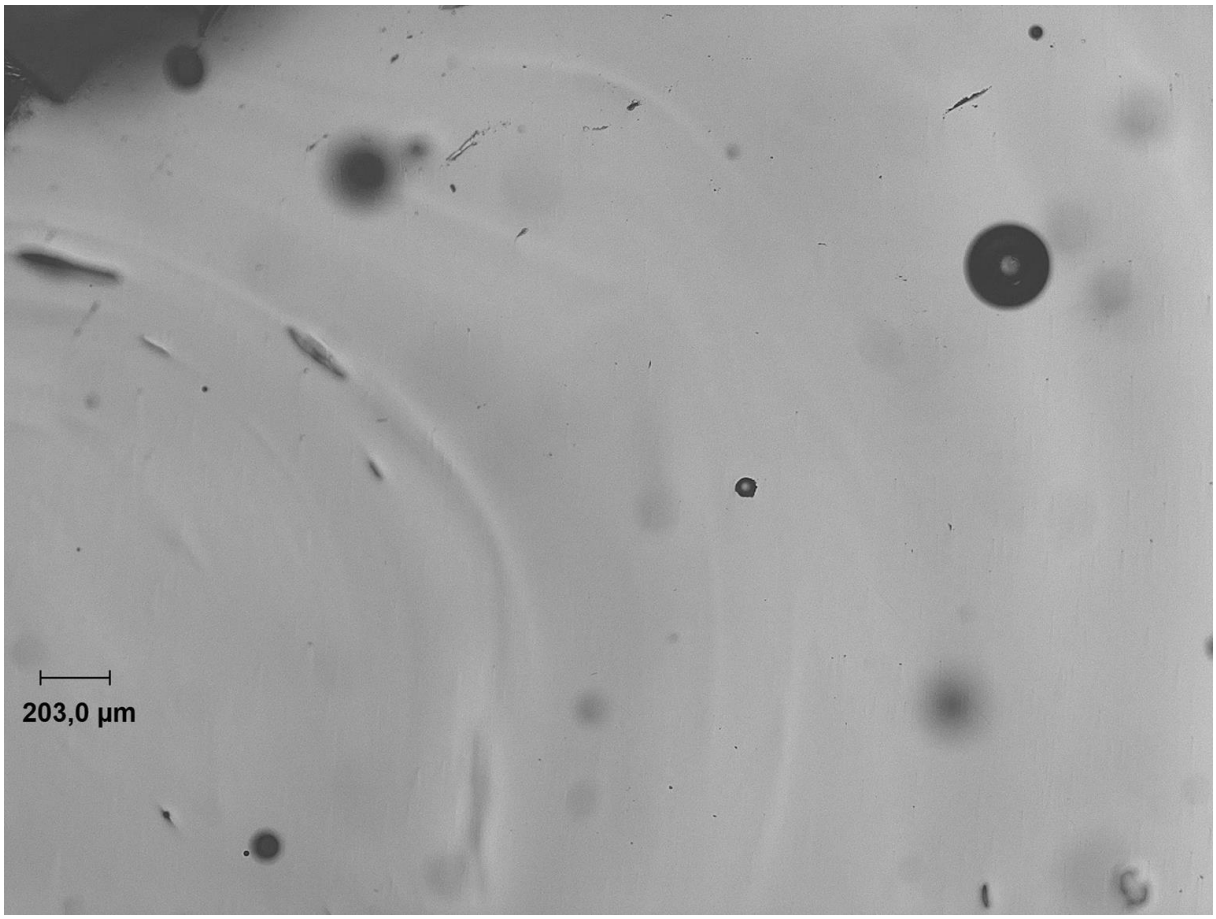

Figure 6 – Optical microscope image (transmitted light) of an Australasian tektite slice. Several bubbles of different dimensions, and flow lines are visible.

Three of the four tektite strewn-fields so far known also present microtektites (diameter usually < 0.1 cm): the North American, the Ivory Coast, and the Australasian SF. These spherules have been found in deep-sea deposits (see, *e.g.* Glass 1967, 1972, 1978, 1990) and are very important for defining the extension of the strewn fields (*e.g.*, Glass & Zwart 1979), for constraining the stratigraphic age of tektites, and to provide an indication regarding the location of possible source craters (*e.g.*, Glass & Pizzuto 1994). Ivory Coast microtektites are found as far as > 2000 km away from their source, whereas Australasian microtektites have been found also at extraordinary distances (>10000 km) from the hypothetical source crater. Microtektites, like tektites, show various morphologies, with oblate/prolate spheres, dumbbell- and teardrop-shaped, and may contain lechatelierite and vesicles. However, microtektites display a larger range of colors than tektites, with the majority being transparent, colorless, or

greenish/yellowish. Trace elements and isotopic abundances confirm that microtektites are genetically related to tektites in the associated strewn field (Frey 1977), but microtektites usually show a wider compositional range than tektites, even if, generally, they are similar to the tektites from the same strewn-field (Table 1). For example, it is possible to recognize IC and AA microtektites based on their alkali earth ratios (MgO/CaO).

There is a particular sub-group of AA microtektites that presents really high Mg contents (HMg; up to 24 wt.% MgO) and low SiO_2 contents than "normal" AA-microtektites, and that have bottle-green color and are highly eroded (Glass & Simonson 2013). A detailed study of major and trace elements of >100 microtektites from the different strewn fields have been done by Glass *et al*. (2004) that besides the HMg microtektites, found also some glasses with high Ni contents (HNi; up to ~470 ppm). HMg microtektites have been found also in the IC strewn-field. The study of the trace elements in microtektites also confirmed that these small distal ejecta derive from upper continental crust.

Everything seemed to point to microtektites being just smaller tektites. However, lately some differences have been found, namely on the Fe oxidation state of North American microtektites (Giuli *et al.* 2013a). The authors have shown that some North American microtektites present higher Fe^{3+}/Fe^{2+} ratio (up to 0.61), compared to the respective tektites, implying that, probably, different formation mechanisms are involved for the formations of such small objects. Interestingly, for these microtektites there is a positive correlation with the distance from the known source crater, and more oxidized conditions are reported for longer distances. This seems to be in contrast with the data available on other microtektites recovered at much further distances (*i.e.* AA microtektites). Because of the relative limited information available on tektite/microtektite formation mechanisms (see below) it is difficult to provide an interpretation of those data. Do microtektites register another "path" of the ejecta, or perhaps a different timeframe? Do they have different cooling rates? Further experimental studies, along

with modelling and further ejecta discoveries will help answering those questions, and probably the broader question of "how do distal ejecta form?".

Table 1: Average major oxide compositions of tektite and microtektites (wt.%). Data from § Glass 2016**; ‡** Giuli *et al.* 2013a**; #** Žák *et al.* 2012**; $** Mizera *et al.* 2016**; *** Giuli *et al.* 2014a **(TAM: microtektites from Victoria Land Transantarctic Mountains); ⊕** Glass *et al.* 2004**. For the original data source and error, see the cited references.**

	NA §	NA micro ‡	CE #	IC §	IC micro ‡	AA $	MN-type $	TAM micro *	AA-HMg micro ⊕
SiO_2	81.80	73.50	80.30	67.58	67.37	73.70	78.00	72.27	54.73
TiO_2	0.51	0.68	0.32	0.56	0.54	0.78	0.62	0.88	0.92
Al_2O_3	11.20	14.08	10.10	16.74	16.68	12.30	10.60	15.07	17.41
FeO	2.64	3.99	1.69	6.16	6.46	4.35	3.81	3.77	6.02
MnO			0.10	0.06		0.10	0.08		
CaO	0.45	1.59	1.35	1.38	1.57	2.41	1.51	3.49	4.82
MgO	0.61	1.81	1.69	3.46	3.72	2.21	1.74	2.87	15.36
Na_2O	0.94	1.87	0.55	1.90	1.89	1.37	1.33	0.25	0.64
K_2O	2.44	2.24	3.48	1.95	1.77	2.78	2.18	0.93	0.11

Other distal ejecta

Besides tektites and microtektites, it is worth mentioning the occurrence of many other spherule-associated layers across the world. For example, a clinopyroxene-bearing spherules layer (cpx-spherules) has been traced in many locations on Earth. The cpx-spherules associated layer is enriched in Ir and is ~10-20 ka older than the North American microtektite one (Glass *et al.* 2004 and references therein). These spherules have been associated to the Popigai complex crater (Siberia, Russia), an extremely large structure (~100 km diameter) of 35.7±0.2 Ma (Melosh 2011).

As mention before, the most notorious and studied distal ejecta deposits are the K-Pg (former KT) spherule ones, associated to another gigantic impact, and to the 170-180 km Chicxulub crater (Yucatan, Mexico). The impact event responsible for this crater had enough energy to distribute ejecta worldwide, and cause the end-Cretaceous mass extinction, around

66 Ma ago. The small K-Pg spherules (100-500 μm), that resemble microtektites, were first detected in the Cretaceous-Paleogene K-Pg layer in Gubbio (I) (Alvarez *et al.* 1980). K-Pg distal impact ejecta horizons are associated with Ir enrichments, siderophile element anomalies, and shocked minerals and high-pressure polymorphs (quartz grains, coesite and stishovite). K-Pg spherule layers have a global geographical extension with more than 350 sites identified, but because of the poor preservation of the claystone at the K-Pg boundary, in the early 80s there were some debates on the origin of these spherules, with some authors supporting an impact hypothesis (*e.g.* Smit & Klaver 1981), and others attributing an authigenic origin for the spherules (*e.g.* Izett 1987). A few years later, many authors, by studying many K-Pg spherules, and in particular the Si-rich spherules preserved at the K-Pg layer at Beloc (Haiti), provided clear evidences of an impact origin, based on geochemical data, enrichment in platinum group elements, the presence of lechatelierite and shocked quartz grains (Bohor 1990; Koeberl 1992b; Koeberl & Sigurdsson 1992; Sigurdsson *et al.* 1991). Despite the alteration of some deposits, according to Morgan *et al.* (2006) there is a correlation between shock markers and paleodistances from the impact site, and in particular the number and size of the spherules and shocked minerals are inversely proportional to their distance from Chicxulub. These evidences have been used to confirm the occurrence of a single highly energetic impact event related to the formation of the K-Pg spherule horizons, and to provide insights on the obliquity of the projectile.

Among the proposed impact-related Cenozoic distal ejecta layers there is one horizon related to a hypothesized impact event that according to Firestone *et al.* (2007), may have occurred at the beginning of the Younger Dryas (YD ~12.8 ka). In this case, impact event is not strictly related to a collision with the Earth surface, but (allegedly) to an airburst, that is a shock wave caused by the explosion of a cosmic object in the atmosphere (such as the well-known 1908 Tunguska airburst, Siberia). The Younger Dryas boundary is a < 5 cm-thick

sediment layer dated ~ 12.8 ka in several sites in North America, and in Belgium and Syria (Bunch *et al.* 2012; Firestone *et al.* 2007; Wittke *et al.* 2013) that contains impact-related markers, such as Ir enriched grains, magnetic micro-spherules (10-250 μm), vesicular carbon spherules, glass-like carbon, shock-fused vesicular lechatelierite, impact nano-diamonds, and fullerenes containing extraterrestrial concentrations of ^{3}He (helium-3 is extremely rare in terrestrial crustal rocks; Koeberl 2013). Still, the YD impact remains just a hypothesis because most of the reported "impact-related" markers could not be confirmed in independent studies or are not considered unambiguously impact proxies. For instance, fullerene with anomalous ^{3}He contents has not been found in all sites, and no shocked minerals have been reported. Moreover, Paquay *et al.* (2009) measured both PGE concentrations and Os isotope ratio (^{187}Os/^{188}Os) in the bulk sediments without finding evidences of extraterrestrial components. In a review, Pinter *et al.* (2011) report that none of the evidences described by Firestone were incontrovertible, and more recently, van Hoesel *et al.* (Van Hoesel *et al.* 2014), in another review on the YD impact markers, concluded that no unambiguous markers have been found so far, and that the data available still cannot support the claim that there was a Younger Dryas impact event.

Enigmatic Impact glasses

Glass & Simonson (2013) in their contribution on distal impact ejecta describe some glasses, almost certainly of impact origin, but not found in stratigraphic contexts. Most of the time, no source craters could be associated to these materials, hence the melting has been often attributed to radiation from airburst. These natural glasses have been found in several locations on Earth and cannot be classified as tektites or spherules. Examples of such glasses are: glass fragments from South Ural (Russia) called urengoites (Deutsch *et al.* 1997) glass fragments

753 from Egypt (Dakhleh glass; Osinski *et al.* 2007), and the famous Libyan Desert Glass, and
754 Darwin Glass (with a putative associated crater; Meisel *et al.* 1990).
755
756 In an area of ~ 6500 km^2 in southwest Egypt, close to the border with Libya, natural Si-
757 rich glass fragments, known as Libyan Desert Glass (LDG) are found (Rocchia *et al.* 1996).
758 Fission track dating provides an average age of ~ 29 Ma (28.5 ± 2.3 Ma to 29.4 ± 0.5 Ma
759 (Storzer & Wagner 1977), and 28.5 ± 0.8 Ma (Bigazzi & Michele 1996). LDG occurs as
760 centimeter- to decimeter-sized, irregularly shaped, and strongly wind-eroded glass pieces
761 (**Figure 7**), and one of the most famous specimens is the one used as the yellowish scarab of
762 Tutankhamen's pectoral. Libyan Desert Glasses are very silica-rich (~ 96.5–99 wt.% SiO_2; see
763 **Figure 1; Table 2**) and shows a limited variation in major and trace element abundances (the
764 remaining few wt.% are oxides of aluminum, iron, calcium, and magnesium). They are
765 homogeneous with a characteristic pale yellow/yellow-green color and characterized by the
766 presence of schlieren (Glass & Simonson 2013). Some minor elongated vesicles and spherulitic
767 inclusions of cristobalite have been reported as well, and in some cases baddeleyite (as high-
768 temperature breakdown product of zircon), rutile, staurolite, cordierite, kyanite, reidite and
769 mullite has been detected (Cavosie & Koeberl 2019; Gomez-Nubla *et al.* 2017; Greshake *et al.*
770 2010, 2018; Rocchia *et al.* 1996; Storzer & Koeberl 1991).
771 Since its discovery, early in the 20th century (Clayton 1934) the origin of the Libyan
772 Desert Glass still represents an unanswered enigma to all scientists and researchers. However,
773 an impact-related origin seems the most plausible mechanism. In fact, LDG fragments are
774 thought to be the remains of a glassy surface layer, resulting from high temperature melting of
775 sandstones/desert sand, caused either by a meteorite impact, or - to explain the absence of an
776 impact crater - by airburst (Aboud 2009; Seebaugh & Strauss 1984). The Rare Earth elements
777 (REE) pattern of LDG is typical of upper continental crust, but the analysis of desert sand and

778 sandstones found in the Libyan Desert Glass strewn-field do not perfectly match, thus no rock
779 precursors and crater could be identified (Storzer & Koeberl 1991). Evidence for an impact
780 origin include the presence of schlieren and flow textures, detectable amount of Ir,
781 lechatelierite, and baddeleyite and, more in general, high pressure–temperature phases (Barrat
782 *et al.* 1997; Storzer & Koeberl 1991; Swaenen *et al.* 2010). Moreover, the high concentration
783 of PGE, the presence of graphite-rich inclusions (ribbons), and reduced Fe species, are
784 additional evidence for an impact origin (Barrat *et al.* 1997; Giuli *et al.* 2003; Pratesi *et al.*
785 2002). Some specimens of LDG present marked layering, with brownish or grayish-bluish
786 streaks (in general, both are referred as dark streaks). The brownish streaks are enriched in
787 siderophile elements, Mg, Fe and Ni, and the Os isotopic data indicates the extraterrestrial
788 component. Observations by Transmission Electron Microscopy (TEM) (Pratesi *et al.* 2002)
789 revealed the occurrence of Al-, Fe- and Mg-enriched amorphous nano-spherules (80-100 nm)
790 in the LDG dark streaks, as a result of silicate–silicate liquid immiscibility. Similarly, also other
791 impact glasses from Zhamanshin crater (blue zhamanshinites; Kazakhstan) contain spherical
792 nano-inclusions (~100 nm) of a second glass enriched in Fe, Ca, Mg and P (Zolensky & Koeberl
793 1991).

794 Based on the amorphous and mineral phases occurring in the different LDG specimens,
795 the range of temperature and pressure have been constrained to T > 1900 K and pressure from
796 10 to > 30 GPa (Pratesi et al. 2002; Gomez-Nubla et al., 2017; Cavoisie and Koeberl 2019).
797 However, while high pressure occurred, most probably during melting and ejection, the
798 quenching of the molten material happened quickly at atmospheric pressure (Greshake *et al.*
799 2018). Moreover, the occurrence of meteoritic component suggests the impact of an
800 extraterrestrial object and not an airburst. This seems to be confirmed by a recent work by
801 Koeberl & Ferrière 2019 that reports the discovery of shock markers (*e.g.* PFs and PDFs on

quartz grains) in bedrock samples recovered in the Libyan Desert Glass strewn-field, and the suggestion of a deeply eroded impact crater in the area.

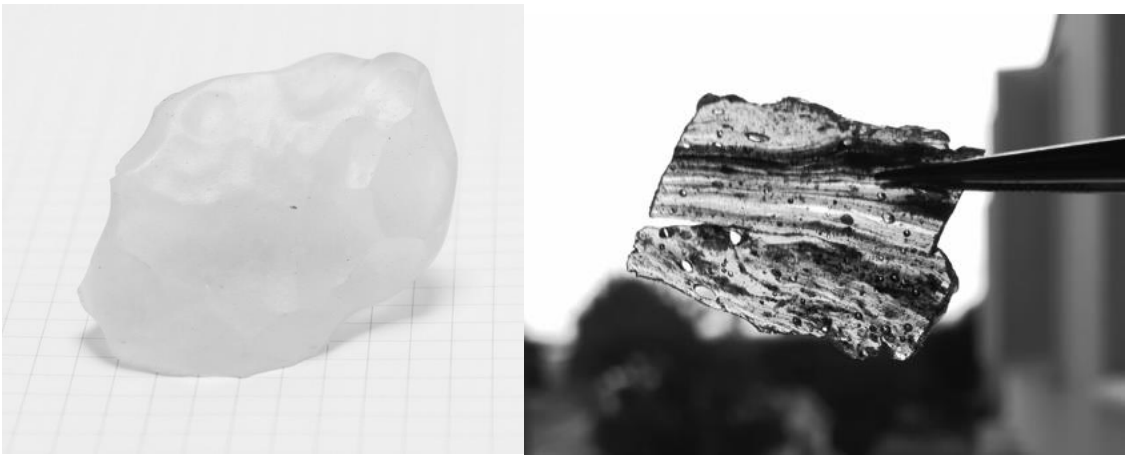

Figure 7 - 1) LDG with the typical aeolian erosion aspect 2) Slice of Darwin glass shows pronounced layering and flow structures, and elongated vesicles.

Another impact glass that cannot be referred to as tektite is found in a strewn-field of ~ 400 km^2 in western Tasmania (Australia): the Darwin glass. The age of this glass, estimated by Ar-Ar methods, is 816±7 ka (Lo *et al.* 2002), thus very close to the Australasian tektites. Though, their major and trace elements compositions are very different, indicating that the temporal association is casual. The Darwin crater, a small (~1.2 km) simple impact crater formed in sedimentary target rocks, was discovered in 1972, and proposed as the source of Darwin glasses (Ford 1972; Fudali & Ford 1979). Howard & Haines (2007) carried out a detailed petrographic study of the crater-filling samples, but no conclusive shock markers have been found (*e.g.*, PDFs in quartz grains). Nevertheless, the geochemistry of target rocks and glasses, the location of the crater, and the glass distribution (Darwin strewn-field) all point to the Darwin crater as source of the ejecta. Darwin glasses occur in an area larger than 400 km^2, with distances of at least 20 km (Howard 2011) from the putative Darwin crater, thus belonging to the distal ejecta group. Glasses generally occur as irregular centimeter-sized fragments, or

masses, even if small splash-forms (spheres and teardrops < 5 mm) can be found across the Darwin strewn-field. The color ranges from white, gray, light or dark green, dark brown, to black, and the glasses are generally vesicular and often exhibit flow structure marked by bands of elliptical vesicles (see **Figures 7 and 8**) (Glass & Simonson 2013). Interesting, the proportion of white glasses is greatest in the proximity of the crater, and the proportion of darker glasses, as well as the proportion of splashform shapes, increase with distance from the putative crater (Gomez-Nubla *et al.* 2015; Howard 2008, 2009). Darwin glasses are SiO_2 rich, and extremely depleted in Na_2O and CaO. The chemistry suggests the presence of (at least) two main glass groups: the first one, which represents ~80% of the samples, is enriched in SiO_2 (average ~ 87 wt.%), whereas the second one has a lower SiO_2 content (average ~ 81 wt.%), higher contents of MgO and FeO, and is enriched in Ni, Co and Cr (Howard 2008) (see **Table 2**). Optical microscope images of a Darwin glass show the contrast between layers of a lighter coloured glass (light brown) and a darker one (dark brown); furthermore, turbulent flow structures and bubbles of different dimensions and shapes are present (**Figure 8**). All textural features visible in this specimen are very similar to those observed by See *et al.* (See *et al.* 1998) in an impact glass bomb from the Ries crater. Raman spectroscopy data associated to the glass specimen shown in **Figures 7 and 8** are reported in **section 4**. Analyses by Raman spectroscopy allowed to identify small inclusions of α-cristobalite, and iron or iron/nickel oxides (Gomez-Nubla *et al.* 2015).

Recently, Raman spectroscopy has been also employed to detect and identify the organic matter in both LDG and Darwin glasses (Gómez-Nubla *et al.* 2018). Based on the results, and the identification of *e.g.* fullerene-type compounds, the authors constrained a pressure of ~15 GPa and temperatures between 670 and 1900 K. The preservation of organic material in inclusions of LDG and Darwin glasses has been explained by the trapping of the

organic matter within the impact melt, and a fast quench that avoided the total decomposition of the material (Gómez-Nubla *et al.* 2018; Howard *et al.* 2013).

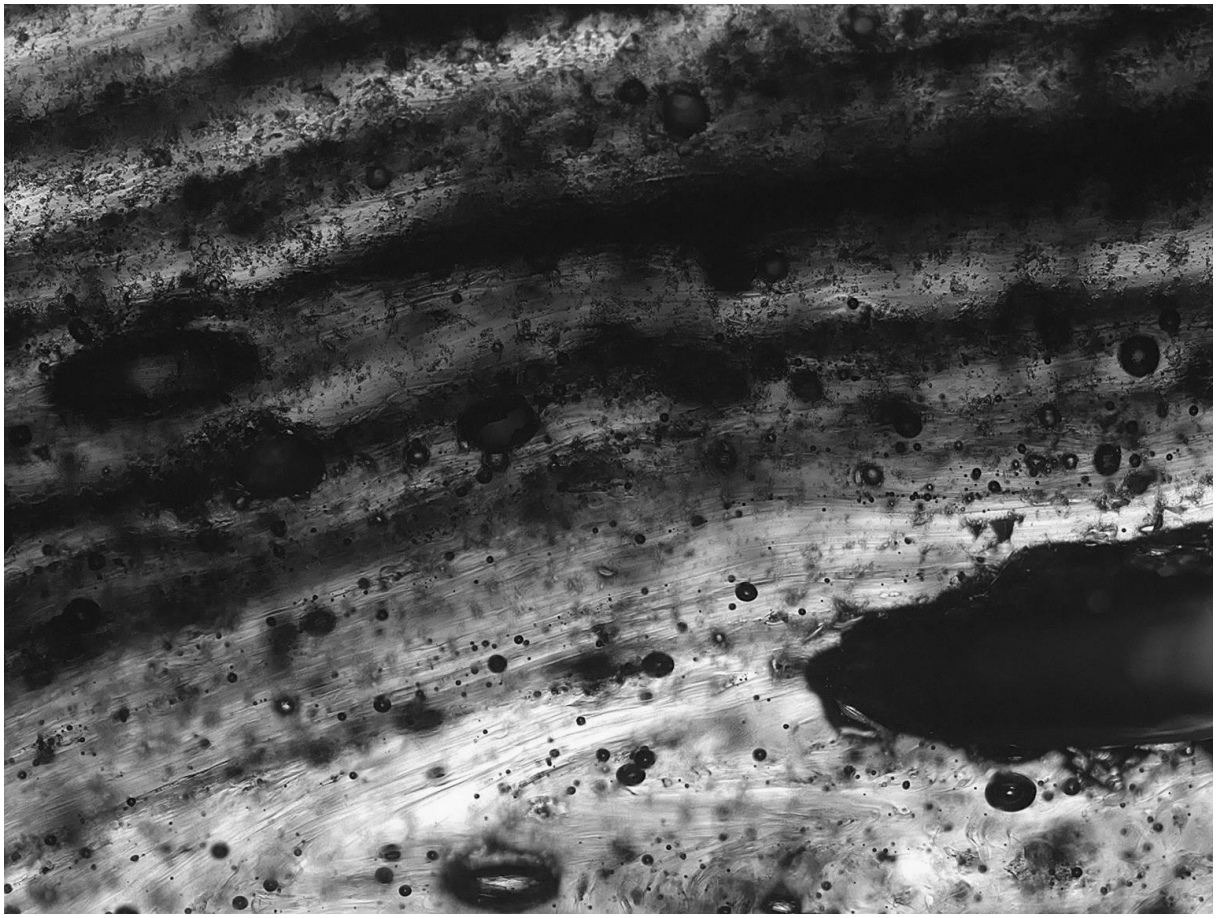

Figure 8 - Optical microscope view (transmitted light) of the Darwin glass slice shown in Figure 7. Darker and lighter layering, flow structures, vesicles and voids are clearly visible.

Formation of distal ejecta

The origin and the formation mechanisms of tektites, microtektites and spherules have been greatly debated. The terrestrial origin of tektites has been finally accepted, even if the strong dispute started in the 50s (*e.g.* Barnes 1958; O'Keefe & Barnes 1958; Urey 1955, 1963) has lasted until recently, with O'Keefe (1994) still supporting the theory that tektites were ejected from volcanoes on the Moon (especially for the unanswered question related to the very low water content of tektites), despite all geochemical and isotopic data available and the

provocative obituary by Schnetzler (1970) and his famous statement "The lunar origin of tektites […] died on July 20, 1969. The cause of death has been diagnosed as a massive overdose of lunar data". If the origin has been settled, the formation mechanisms are not completely clear yet. New distal ejecta finding, improved experimental data and numerical modelling have strongly enhanced the understanding of the physical-chemical conditions occurring during a hypervelocity impact (Melosh 1989, 2013). Nevertheless, the reason(s) why only a few impacts have produced significant amounts of distal ejecta is uncertain yet. Moreover, the spherule formation from the plume is not fully constrained as well, because physical and mathematical models are hampered by the limited information available on how materials respond to extremely high stresses in highly non-equilibrium conditions. One of the most important factors for distal ejecta formation is thought to be the obliquity of the impact (the angle between the projectile and target impact), which determine the maximum shock pressure and temperature regimes, and lately, the presence of water in the target rocks has been pointed out as a key factor as well (Artemieva 2002; Howard 2011; Stöffler *et al.* 2002).

Distal ejecta are believed to be formed during the very initial stage of the excavation (cratering process) when the projectile and the target materials (with a volume comparable to that of the impactor) are highly shocked, melted and vaporized. The highly pressurized mixture of vaporized rocks, molten materials, small solid fragments, and hot atmospheric gases constitute the so-called vapor plume (aka impact plume or fireball) (Melosh 2013), that expands away from the forming crater. The vapor plume pushes away the ambient atmosphere in its path and this allows ejected melt to follow long ballistic trajectories (*cf.* Howard 2011; see also Melosh 1989), and for large enough impacts the vapor plume might expand and burst the top of the atmosphere allowing materials to be dispersed at great distances, even at the global scale. Numerical modeling on spherules (or tektites) nucleation and condensation from the vapor plume has been done by *e.g.* Johnson & Melosh 2012, 2014; Melosh 1989; Pierazzo *et al.* 1998.

889 Johnson & Melosh 2012, 2014 differentiate two origins for spherules, based on their
890 thermodynamic histories: i) vapor condensed droplets and ii) melt droplets, in agreement with
891 early observations on other ejecta (Engelhardt *et al.* 1987). Because of the extremely high
892 temperatures expected in the impact plume, the melt will have an extremely low viscosity ($7 \times$
893 10^{-6} Pa s, according to Melosh & Artemieva 2004), and volatile-bearing bubbles will rapidly
894 travel through the melt and burst at the liquid surface, resulting in a liquid phase quickly
895 depleted in water and other volatile elements, such as Na and K (Melosh & Artemieva 2004).
896 The presence of a superheated melt in the vapor plum might explain not only the occurrence of
897 alkali depletion, and the low water content in the ejecta, but also the oxygen volatilization and,
898 in turn, the highly reducing conditions.
899
900 3.1.2 Proximal impactite
901 Glasses deposited within five crater radii from the impact site are referred to as proximal.
902 These amorphous materials can resemble tektites, but they show higher chemical heterogeneity,
903 relatively higher water contents (0.02 to 0.06 wt.% H_2O), and contaminations from the impactor
904 (Devouard *et al.* 2014; Koeberl *et al.* 2019; McPherson *et al.* 1984). Example of glasses
905 associated with impact sites are Irghizites (Kazakhstan), Aouelloul glasses (Mauritania), Lonar
906 Crater Glass (India), Waber Glass (Saudi Arabia) and Atacamaites (Chile).
907 Associated to the Zhamanshin impact structure (Kazakhstan) there are a variety of impact
908 glasses. The main groups are i) Irghizites, glasses with aerodynamic flight-shapes that resemble
909 tektites, but with higher water contents, and with an average SiO_2 content of ~74 wt.%; ii)
910 Zhamanshinites that can be found closer to the source crater and are much larger than Irghizites.
911 Zhamanshinites are very heterogeneous, with layered structures, flow structures and based on
912 the chemistry they are further differentiated in different subgroups (Fredriksson *et al.* 1977;
913 Koeber & Fredriksson 1986), with glasses Si-enriched (> 70 wt.% SiO_2), and glasses strongly

depleted in silica (< 55 wt.%), called basic impactites. An additional amorphous material is referred to as blue Zhamanshinite. It has high SiO_2 and CaO contents, and present evidences of liquid immiscibility with the occurrence of amorphous inclusions that provide the characteristic turquoise to very dark blue color (Koeber & Fredriksson 1986; Koeberl 1988; Zolensky & Koeberl 1991Koeberl 1988; Zolensky& Koeberl 1991). Indeed, the nano-sized Ca-Fe-Mg-P-rich silicate immiscible liquid inclusions are responsible of the scatter of light (Rayleigh scattering) that results in the blue coloring of the glass.

Africa has 19 confirmed impact structures (Reimold & Koeberl 2014), and among them there is the Aouelloul structure in Mauritania, a relatively young (3.1± 0.3 Ma) crater of ~390 m diameter. The enrichment in siderophile elements, and the occurrence of lechatelierite, baddeleyite, Ni-rich Fe- spherules are the impact marker identified. The glasses associated (Aouelloul glasses) spread in proximity of the crater, and similarly to the Darwin glasses, are very heterogeneous. They are water-depleted silicate glasses, with abundant schlieren texture and different bulk chemistries, and with the presence of unambiguous meteoritic component.

Wabar crater is a very young impact structure in Saudi Arabia (290 ± 38 years). The associated glasses are both large fragments and small (≤1 cm) glassy aerodynamic flight-shaped and spheres [Prescott et al. 2004; Hamann et al. 2013]. Wabar glasses are known to have several chemical heterogeneities, with flow structures, emulsions of Fe-rich ultrabasic silicate glasses, FeNi globules and areas marked with light- and dark-brown glasses, respectively depleted or enriched in Fe (Hamann *et al.* 2013; Hörz *et al.* 1989; Ottemann 1966; see **Table 2**). See *et al.* (1998) by studying the glasses microstructure, highlighted the textural and chemical heterogeneity that are present in these impact glasses, and the occurrence of interstitial enrichments of Fe and Ni, most probably resulting from the impactor.

From Atacama Desert (Chile) thousands of aerodynamically shaped black glasses have been recovered and named atacamaites. These glasses have minor vesicularity, inclusions of an

939 extremely silica rich glass (lechatelierite), turbulent flow structures, strong chemical variations
940 (*e.g.* FeO contents vary from 5 wt.% to 15 wt.%), and extremely high contents of Ni, Co, Re,
941 Ir and Pt (orders of magnitude higher than the average upper continental crust). Moreover, water
942 contents are higher (~ 130 ppm) than those associated to tektites. All these characteristics point
943 to the impact nature of these glasses (Devouard *et al.* 2014; Dos Santos *et al.* 2015; Koeberl *et*
944 *al.* 2019).
945
946 For sake of comprehensiveness, we will briefly describe an example of a proximal
947 impact breccia, the suevite, from the Ries crater type locality. An exhaustive review on Ries
948 crater and suevite is reported by Stöffler *et al.* (Artemieva *et al.* 2013) (the modelling part is in
949 Artemieva *et al.* 2013). The term suevite was firstly used to describe an impact breccia
950 formed at the Ries impact crater (Bavaria, Germany); nowadays the term is used more in general
951 to describe polymict (consisting of heterogeneous fragments) impact breccia containing clastic
952 matrix/groundmass from the target rocks, shocked minerals, and glass. At the Ries impact site,
953 suevite can be found both in the crater and outside the rim (outer or fallout suevite), associated
954 to the different (five) shock stages. Because of the occurrence of a full set of rocks subjected to
955 different degrees of shock metamorphism (and distal ejecta as well), the Ries crater is one of
956 the most studied, and has been the type locality in order to discover and classify all shocked
957 materials (Artemieva *et al.* 2013; Stöffler 1971). **Figure 9** reports a photo of a glass-rich suevitic
958 impact breccia (fallout suevite from Otting quarry; Ries crater, Germany). The heterogeneous
959 nature of the sample can be appreciated, with lithics, relict mineral grains and abundant glass
960 portions. From this locality is was first reported the occurrence of coesite (Shoemaker & Chao
961 1961). According to Stöffler et al. (Artemieva *et al.* 2013 and references therein) the fallout
962 suevite (also called outer suevite) is almost completely constituted of lithic clasts derived from
963 the target crystalline basement rocks, and only a few percent is of sedimentary origin (< 6%
964 sedimentary lithic) and contain rocks of all stages of shock metamorphism, from the unshocked

965 materials of stage 0 (0-10 GPa), to moderate shocked (stages I and II: 10-60 GPa), up to stage
966 IV (> 60GPa) and there is the occurrence of abundant glass materials.
967

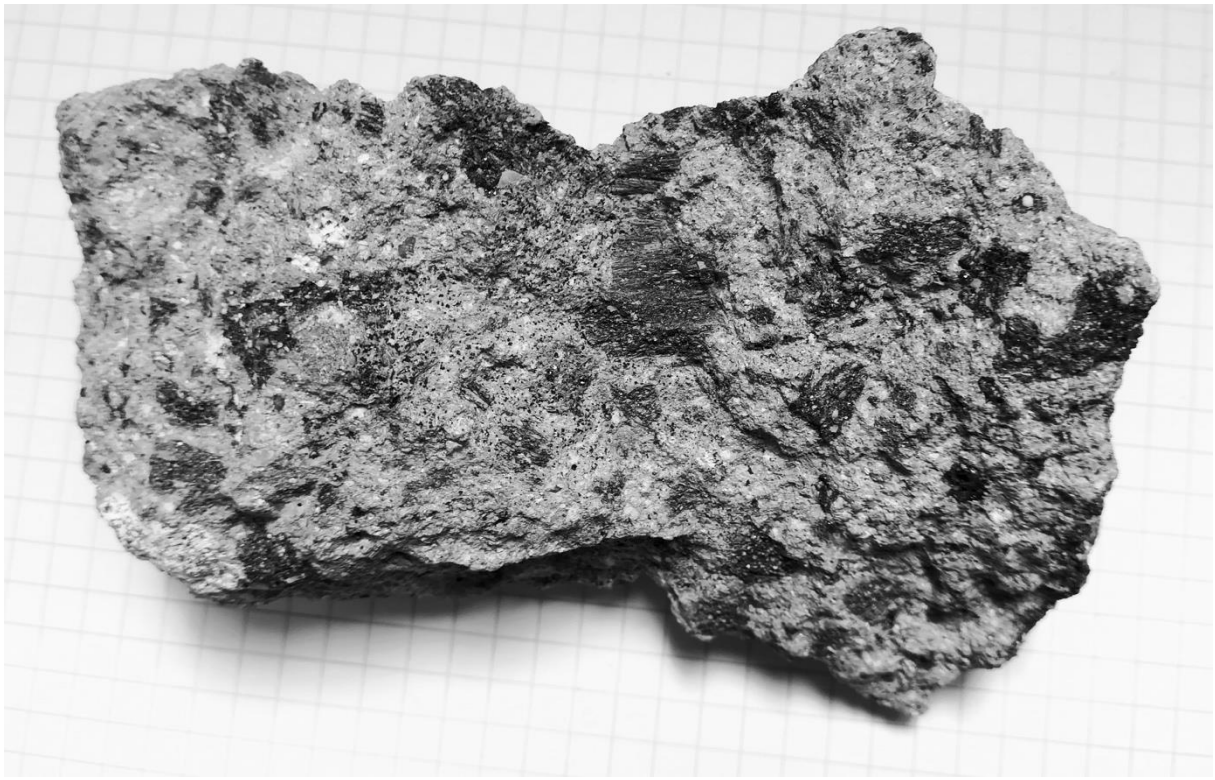

968

969 **Figure 9 - Fallout suevite from Otting quarry (Ries crater, Germany). The polymictic sample**
970 **has lithics (brighter spots), relict mineral grains and abundant glass (darker portions).**
971

972 Oberdorfer (1905), in suevite deposits in the west side of the Ries crater, observed the
973 presence of spherical dark-brown amorphous bodies surrounded by a light brown glass, with
974 textural features indicative of silicate-silicate melt immiscibility. Other textural evidences of
975 liquid immiscibility were reported by Graup (1999), but in this case for an immiscibility
976 between silicate and carbonate melts. Crystalline calcite is a common constituent of suevite,
977 and it was believed to derive from post-impact hydrothermal activities (Engelhardt 1967, 1972).
978 However, because of the presence of gas vesicles in carbonate flow lines, or carbonate globules
979 embedded in silicate glass (and *vice versa*), and the presence of deformed and coalescing

spheres of carbonate within the silicate melt, the carbonate component is likely a result of impact-shock melting, and not of secondary origin (Graup 1999).

As observed above, impact glasses (including the enigmatic ones) are more heterogeneous than distal ejecta (*i.e.* tektites). For example, Irghizites, Wabar and Darwin glasses clearly present at least two major chemical bulk compositions. In **Table 2** is reported the average major oxide composition for some of the impact glasses discussed here. The chemical variability among the same impact glasses, and with respect tektites (see data in **Table 1**) reflects the differences in the mechanisms of formation of those glasses, especially related to the different time-scales.

Table 2: Average major oxide compositions of impact glasses (wt.%). Data from § Koeberl 1997; ⊕ Giuli *et al.* 2003; # Ottemann 1966; ‡ Howard 2008; $ unpublished data.

	LDG §	LDG dark streak ⊕	Wabar dark #	Wabar light #	Aouelloul #	Suevite glass - Ries #	Darwin ‡	Darwin* $	Atakamaite $
SiO_2	98.4	95.85	87.45	92.88	86.51	66.19	76.47 - 93.85	82.74	68.74
TiO_2	0.12	0.18	0.15	0.12	0.55	0.82	0.22 - 0.8	0.609	0.43
Al_2O_3	1.19	1.48	1.77	2.64	5.76	14.74	3.14 - 11.45	7.89	10.66
FeO	0.12	0.98	5.77	0.53	1.59	3.86	0.84 - 5.87	2.39	5.40
MnO		0.02						0.01	0.06
CaO	0.01	0.08	1.90	1.46	0.73	3.96	0.02 - 0.25	0.04	3.59
MgO	0.01	1.38	0.60	0.47	0.91	2.60	0.24 - 4.0	0.87	1.52
Na_2O	0.005	0.02	0.39	0.42	0.14	3.62	0.0 - 0.21	0.09	2.77
K_2O	0.009	0.01	0.58	1.61	2.05	3.26	0.75 – 2.71	2.05	2.61

Note: * average chemical composition of the specimen shown in **Figure 8**

997 **3.2 Fulgurite**

998 Fulgurites are formed as a result of fusion and modifications of rocks (*s.l.*) by lightning,
999 and the name derives from the Latin word "*fulgur*" (lightning). Usually they consist of
1000 irregularly shaped tubes ranging from approximately 1 cm in diameter to 1 mm, even if they
1001 may extend laterally or vertically for up to 10 m (Essene & Fisher 1986). Famous fulgurites
1002 specimens are those coming from the Saharan desert; however, fulgurites can occur on any soil,
1003 either formed naturally or triggered in proximity of high voltage power lines.

1004 The study of the mineralogy and petrology of these specimens, and of their mechanisms
1005 of formation has started to become more and more significant. Starting from the curiosity of
1006 understanding more in detail these fascinating objects, researcher from physics, atmospheric
1007 sciences, geochemistry, materials science, impact-related sciences have gathered and compared
1008 many information, and the results are well beyond the pure scientific curiosity, with key
1009 implications in biogeochemistry and formation of life. In this section we will try to introduce
1010 the lightning process, the fulgurite morphology and mineralogy, and we will try to arouse
1011 interest on the multidisciplinary aspects related to fulgurites.

1012

1013 Lightning is a very common phenomenon but is not uniformly distributed across the Earth
1014 (see image from Lightning Imaging Sensor (LIS) NASA… Ask for permission!) and equatorial
1015 conditions (warm, moisture!) greatly favor the occurrence of lightning. As a curiosity, the place
1016 on Earth with the highest lightning flashes for year is Lake Maracaibo (Venezuela) with an
1017 average of ~232 flashes (per km^2 per year).

1018
1019

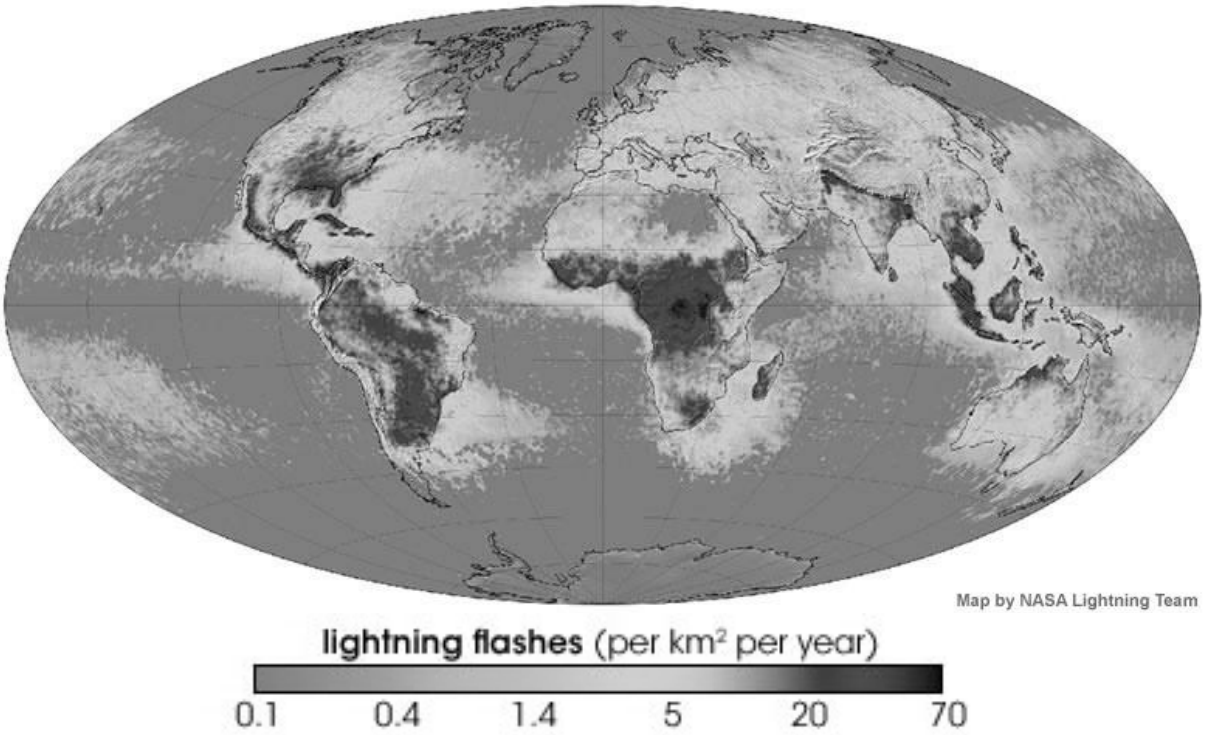

Figure 10: World Lightning Map shows the average yearly counts of lightning flashes per square kilometer based on data collected by NASA's LIS between 1995 and 2002. Localities with the largest number of lightning strikes are in the Equatorial area.

This common phenomenon is extremely energetic, and lightning may dissipate ~ 10^9 J (Borucki & Chameides 1984; Rakov & Uman 2003), raising, instantaneously (< milliseconds), the surrounding air temperatures in the range of 10^5 K (Uman 1964; Uman & Krider 1989). Thus, a really high amount of energy strikes the surface target material, providing a local temperature rise higher than 2000 K, and with even greater temperatures expected on the "current" path (Uman & Krider 1989). Such amount of energy is able to melt/vaporize the inorganic target materials, and incinerating the organic ones along the current path, inducing the formation of voids and vesicles from the release of the volatilized components. The heating rates have been constrained to be in the order of 10^3 K/s (Carter *et al.* 2010; Jones *et al.* 2005; Krider *et al.* 1968; Uman 1964), whereas the cooling rates are estimated in the order of 10^8 K/s (Rietmeijer *et al.* 1999; Switzer & Melson 1972) because of the formation of very homogeneous glass layers and the abundance occurrence of lechatelierite. The result of such fast event is a

cylinder (often presenting lateral branches) with an inner smooth glassy portion surrounded by an irregular outer surface that can be composed of melted, partially melted and unmelted minerals grains and rock fragments, and with many spherical and elongated vesicles occurring in all portions (**Figure 11**).

Figure 11 –Fulgurite specimens showing different morphologies. TO CHANGE?!?

Lightning strikes are, therefore, rapid high energetic phenomena able to induce strong physical and chemical modifications in the target materials, and the morphology of the fulgurite specimens formed will be strongly dependent on energy and timescale of the striking, on target composition and heterogeneity, and so on. The bulk composition of fulgurites is quite broad when considering the whole samples, as a reflection of the different target materials (**Figure 1**). However, the chemistry of the glassy part is much narrower and reveals a volatilization of most of the major elements, resulting in an amorphous phase enriched in silica, and depleted in alkalis. Most of the studies report the occurrence of glass heterogeneities, with lechatelierite glass (98-100 wt.% SiO_2) occurring in different percentages, and secondary glass phases having relatively lower amounts of SiO_2, and higher proportions of Al_2O_3 and FeO (Essene & Fisher

1986; Frenzel & Stahle 1984; Pasek *et al.* 2012). Pasek et al. (2012) established a classification for fulgurites based on morphology, mineralogy and petrology, providing five main types depending on the target rocks (sand, soil, rocks):

- Fulgurites formed in quartz sand are classified as type I, and usually present thin glassy walls; type I can contain one or two melts consisting prevalently of lechatelierite, and sometimes, also a SiO_2-rich melt with higher concentrations of Al and/or Fe. In the groundmass has been reported also enrichments in Zr oxide- and Fe–Ti oxide- rich glass.
- Fulgurites type II has a thicker glass portion compared to type I. The amorphous portion is more compositionally varied (< 50% lechatelierite), because formed in different environments than silica sand, such as unconsolidated soils containing clays minerals, small rocks, and so on.
- Type III consists of lechatelierite and feldspar glasses, and a calcite-rich matrix. Fulgurites type III are mostly found in calcite-rich soils and are the densest (average density[1] 2.1 ± 0.5 g/cm^3).
- Type IV fulgurites are heterogeneous melts, with the inner portion rarely consisting of lechatelierite, and the outer portion consisting of unmelted (or partially melted) rocks and mineral grains. These fulgurites form usually in bulk rocks and have densities similar to those of the target rocks.
- Type V are droplet fulgurites that have a homogeneous glass matrix. The two main oxides contained in type V droplets are enriched in SiO_2 and K_2O relative to the originating fulgurite, whereas other oxides are depleted.

An updated classification (Pasek & Pasek 2018) includes also specimens artificially formed, either from high voltage power lines, or triggered by high-voltage electrical arcing.

[1] The density value reported is related to the density of the material as approximated by a whole fulgurite cylinder Pasek *et al.* 2012..

Since fulgurites result from a quick high energetic event that produces also a shock wave, in many fulgurite specimens shock markers typical of impact glasses have been identified. For instance, shock lamellae in quartz, kink bands in plagioclase have been reported, with estimated shock pressures >10 GPa [Gieré *et al.* 2015]. Other studies (either experimental or based on modeling) reported even higher shock peak pressure, above 20 GPa [Carter *et al.* 2010; Ende *et al.* 2012). Artificial produced (triggered) fulgurites confirmed that temperature and pressure regimes needed to produce shocked materials can be achieved by lightning strikes (Chen *et al.* 2017). The occurrence of such shock features in fulgurites, until then considered diagnostic of impactites, raised questions about samples of uncertain origin, such as irregular glassy objects having shocked quartz grains, but unlikely related to any impact event (Melosh 2017).

Besides the occurrence of shock markers, in many fulgurites have been observed O-free phases and metals indicative of extremely reducing conditions, such as those typical of meteorite phases. These findings have extremely important implications, especially concerning the origin of life (see below). The occurrence of metallic phases have been reported since long (Anderson 1925; Essene & Fisher 1986; Wasserman & Melosh 2001), and Essene & Fisher 1986, explained the occurrence of metallic globules rich in silicon, spheroids of silicon-bearing metals (99.5 at.% of metallic silicon phase with minor amounts of titanium, iron, and phosphorus), and Fe-rich spherules, via thermodynamic calculations that indicate that extremely high temperatures (> 2000 K) and reducing conditions close to the SiO_2-Si buffer were needed. However, the authors could not decipher (and rule out) the role of other agents, such as the presence of carbonaceous materials, or the degassing of oxygen or the formation of nitrogen oxide gases.

Other metallic phases, such as Fe-Si-Al-Ti metallic droplets, or phosphide phases usually common in meteorites (*e.g.* Fe_2Si, Fe_3P) have been reported as well (Pasek *et al.* 2012 and

references therein]. Rowan & Ahrens 1994 report phases reduction in MORB glasses by shock experiments. Shock pressures between ~0.8 and ~6 GPa induced a change of the glass chemistry (enrichment in SiO_2) and the formation of Fe-, Si- and Mo-rich metallic microspheres embedded in the shocked glass. Based on the experimental conditions and the occurrence of iron silicide alloys, the authors estimated that an oxygen fugacity ~ 8 log units below the initial one was needed in order to form such metallic phases. Jones *et al.* (2005) artificially (triggered-lightning) produced specimens composed of 99.9% pure binary oxides of manganese and nickel in order to study the reduction mechanisms, and while they observed the formation of nickel oxide particles, the manganese oxide fulgurite showed no metallic phase formation. Thus, the thermodynamical stability of the oxides involved has a key role in the reduction mechanisms. Based on their experiments, Jones *et al.* (2005) suggest different possible mechanisms for the reduction associated to lightning, and they highlighted that the presence of carbon is not required for oxide reduction during fulgurite formation.

The presence of reduced phosphorous species in fulgurites is particularly important. A relative enrichment in phosphorous is not unusual in fulgurites (Martin Crespo *et al.* 2009; Pasek *et al.* 2012; Pasek & Block 2009), but the occurrence of phosphides has different implications. In iron meteorites, pallasites and enstatite chondrites, phosphorus is commonly occurring as phosphide (*e.g.* schreibersite $(Fe,Ni)_3P$), which slowly react with water to produce reduced forms (PO_3^{3-} phosphite). Contrarily, on Earth, phosphorus occurs in minerals with its stable form P^{5+} (PO_4^{3-} phosphate). Besides the mineral supergroup apatite (the primary source of P), this element is a common constituent of organic molecules (DNA, RNA, and so on…). On Earth surface, a possible mechanism for reduction of phosphate species may be lightning, as shown by simulated discharge experiments from Glindemann *et al.* 1999, and from the studies on many fulgurite specimens by Pasek and coauthors. For example, Pasek and Block

(2009) report that the reduction of PO_4^{3-} species to reduced forms occurs commonly in many target soils, and they provided two potential causes of P reduction during fulgurites formation:

1) the reduction of phosphate to phosphide, and a later reaction with water; this process is analogues of that of meteoritic schreibersite that react with water to produce reduced forms *e.g.* H-phosphonic acid H_3PO_3 (*e.g.* Bryant *et al.* 2009);

2) the direct reduction from PO_4^{3-} to PO_3^{3-} species; thermodynamical calculations indicate that phosphates ($CaHPO_4$) could be reduced to phosphite species ($CaHPO_3$) at temperatures ~2000 K, under oxygen fugacity conditions of ~ -5 (as $\log(fO_2)$) (Pasek & Block 2009).

The phosphides species occurring during meteoritic impacts, and especially during the Hadean-Archean heavy meteorite bombardment have been proposed as a way of altering global phosphorus biogeochemical cycle, and the source of reactive phosphorus required for the processes of prebiotic phosphorylation on the early Earth (Pasek 2008, 2017; Pasek & Block 2009).

Case study: fulgurite

A fulgurite with a dark thick glassy inner core has been used for a series of analysis. The specimen is highly vesiculated and the inner glass core has a variable thickness up to 1 mm. The outer portion presents unmelted white/grey grains of quartz, and probably salts species. The specimen has been sliced and the cross section polished (**Figure 12**). Optical microscope images, and Raman spectroscopy analysis have been coupled to SEM/EDS data in order to provide an overview of all the phases occurring in this fulgurite.

The polished slice has been observed with an optical microscope by reflected light, and SEM. The glass matrix of the inner part seems to be very homogeneous, with no relict mineral grains detectable, and a few bubbles if any. Moving from the inner portion toward the external wall (see **Figure 12**), vesicles, mostly elongated, are clearly increasing in amount, and the matrix become more heterogeneous. The fulgurite specimen has several outer branches, and many large voids.

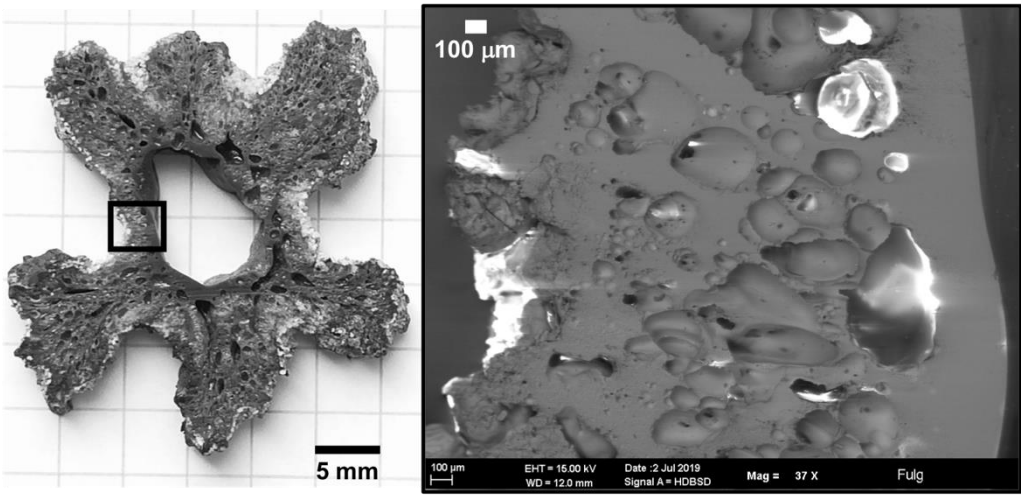

Figure 12: Photograph of the sliced fulgurite (left), and SEM image (right) of the thinner portion where both inner and outer walls can be observed. The inner wall has a smoother surface, in contrast with the rough outer part. Brighter areas in the left image are residual of carbon coating.

Backscattered electron images of the fulgurite (**Figure 13**) show the increasing number of elongated bubbles, which radially distribute in the branches. The matrix is predominantly amorphous and fairly homogeneous close to the inner wall, while all outer branches are more

heterogeneous, with completely foamed glass portions, unmelted quartz grains, regions with small zoned crystals, and tiny bright spots, too small to be characterized.

EDS analyses of the inner glass portion reveals the homogeneous presence of lechatelierite, with small amounts of Al_2O_3 ($SiO_2 \geq 99$ wt.%, $Al_2O_3 \leq 1$ wt.%). When moving from the smooth inner to the rough outer walls the chemical compositions marginally differ, but without a defined trend. The SiO_2 content ranges between 96.6 and 99.5 wt.% with some random points having higher Al_2O_3 amounts (~ 2.4 wt.%) and traces of FeO, MgO, CaO and K_2O (all < 0.4 wt.%).

The areas where the branches depart and all the branches themselves have areas (pockets) and veins-like features that especially surround bubbles (see arrows in **Figure 13**). These portions are highlighted in the BSE images by the different contrast (light grey) and the EDS analysis indicate lower Si contents (down to ~75 wt.%), and higher amounts of Al_2O_3 (up to ~ 14 wt.%), and the presence of many other elements, including FeO (3-6.5 wt.%), MgO (1-1.5 wt.%), K_2O (0.5-1 wt.%), CaO (~ 0.4 wt.%) and TiO_2 (~ 0.3 wt.%). The elemental mapping of one of the regions rich in pockets and veins is reported in **Figure 14.** The primary matrix is composed almost exclusively by SiO_2, and only a 0.5-1.5 wt.% of Al_2O_3. The bubbles are surrounded by large light grey pockets and veins that contain the secondary melt relatively depleted in silica, and enriched in Al, Fe, and alkali/alkali-earth elements. In a few light grey spots there are also traces of P_2O_5 and Na_2O (~ 0.3 wt.%).

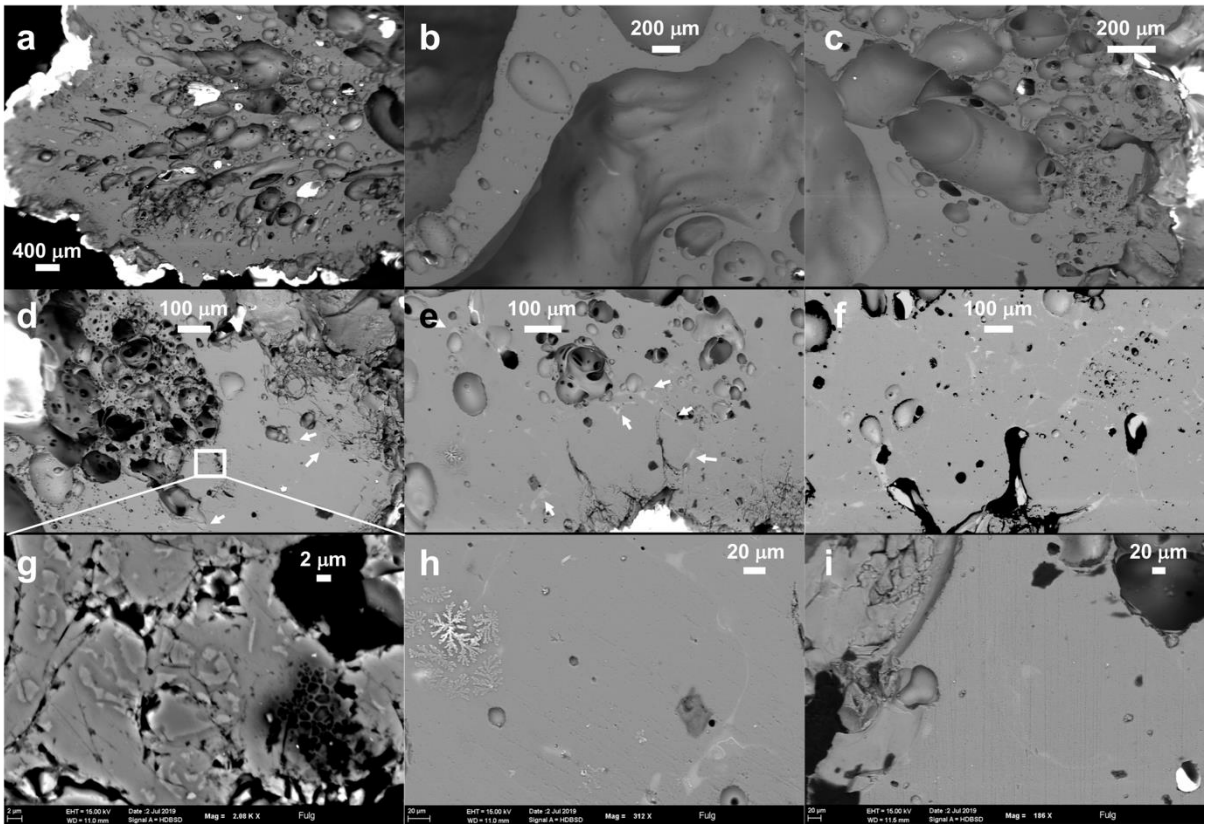

Figure 13: backscatter electron images of the fulgurite at different magnifications to emphasize the heterogeneity of the sample. Overview of the a) outer branch, b) inner glass wall, c) outer portion in the thinner area; d-e-f) outer portions with heterogeneous features, such as foamed area, aligned bubbles, relict quartz grains and pocket and veins of glass with different chemistry (light grey; arrows); g-h-i) higher magnifications.

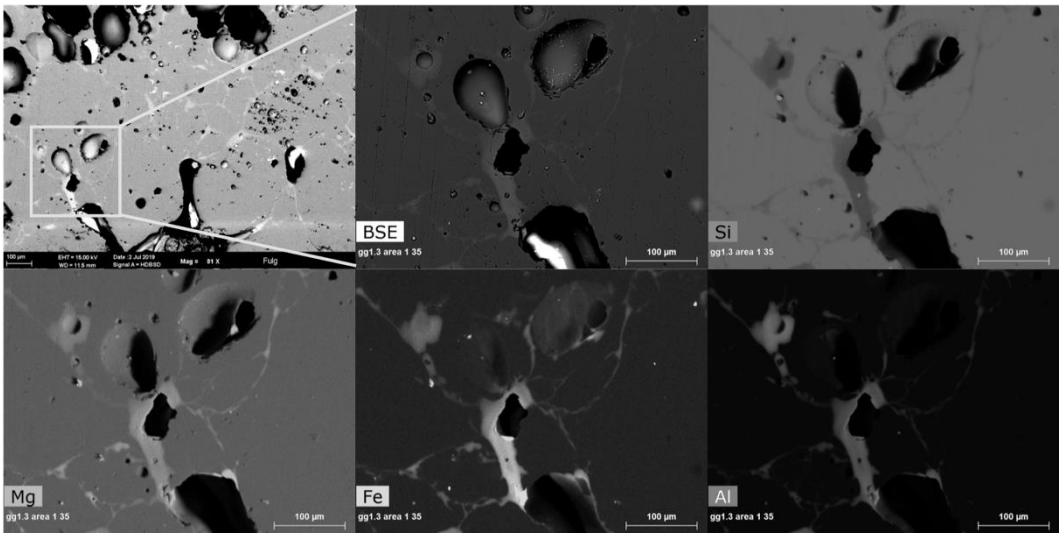

Figure 14: Elemental mapping of one of the regions rich in pockets and veins. The primary glass matrix is composed of ~99 wt.% SiO_2, and voids and bubbles are surrounded by a secondary melt, relatively depleted in Si, and enriched in Al, Mg and Fe. Scale bar in all images is 100 µm.

Raman spectra were collected in several portions of the sliced fulgurite, with a 488 nm excitation laser, in order to characterize the amorphous and the mineral phases. The outer whiter grains, supposedly residual of the target rocks, are mainly composed of quartz and some salts, such as NaCl (from EDS point analyses). The spectra of the outer grains perfectly match the spectra of α-quartz (see **Figure 15A**), with the presence of a sharp intense peak at ~464 cm^{-1}, and a broad band at ~205 cm^{-1} (A_1 modes), and also the *E* modes at ~127 cm^{-1} and 263 cm^{-1}. The differences in the relative intensity of the *E* modes between the reference quartz spectrum and the spectrum of the outer grains (point 1 in **Figure 15A**) is due to sample orientation. Similar spectra were obtained in some of the branches, although with some of the main peaks shifted (point 2 in **Figure 15A**). Indeed, all peaks match vibrations of alpha-quartz, but with shifts of the vibrational modes that indicate the occurrence of shock pressures (**Table 3**). For instance, while the main peak moves ~ 3.1 cm^{-1} toward lower frequencies, the broad peak at 205 cm^{-1} shifts more than 10 cm^{-1} downward, and the small peak at 354 cm^{-1} remains unchanged. These uneven shifts of the quartz peaks indicate the presence of shocked quartz, and based on the experimental work done by McMillan *et al.* (1992), the shifts observed provide a shock peak pressure between 25 and 28 GPa, similarly to what reported by Carter *et al.* (2010).

The Raman spectrum of the glass on the inner wall (point 3 in **Figure 15B**) has the clear broad features of amorphous silica and nearly perfectly match the spectrum of SiO_2 suprasil, used here as reference (SiO_2 in **Figure 15B**). These spectra agree with the SEM/EDS analysis and the occurrence of a homogeneous lechatelierite glass in the inner wall. When moving from the inner wall toward the outer one (points 4 to 7 in **Figure 15C**), the shape of the Raman spectra is very similar, and small variations can be attributed to the different concentration of Al_2O_3 in the amorphous matrix. Moreover, the two last spectra show the presence of small sharp peaks,

that indicate the occurrence of microcrystalline quartz. Based on the position of the main peaks here the shifts suggest higher shock pressure, of ~ 30-31 GPa (**Table 3**).

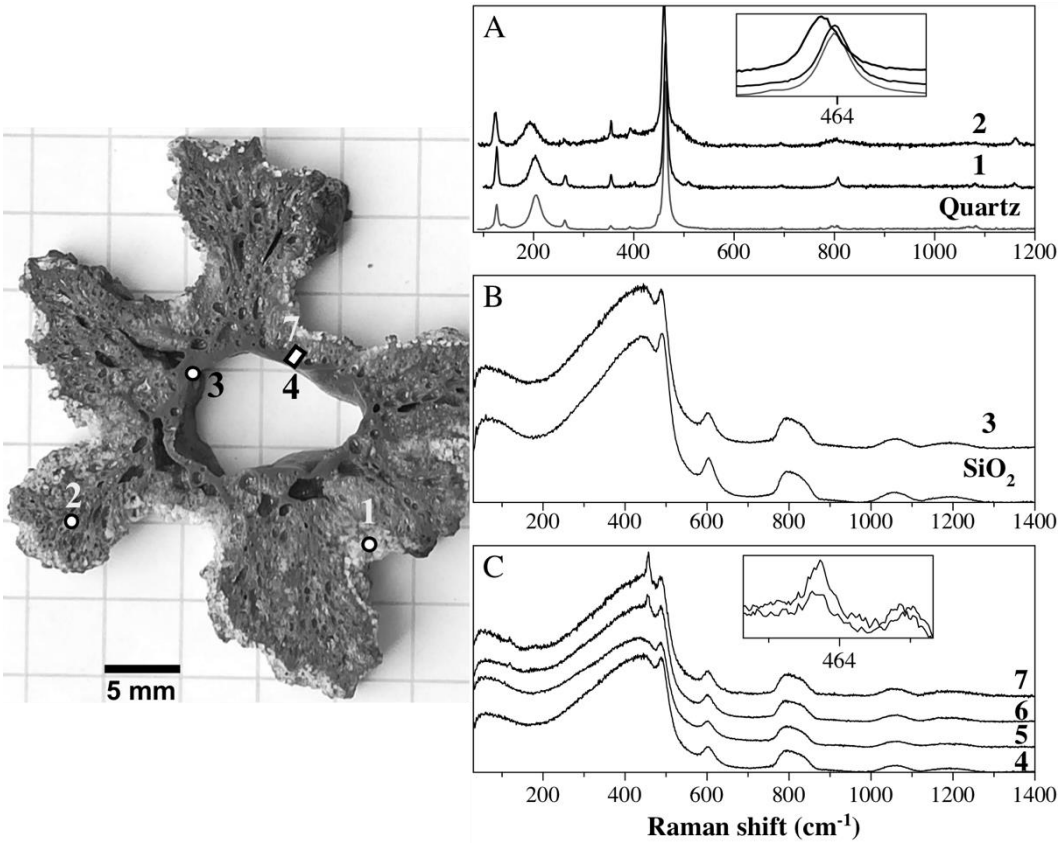

Figure 15: Raman spectra of different portions of the fulgurite (numbers from 1 to 7) and crystalline references. The outer unmelted grain and a small grain in the branch present vibrations associated to alpha-quartz (2). The glass on the inner wall (3) is very polymerized and the spectra is very similar to that of a pure SiO_2 glass. Moving from the inner wall toward the outer part (from 4 to 7) the homogeneous glass matrix start to be slightly more heterogeneous with the presence of a small amount of quartz (sharp peaks in 6 and 7 and inset).

Table 3: Frequencies of the main vibration modes of α-quartz (reference phase), and of the crystalline phases occurring in the fulgurite specimen. Numbers refer to the sampling spots reported in Figure 15.

Reference α-quartz	Spectrum 1	Spectrum 2	Spectrum 6	Spectrum 7
126.8	126.8 cm-1	124.1	120	120
205.1	204.5	194.1		
263.1	263.6	262.1		
354.2	354.2	354.2		
463.6	463.6	460.5	457.8	457.8

3.3 – Trinitite or nuclear glass

Within glasses formed by highly energetic events, there is a glass that is not natural, but neither man-made in the strict definitions. During the first atomic bomb test in Alamogordo (USA Trinity test, 1945), the detonation of the nuclear weapon on the desert sand has created a *"Lake of Jade […] a lake of glistening incrustation of blue-green glass 2400 feet in diameter"* as reported by Time Magazine (Science: Atomic footprint, 17 Sept 1945). The green amorphous material has been called trinitite, or nuclear glass. Another nuclear test that produced amorphous material is the first underground nuclear explosion, the so-called Rainier test (1957).

The study of these glasses has mainly focused on the radioactivity of the materials, and on the incorporation and distribution of radionuclides, although, more recently, more detailed chemical, mineralogical and geochemical investigations have been reported. Moreover, because of the mechanisms of formation, trinitite could be regarded as an analogous of impactites.

In the following, we are going to discuss about the event associated to the formation of trinitite, and we will provide information on the different geochemical aspects of this glass.

Figure 16. Photograph of a bottle green trinitite.

Trinitite glasses are a record of the first atomic bomb blast on July 16, 1945. The detonation of the 21 kilotons plutonium bomb and the resulting fireball melted/vaporized the arkose/arkosic sand desert and formed a large crater glazed with green fused silica sand. The explosion released an extreme high amount of energy, with an estimated yield of 9-18 kt, and average temperature of 8430 K (Hermes & Strickfaden 2005). The heating rate was extremely high with a very short duration of ~ 3 s and this explain the glass formation and why some minerals (zircon and quartz grains) were only partially melted (Hermes & Strickfaden 2005).

The green fused silica sand was first described by Ross (1948) that, based on the optical properties, reports the occurrence of two different melts. In general, he described trinitite as a highly vesiculated pale bottle green glass that present distinct flow lines. One of the glass phases has a refractive index (RI) between 1.51 and 1.54 and derives from feldspars, clay fraction and accessory minerals (calcite, hornblende, augite). The second amorphous phase has a lower index of refraction (close to 1.46), indicating that this material is nearly pure SiO_2 glass derived from the fusion of the quartz component of the arkosic sand. Ross (1948) observed also the occurrence of small glass areas with glasses red or grey in color, both containing copper, and suggested the it was a contamination from the explosion device.

Since the nuclear explosion, most of the studies have been done on the radioactive nuclides present in the materials (*e.g.* Atkatz & Bragg 1995; Eby *et al.* 2010; Parekh *et al.* 2006; Wallace *et al.* 2013). Indeed, the migration of actinides at historical test sites are considered very important, since it is closely related to the waste management and to the storage of high-level nuclear waste (Hu *et al.* 2008; Pacold *et al.* 2016; Tompson *et al.* 2002, 2006). However, for long time the study from Ross was the only mineralogical investigation available on trinitite (except a magnetic susceptibility study by Glass *et al.* 1987; see below). Only in the last decade the interest for these materials raised again, mainly because of the nuclear forensic applications,

and many studies on the mineralogy, petrology, geochemistry and on the average Fe or Ti redox state have been published. For example, Eby *et al.* (2010) report the occurrence of four different type of glass:

1) glassy and vesicular green top surface coated with sand grains (the top part of the trinitite layer) (**Figure 16**);

2) a Cu-rich glass (red trinitite) containing metallic chondrules;

3) green trinitite (scoriaceous fragments);

4) trinitite ejecta, which include aerodynamically shaped droplets, beads, and dumbbell glasses. The latters were discovered a few years after the detonation as mm-sized specimens. Supposedly, part of the molten material was transported by the hot gas cloud and spread over a wide area into beads and dumbbell shapes (Eby *et al.* 2010). The red trinitite contains several metallic chondrules having Cu, Fe and Pb deriving from the explosion (blast tower and trinity device), confirming the hypothesis of Ross (1948). The most common material is the green trinitite that consists of vesiculated and amorphous scoria-like fragments, and it is extremely heterogeneous. Light microscopy, SEM and BSE analysis show the presence of euhedral heated sand grains, large flow bands and strong chemical variability (Bellucci *et al.* 2014; Eby *et al.* 2010, 2015; Fahey *et al.* 2010) (see **Figure 17**). The more recent analysis confirmed the early observation done by Ross (1948) on the bulk chemistry. Trinitite glasses have two major glass compositions, one essentially consisting of lechatelierite, and a second one, depleted in silica, with a much higher variability (SiO_2 range = 55 - 80 wt.%). Moreover, Eby *et al.* (2015) reports the occurrence of planar deformation features in quartz grains, a typical evidence of shock metamorphism in impactites and fulgurites.

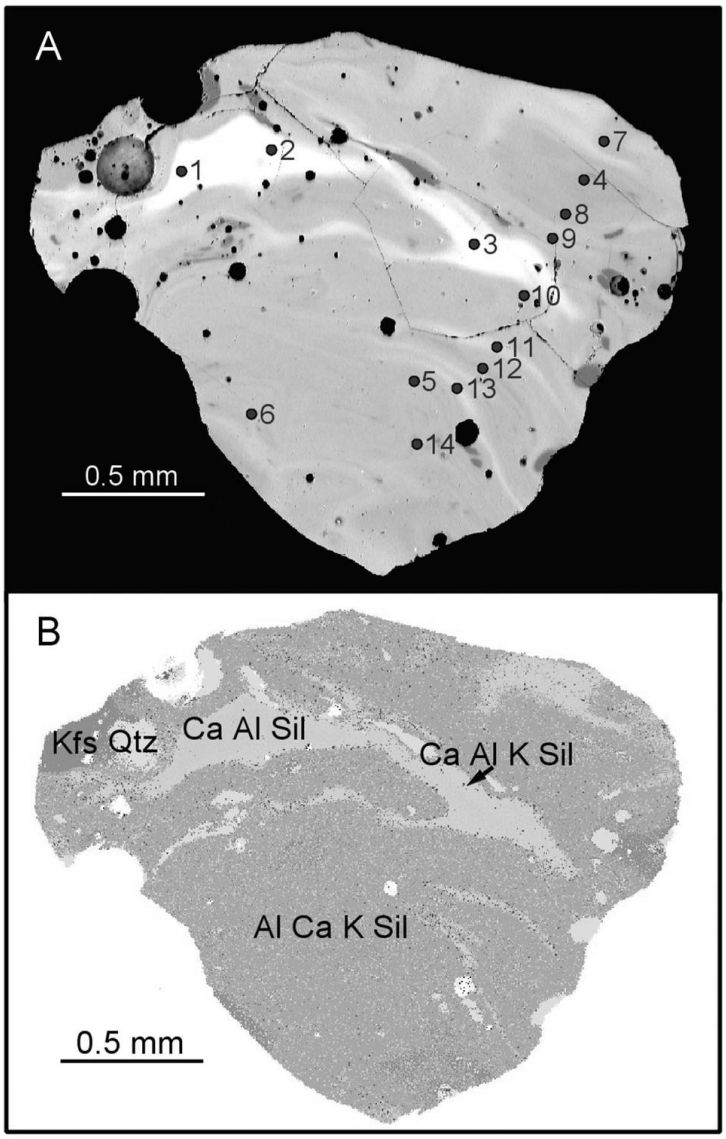

Figure 17 (a) Backscattered electrons (BSE) and (b) QEMSCAN (Quantitative Evaluation of Minerals by SCANning electron microscopy) images for a green trinitite fragment. Besides the partially melted K-feldspar (Kfs) and quartz grains (Qtz) there are evident flow structures, and the occurrence of different glass compositions. The brightest areas are enriched in calcium content. Numbers represents the point analysis. Figure from Eby et al. 2015 (American Mineralogist. 2015;100(2-3):427-441. doi:10.2138/am-2015-4921) MSA copyright.

Because of the resemblance between trinitite ejecta and distal impact ejecta, trinitite glasses have been compared to tektite and microtektites (Glass *et al.* 1987). The similarities between the two products were confirmed, especially regarding the water contents (between 0.01 and 0.05 wt.%) and the predominant reducing conditions ($Fe^{3+}/Fe_{tot} < 0.1 \pm 0.1$; Glass *et al.* 1987; Giuli *et al.* 2010b; Eby *et al.* 2015). The study of the mineralogy and chemical variability of the glass samples has constrained the conditions occurring during the atomic

detonation (Pressure-Temperature (P-T) regime), with temperatures on the order of ~ 1870 K and pressure ≥ 8 GPa (Eby *et al.* 2015). A recent study highlights also the occurrence of nano-structures in zircon grains, and in particular the presence of baddeleyite fibers surrounding the core of unaltered zircons (Lussier et al. 2017). These fibrous that seem to irradiate from the zircon grains, are not in physical contact with the core. Based on Raman, TEM and electron diffraction data, the P-T regime was constrained to T > 1770 K and P < 10 GPa (Lussier et al. 2017). Because of the disagreement between temperatures estimated by trinitite glasses and fireball (~ 1800 K *vs.* ~ 8000 K, respectively), it was suggested that the very short duration of the nuclear event has a major impact on the physical properties registered by glasses and minerals (Eby *et al.* 2015).

The study of the glasses formed during nuclear events provides information on the type of device that was detonated and its origin, thus it has nuclear forensic applications. Recently, Molgaard *et al.* 2015 produced synthetic nuclear glasses, comparable with trinitite glasses, as surrogates that could be used to simulate a variety of scenarios and could be used as a tool for developing and validating (nuclear) forensic analysis methods.

5. Glass properties

The study of the glasses described in the previous sections can provide important information of the formation mechanisms of these amorphous materials, and on the related events. In particular, the information provided by the study of shock metamorphism materials have implications well beyond earth sciences, since they involve also planetary science, biogeochemistry, and materials science.

By looking at different scales, it is possible to obtain information on the glass average redox conditions during fast cooling, on the short and medium range silicate network, on liquid immiscibility phenomena, and on the macroscopic properties (optical, physical, magnetic and so on…). All these data can be used to constrain the regimes of temperature and pressure during formations, evaporation and condensation stages, the timescale of the processes, and the thermal history of glasses. Altogether with the data from experimental studies (*e.g.* shock experiments) they are the base for simulations and numerical models of crater formation. In the following we report some of the characteristic of the amorphous materials and a compilation of Fe redox state and Raman spectroscopy data, collected on a variety of non-magmatic glasses.

Liquid immiscibility

A common feature of many natural glasses is the occurrence of two coexisting different melt phases, with features similar to liquid-liquid immiscibility. For example, in the previous sections, the presence of compositional heterogeneities on a variety of scales has been described for several impact related glasses (*e.g.* Libyan desert glass, Darwin glass), fulgurites and trinitite. Moreover, the occurrence of ferromagnesian droplets coalescing into a felsic amorphous matrix has been reported also for pyrometamorphic materials (*e.g.* Capitanio *et al.* 2004).

Multicomponent silicate systems are stable over wide ranges of P-T-X-fO_2 (pressure, temperature, bulk composition, oxygen fugacity), nevertheless, they might exhibit immiscibility at particular conditions (*e.g.* Hamann *et al.* 2018; Hudon & Baker 2002; Roedder 1992). Silicate-silicate liquid immiscibility is a common phenomenon observed in many natural igneous melts on Earth, and in lunar mare basalts (as a late-stage immiscibility), including meteorites (*e.g.* Hudon *et al.* 2004; Roedder 1978) and is a fundamental research field in glass and ceramic industry (phase separation; see Vogel 1994 for a review). The silicate-silicate (or carbonate) fluid immiscibility arises from differences in physical properties between two separate phases, and usually the immiscibility is characterized of coexisting felsic and mafic components; however, the chemical distribution is highly dependent on the duration of melting, the cooling rate and ambient atmosphere (reducing or oxidizing conditions). In highly energetic events, there are dynamic pressure and temperature conditions that allow the physical and chemical interaction (respectively, mingling and mixing) of very different target materials; however, because of the timescale of these processes, equilibrium conditions are hardly achieved, opposite to magmatic processes where a complete homogenization can be attained (for more information on Magma mixing see chapter **Morgavi, this volume**).

Liquid-liquid immiscibility arises from the different structural role of the cations in the glass. For instance, the main cation building the network in natural compositions is Si^{4+} (altogether with AlO_4 tetrahedra), which is bonded by four oxygen ions to form a tetrahedral coordination; each oxygen is shared by neighboring tetrahedra (bridging oxygens) to form a three-dimensional network held together by strong covalent bonds. The other cations present in a natural composition have different structural roles, and may either aid or disrupt the silicate network, thus they are called, respectively, network-formers or network modifiers (see **Chapter XX**, this volume). According to Veksler (2004) the cations that the most influence the liquid-liquid immiscibility fields are aluminum and alkali/alkali earths, and in turn, the peraluminous

or peralkaline nature of the melts, and cations that present high field strength tend to concentrate in the Si-poor phase.

Liquid immiscibility seems to be a very common feature of glasses deriving from highly energetic events, and recently, Hamann *et al.* (2018) discuss the importance of liquid immiscibility in impact processes, and the mechanisms that lead to the formation of melt heterogeneities and unmixing of silicate phases. In particular, besides the classical liquid-liquid immiscibility (rising from phase separation of a melt), the authors define other two main mechanisms that could produce the heterogeneities observed in silica impact glasses: i) mingling or incomplete mixing due to the short time-scale associated with highly energetic events; ii) emulsification of incompatible melts (deriving from the target rocks and impactor), without mixing. Moreover, Hamann *et al.* (2018) report that, despite the huge differences from phase separated volcanic rocks (both in terms of composition and T-P-time conditions), impact glasses show a very similar major element partition between phases.

Heterogeneity in glasses from high energetic events have been described in detail for Libyan Desert glass, blue zhamanshinites, and also trinitite and fulgurite glasses. In all specimens the occurrence of amorphous nanospherules, as a result of silicate–silicate liquid immiscibility, have been observed (Feng *et al.* 2019; Pratesi *et al.* 2002; Zolensky & Koeberl 1991). Other immiscibility like features can be found also in suevite glasses from Ries crater where mixture of carbonate impact melt and silicate melt have been reported (Graup 1999).

Reduced iron species

As discussed in the previous sections, the highly reducing conditions of glasses/rocks formed from highly energetic events have many repercussions, not only on the formation mechanisms of the samples themselves, but also on the understanding of the processes that occurred during the heavy meteorite bombardment, and on the evolution of the early Earth or to understand planetary impact cratering processes and differentiation. Among the characteristics common to all distal ejecta there is the occurrence of very high amount of reduced iron species Fe^{2+} in the melts, and several mechanisms have been proposed to explain the presence of reduced species, and its preservation during the "travel", and the quench (*e.g.* see Engelhardt *et al.* 1987; Ganino *et al.* 2018; Lukanin & Kadik 2007).

Iron is by far the most common multivalent element in all natural amorphous materials, with two valence states (Fe^{3+}, Fe^{2+}) that are stable over a large range of P-T conditions. In the study of glasses derived by impact or other highly energetic events, the occurrence of reduced iron has become one of the common markers to differentiate those samples from volcanic rocks. Moreover, in order to constrain some of the condition of formation of natural glasses, the study of iron valence has been one of the most common tools. An overview of the average Fe valence in these samples is provided in **Figure 18**, where $Fe^{3+}/(Fe^{2+} + Fe^{3+})$ (hereafter, Fe^{3+}/Fe_{tot}) ratios, are reported for many natural glasses. The data for tektite and microtektites where obtained by several techniques (wet chemistry, Mossbauer, XAS; see below for details). Tektites, from the different strewn-fields, aside some extreme values reported in the literature, all show an average Fe redox ratio $Fe^{3+}/Fe_{tot} \sim 0.09$ (±0.10; vertical grey line), thus indicating a similar thermal history and similar P-T-fO_2 conditions, despite their different geographical distribution. In Muong-Nong-type tektites (MN) and North American microtektites (NA mT), the large range of Fe^{3+}/Fe_{tot} ratios is, in the first case, typical of the layered tektites, and in the second one, an unique case among microtektites (see section 3.1). Distal ejecta have considerably lower

1429 Fe^{3+}/Fe_{tot} ratios than impact glasses, or Fe valences associated to average crustal target rocks
1430 (the possible precursor material).
1431

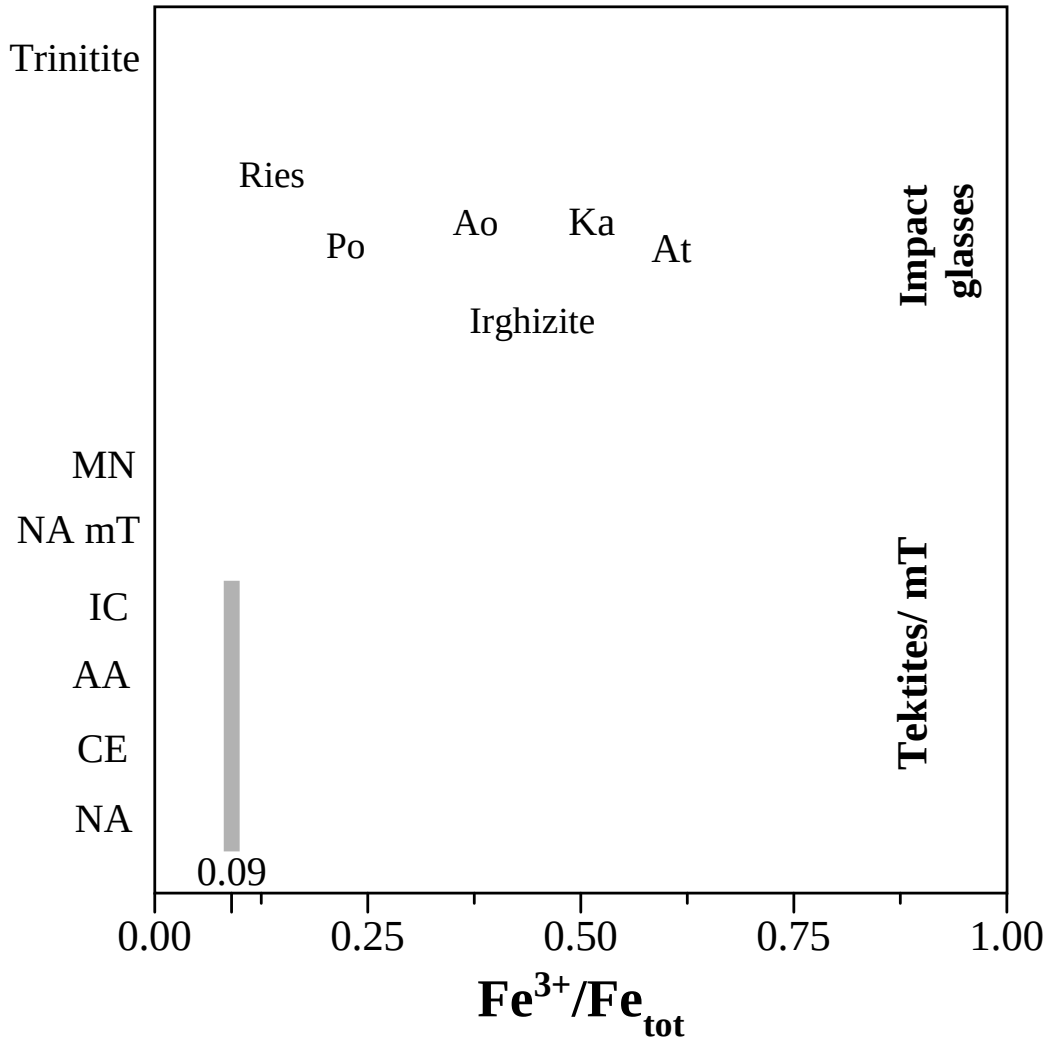

1432

1433 **Figure 18: Ranges of Fe redox state (as Fe^{3+}/Fe_{tot}) of tektites and microtektites from the different strewn**
1434 **fields are compared to the Fe^{3+}/Fe_{tot} of impact glasses (proximal from Zhamanshin, Popigai. Kara,**
1435 **Aouelloul, Atacama and Ries craters) and trinitite glasses. For tektites, both the extreme values and the**
1436 **average one (~0.09) are reported. North American microtektites and Muong-Nong tektites are the only**
1437 **distal ejecta specimens that show a broader range of Fe redox states (see section 4), with values that overlap**
1438 **the proximal impact glasses.**
1439

1440 Several techniques have been used to infer the Fe oxidation state. The earlier works
1441 reported quite broad ranges regarding the Fe^{3+}/Fe_{tot} with values between 0 and ~ 0.5. The
1442 analyses were based or on magnetic susceptibility or, more commonly, on wet-chemistry
1443 methods (*e.g.* Bouška 1994; Bouška & Povondra 1964; Cuttitta *et al.* 1972; Schnetzler & Pinson

1964; Schreiber *et al.* 1984; Thorpe *et al.* 1963). Early spectroscopic data (Mössbauer) were obtained for a large dataset (tektites from various locations by Evans & Leung 1979; Fudali *et al.* 1987) finding no detectable ferric iron in one case, and up to 0.12% in the second case. Lately, very similar results on the average Fe redox state were obtained (*e.g.* Dunlap 1997; Rossano *et al.* 1999). Mössbauer spectroscopy, respect wet chemistry, provided additional information on the Fe local environment. The early studies reported a coordination environment for ferrous iron around 6, with a minor presence of 4-fold coordinated species, but more recently it was reported the main presence of ferrous sites with coordination between 4 and 5 (trigonal bipyramids) (*e.g.* Dunlap *et al.* 1998; Dunlap & Sibley 2004; Rossano *et al.* 1999; Volovetsky *et al.* 2008).

Another spectroscopy technique that is element selective is X-Ray Absorption Spectroscopy (XAS). The study of the absorption edge region (XANES), including the small feature before the whiteline called pre-edge peak, and the extended energy region (EXAFS) provide information on an element average valence state and coordination number. This technique has been used to study Fe, Al, Ti structural environment in many natural amorphous materials, to provide insights on pressure and oxygen fugacity conditions during cooling. Because iron is the most common multivalent transition elements in natural melts, it has been extensively studied both in natural and synthetic systems, thus, accurate information can be derived by the study of the Fe K-edge XAS spectra of tektites, impact glasses and so on. XAS spectra related to reduced Fe^{2+} and oxidized Fe^{3+} glasses show differences in their energy position, as well as in their shape, with the spectrum related to oxidized species shifted toward higher energies (**Figure 19A**). The small feature before the absorption edge (inset in **Figure 19A**) is the pre-edge peak that presents different energy positions and intensities depending, respectively, on Fe oxidation state and average coordination number (local symmetry), and the deconvolution of this small feature for many crystalline compounds allowed to create the

variogram reported in **Figure 19B** and to derive quantitative information on the Fe structural role; indeed, the intensity of the pre-edge is related to the number of first neighbors and site geometry, whereas the centroid position is related to the average valence. For a review on the technique and on studies related to iron in silicate glasses, melts and minerals, the readers are referred to Calas & Petiau 1983; Giuli *et al.* 2002, 2012; Henderson *et al.* 2014; Mottana 2004; Wilke *et al.* 2001, 2004, 2007.

The results obtained from the study of the Fe K-edge pre-edge peak for an extensive dataset of tektites and microtektites provide very consistent results, with all distal ejecta having similar values both as average oxidation state and coordination environment. The pre-edge peak variogram in **Figure 19B** shows that tektite and microtektites cluster in a position that is compatible with the presence of highly amount of reduced species ($\geq$ 90% Fe^{2+}), and an average coordination between 4 and 5. Trinitite glass as well has a similar behavior and the iron structural environment resemble that of distal ejecta. Impact glasses from different localities have much higher centroid energy values, corresponding to higher amount of trivalent iron (data in **Figure 19B** from Giuli *et al.* 2002, 2010a, 2010b, 2013b, 2014a, 2014b). Beside the analysis of the Fe pre-edge peak, the analysis of the extended region of the Fe K-edge XAS spectra allowed to derive average <Fe-O> distances of 2.00 ± 0.02 Å, values compatible with the presence of ferrous species with coordination between 4 and 5 (Giuli et al. 2002).

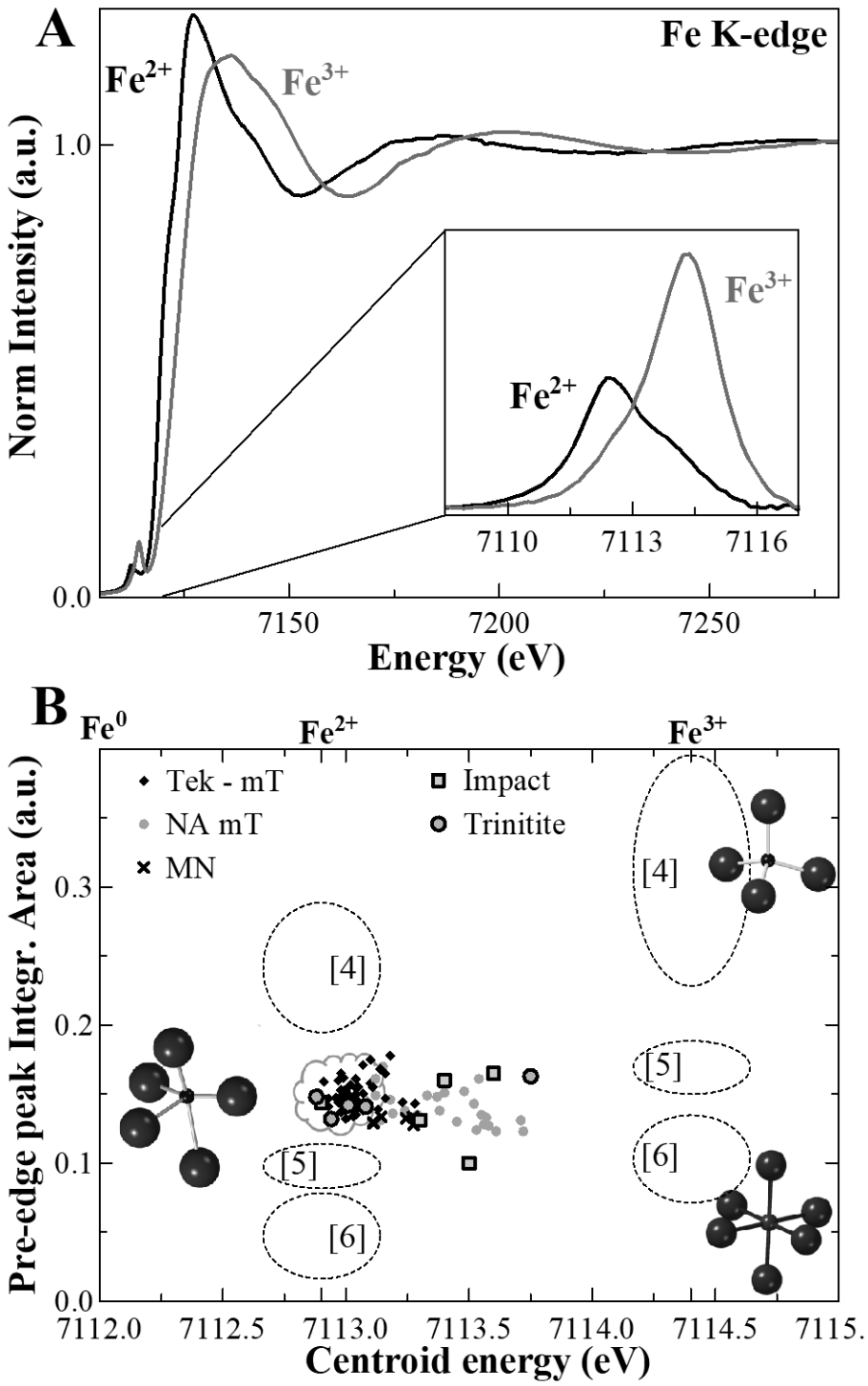

Figure 19: A) XAS at the Fe K-edge for two glasses having reduced and oxidized iron species. The inset shows in detail the background subtracted pre-edge peaks (data from Cicconi *et al.* 2015). B) Centroid energy position against the Fe pre-edge peak integrated intensity. The dashed ovals represent different coordination environments of the iron species in minerals. This variogram is obtained from the study of the Fe K-edge pre-edge peak of several tektite, microtektites from the different strewn-fields, impact glasses and trinitite glasses. Nearly all the distal ejecta cluster in a small area, here highlighted by the cloud shape. Data from Giuli *et al.* 2002, 2010a, 2010b, 2013b, 2014a, 2014b**. Figure modified after** Cicconi *et al.* 2020

Glass structure

Most of the natural materials discussed in this chapter are SiO_2-rich aluminosilicate glasses. The study of the silicate network arrangement can provide information on glass polymerization, temperature and pressure regimes, as observed in **Figure 3**. One of the most studied phases is SiO_2, either the amorphous phase or the crystalline polymorphs, and for sake of clarity, we compare the properties of amorphous SiO_2 with those of the other crystalline phases in **Table 4**. There are 11 known SiO_2 polymorphs formed depending on the different pressure and temperature systems, and here we report the most common ones in natural glasses. Quartz, tridymite and cristobalite are low pressure polymorphs, whereas coesite and stishovite are the high pressure ones (see **Figure 3**). The arrangement of the silica is always the same in all polymorphs, namely having a silicon surrounded by four oxygens arranged in a tetrahedra (4-fold coordinated), except stishovite where silicon is surrounded by six oxygens.

Table 4: Some properties of lechatelierite glass and crystalline SiO_2 polymorphs.

name	Density (g/cm^3)	Refractive Index	<Si-O> (Å)
Lechatelierite	2.20	1.458	1.62
α-quartz	2.65	1.549	1.61
β-quartz	2.53	1.537	1.59
α-tridymite	2.25	1.471	1.59
α-cristobalite	2.32	1.484	1.60
Coesite	2.92	1.596	1.61
Stishovite*	4.29	1.81	1.78

* silicon coordination is 6.

Raman spectroscopy is a very powerful technique that allow to derive information on the silicate melt short- and medium-range orders, thermal history, pressure regimes, and to provide an overview of sample heterogeneity. Moreover, Raman has been widely used on obsidian specimens in order to get information of the provenience (determination of the

geographic origin) of archeological obsidians (*e.g.* Bellot-Gurlet *et al.* 2004). Besides magmatic glasses, some of the first studies that exploit Raman technique to understand the origin of other natural glasses were done as early as in the 80s, and by using polarized Raman spectra the authors tried to derive information on the thermal history of Libyan Desert Glasses (Galeener *et al.* 1984), or proximal and distal ejecta (Jakes *et al.* 1992). Despite these early investigations, it is surprising that in the last decades, not so many studies have used this technique to understand possible modifications in the glass connectivity, but rather to determine the crystalline phases present, and the peak shock pressure (for instance, see case study in section 3.2).

In the following, we will report a series of Raman spectra collected for several glasses described within this chapter. A short description of the main vibration modes of silicate glasses is reported for sake of clarity; however, for a comprehensive description of Raman spectroscopy and on the silicate network short- and medium-range order, the readers should refer to dedicated text (Neuville *et al.* 2014; **Henderson_Stebbins this volume**). Raman spectra for other natural glasses, including magmatic ones, are reported in Cicconi & Neuville (2019).

Raman spectra of silicate glasses have the main vibration modes in the 10-1300 cm^{-1} frequency range, which can be divided in different major regions: a very low wavenumber region (< 250 cm^{-1}), which provides information on tetrahedral arrangement (see Neuville *et al.* 2014 for more details). The frequency range between ~400 and ~650 cm^{-1} can be related to vibrations of the tetrahedra-rings (**Figure 20**), with the main asymmetric band (R) usually assigned to symmetric vibrations of T-O-T in ≥ 5-membered rings (*e.g.* T is the Si^{4+} - or Al^{3+} - centered tetrahedron). Depending on glass polymerization, two additional sharper bands can be observed (**Figure 20**), the so -called defect bands, D_1 (~490 cm^{-1}) and D_2 (~600 cm^{-1}), assigned to breading modes of 4- and 3-membered rings, respectively. The frequency position and the

shape of the R band strongly depend on the silica network, and for instance, it shifts toward higher frequencies by densification of SiO_2 glasses (Deschamps *et al.* 2013), or by changing glass connectivity (*e.g.* by adding network modifier cations) (Neuville *et al.* 2014), thus by varying T-O-T inter-tetrahedral angles, and T-O average distances. The high wavenumber region, extending from ~ 900 to 1300 cm^{-1}, contains T-O asymmetric stretching vibrations; usually these stretching modes are labelled according to T polymerization: $Q^{0–4}$, where *Q* represents the Si(Al) centered tetrahedron, and *0–4* represents the number of bridging oxygens (BO). This region is also called *Q*-range or *Q*-envelope (**Figure 20**). By decreasing glass polymerization (*e.g.* by adding network modifier cations), the *Q*-range strongly increases in intensity and shift toward lower frequencies because other bands, related to different *Q* species (Q^3, Q^2) appear in the 900-1200 cm^{-1} region (*e.g.* Neuville *et al.* 2014).

There are several studies dedicated to the modification occurring to the structure of pure silica glass upon compression by hydrostatic pressure (*i.e.*, DAC – diamond anvil cell) or shock experiments. These investigations report that there is a permanent increase in silica glass density (densification), and for example, the density of a SiO_2 glass increases steadily up to values 20-21% higher, approaching the density of crystalline SiO_2 (Bridgman & Šimon 1953; Cohen & Roy 1961, 1965; Susman *et al.* 1991), and for applied pressure below 28 GPa, this densification is not due to changes of silicon coordination, but rather to structural changes, mainly related to variations in intertetrahedral angles distribution and the ring statistic, without variations in Si-O coordination (Deschamps *et al.* 2013; Sugiura *et al.* 1997). Okuno *et al.* (1999) carried out shock wave experiments on a SiO_2 glass by impacting glass with a steel flyer (speed up to ~2 km/s) for pressures in the range of 17.8 GPa to 43.4 GPa, and they observed the maximum density increment (maximum changes in silica network) at 26.3 GPa, The study of the Raman signals of compressed or shocked glasses has allowed to get many information

on the variations that may occur in the silicate network after high grade shock metamorphisms, and to identify the peak pressure values.

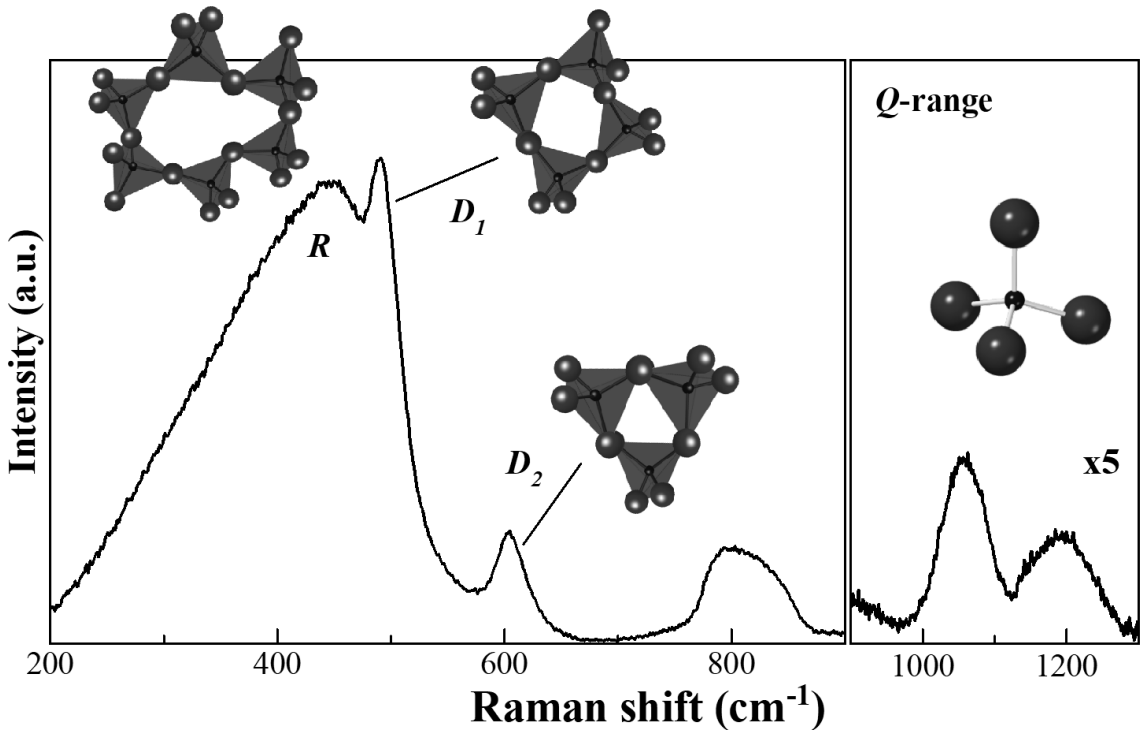

Figure 20: Background subtracted Raman spectrum of a commercial pure SiO_2 glass. The different bands can be attributed to specific Si-O-Si and Si-O vibration modes See text for details on band labels.

A common feature of many natural glasses is the occurrence of lechatelierite, that is amorphous SiO_2, or glass phases enriched in silica content. For example, different Libyan Desert Glass (LDG) clear fragments have been analyzed by using a 488 nm laser excitation, and all Raman signals present vibrations with frequency positions and intensities very similar to that of a lechatelierite glass, including the two sharp peaks related to the breading modes of 4- and 3-membered rings (defect lines). Some authors used the relative intensity of the defect bands in the Raman spectra to get information on the thermal history of natural glasses (Champagnon *et al.* 1997; Galeener *et al.* 1984), and for example Galeener *et al.* reported a fictive temperature (Tf) of 1000 ± 50 ºC for LDG, and suggested that the molten material cooled down to temperature below Tf in a period ranging between a few minutes and days.

The whole region in the frequency range 700 – 1300 cm^{-1} of the LDG Raman spectrum has a higher background, and all fragments analyzed present a contribution around 940 cm^{-1} that is not present neither in the commercial SiO_2 glass, or in the lechatelierite spectrum (**Figure 21**). Because this band is not related to luminescence (electronic transitions), it must be related to other cations present in the Libyan Desert Glasses. Stretching modes related to 4-fold coordinated Al^{3+} will mainly influence the relative intensity and frequency position of the band at ~1200 cm^{-1}, and the intensity of the defect lines because of the changes in the ring statistic; hence, the higher background and the band at ~ 940 cm^{-1} might be related to other (relatively) abundant cations, such as Ti^{4+} and Fe^{3+} species (~ 0.1 wt.%).

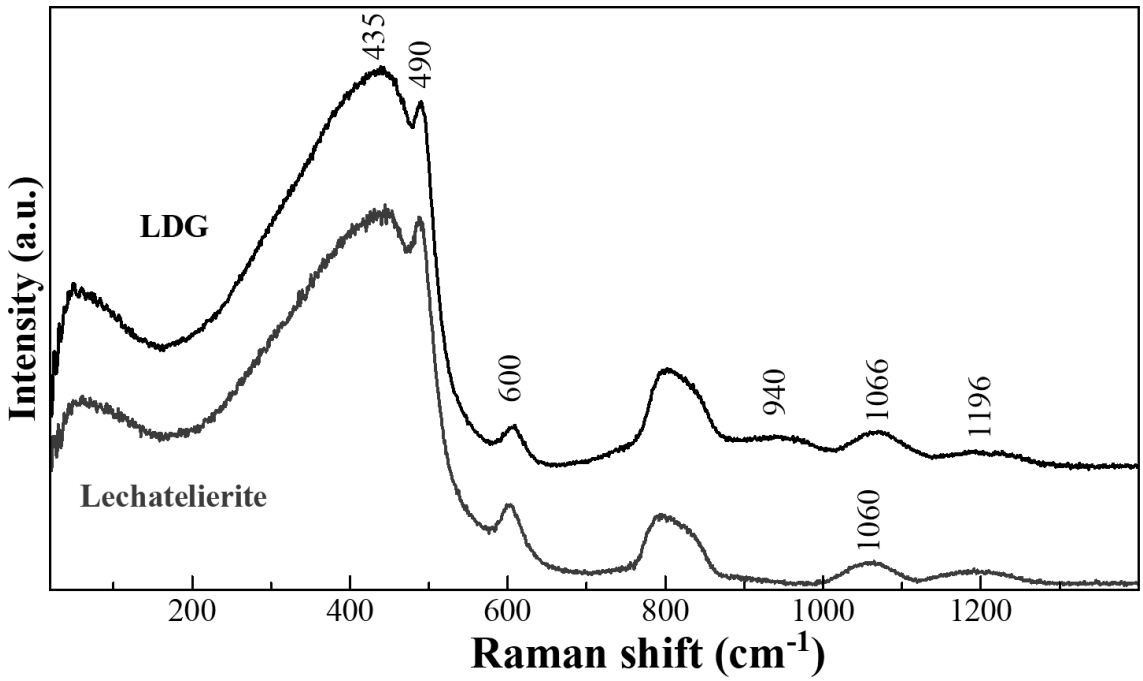

Figure 21: Raman spectra in the frequency range 20-1400 cm^{-1} of lechatelierite and Libyan Desert Glass (LDG). The frequency position of the main vibrations is reported.

Darwin glasses are chemically varied, and the Raman signals reflect the heterogeneity of these samples. Indeed, depending on the portion analyzed it is possible to get vibrations almost completely related to amorphous SiO_2 (*i.e.*, lechatelierite) or vibration modes that indicate a more depolymerized silicate network (**Figure 22**). For instance, the layered structure

of the Darwin glass shown in **Figures 7 and 8** have vibrations related to a highly polymerized glass in the light layering, whereas the darker layers have lower intensities of the defect lines D_1 and D_2, and stronger bands in the high frequency region, most probably related to higher amounts of non-bridging oxygens (NBO). The frequency region between 860 and 1400 cm^{-1} in the dark portion has an integrated area almost three times higher than in the light layers, and these modifications can be attributed to change in the bulk chemistry (see **Table 2**). In the dark glass portion there is also the appearance of an additional contribution around 940 cm^{-1}.

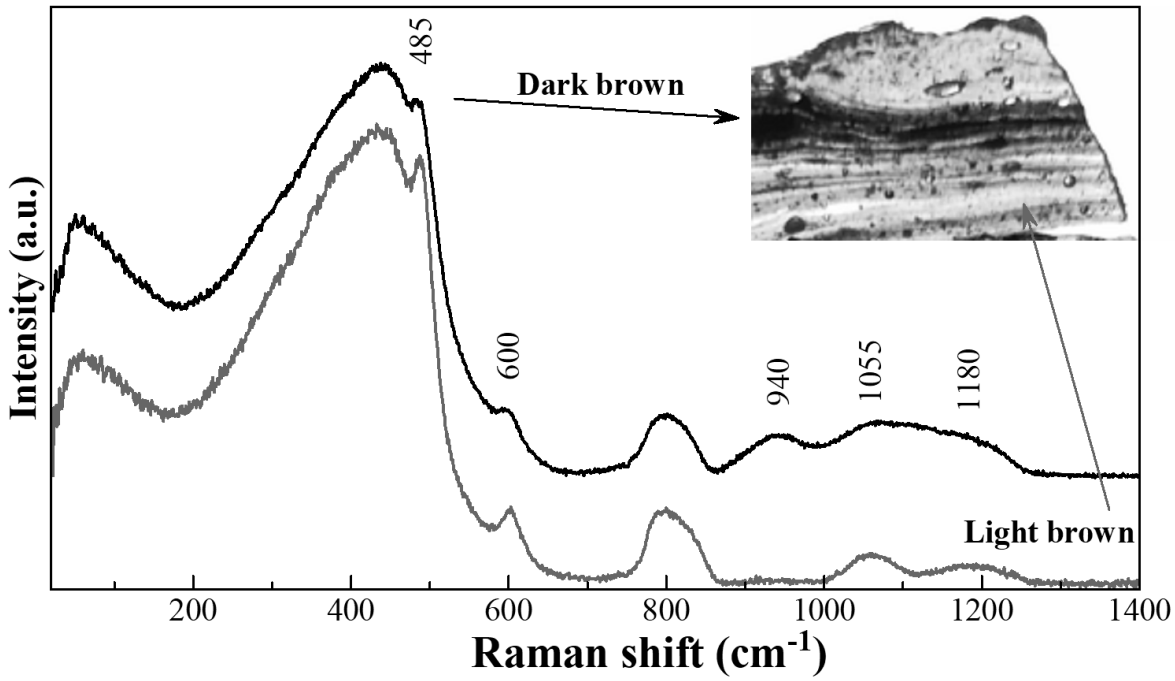

Figure 22: Raman spectra in the frequency range 20-1400 cm^{-1} of the light and of the dark brown layers in a Darwin glass specimen. The frequency position of the main vibrations is reported.

Distal ejecta and impact glasses have high SiO_2 contents (typically > 65 wt.%; see **Tables 1 and 2**), thus the typical vibrations of silica rich glasses are clearly observed, even if, sometimes, the defect lines are barely visible (**Figure 23**). Again, the high frequency regions show further contributions, and are very different from the lechatelierite glass, or more in general from the SiO_2-richer LDG samples. Atacamaite sample is the most different one, with strong variations in the frequency position of the vibrational bands, and an intense *Q*-envelope.

These modifications on the Raman spectrum of atacamaite glass reflect the average bulk chemistry of the glass, and especially the relatively low SiO_2 content, and the high Al_2O_3, FeO and CaO contents.

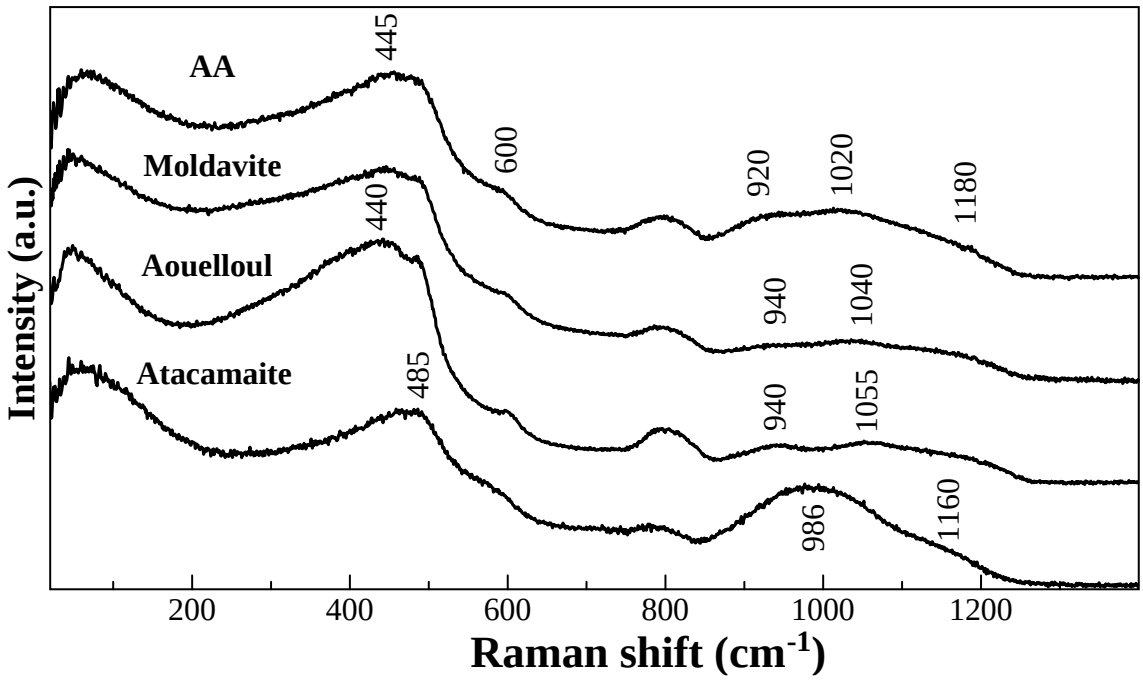

Figure 23: Raman spectra in the frequency range 20-1400 cm^{-1} of several impact related glasses: two tektites, respectively from the Australasian (AA) and Central European (moldavite) strewn fields, and two proximal impact glasses (Atacamaite and Aouelloul). The frequency position of the main vibrations is reported.

Figure 24 report the Raman spectrum of a bottle green trinitite specimen, and only the most homogeneous inner glass portion was considered. At the microscale, trinitite specimens are chemically highly heterogeneous (see section 3.3) with SiO_2 contents that range between ~ 90 and 60 wt.% (Eby et al. 2010). In the specimen available the Raman spectra collected do not show Si-rich portions, and the majority of the data collected points to an aluminosilicate glass composition with SiO_2 contents << 75 wt.%. The high frequency range has very intense and broad bands, with the highest contribution peaking at ~1030 cm^{-1}. Depending on the glass portion considered the intensity of the shoulder at ~940 slightly varies, and the R band decreases

its intensity. These small variations can be related to the different proportions of network modifier cations, and in turn, to the SiO_2 content variability.

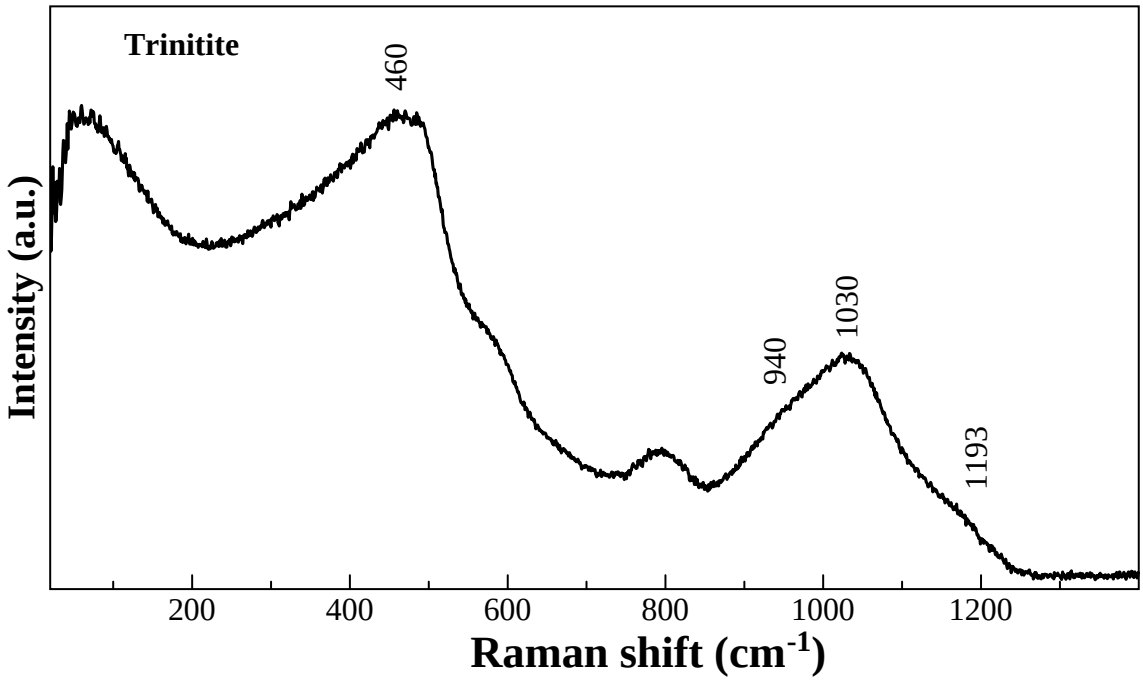

Figure 24: Raman spectra in the frequency range 20-1400 cm^{-1} of a trinitite sample. The frequency position of the main vibrations is reported.

The Raman spectra shown here are just an overview of the variability of the glass structures, and demonstrate the potentiality of using Raman spectroscopy, especially for investigations at the microscales. Despite the chemical complexity of a multicomponent natural glass, the vibrational bands can be interpreted based on the study of simplified synthetic compositions, and it is possible to correlate the degree of polymerization to the Raman features. All changes occurring in the low frequency region can be mainly associated to the changes in the bulk composition, and more in detail, on the Si content that drives the glass network polymerization. For an almost constant bulk composition, it would be possible to use the glass-memory effect and study the variations of the intensity of the defect lines, and the variations in the position of the main R band, in order to relate them to the pressure or the thermal history of

the glasses. The high frequency region contains the T-O stretching modes related to Si^{4+}, but also of other network former cations, such as Al^{3+}. The variations observed in all glasses, compared to the bands of lechatelierite, could be related to the different proportions of network modifiers that creates higher amounts of NBO, and charge compensator cations, that will influence the covalency character of the bonds. Moreover, other cations, such as the 4-fold coordinated Fe^{3+}, can also provide stretching vibrations in the high frequency region. For instance, in aluminosilicate and silicate glasses, both natural and synthetic, it has been reported that the bands between 800 and 1200 cm^{-1} are very sensitive to the average iron valence state (e.g. Di Muro et al. 2009; Di Genova et al. 2016; Le Losq et al. 2019). Thus, in the case of Darwin brown glass, and atacamaite, the contribution observed could be related to the presence of higher amounts of 4-fold coordinated Fe^{3+}.

We have described several natural glasses not deriving from volcanic processes, and we observed that glasses formed as a consequence of highly energetic event share many characteristics, such as:

- Compositional similarities (*e.g.* the presence of lechatelierite)
- Liquid-liquid immiscibility
- Highly reduced species
- Shocked minerals

The study of fulgurites and trinitite glasses may serve as a proxy for impact-induced mineralogic and petrologic changes, and to better understand the formation of glasses from highly disequilibrium conditions.

NOT INCLUDED – no time for mapping.

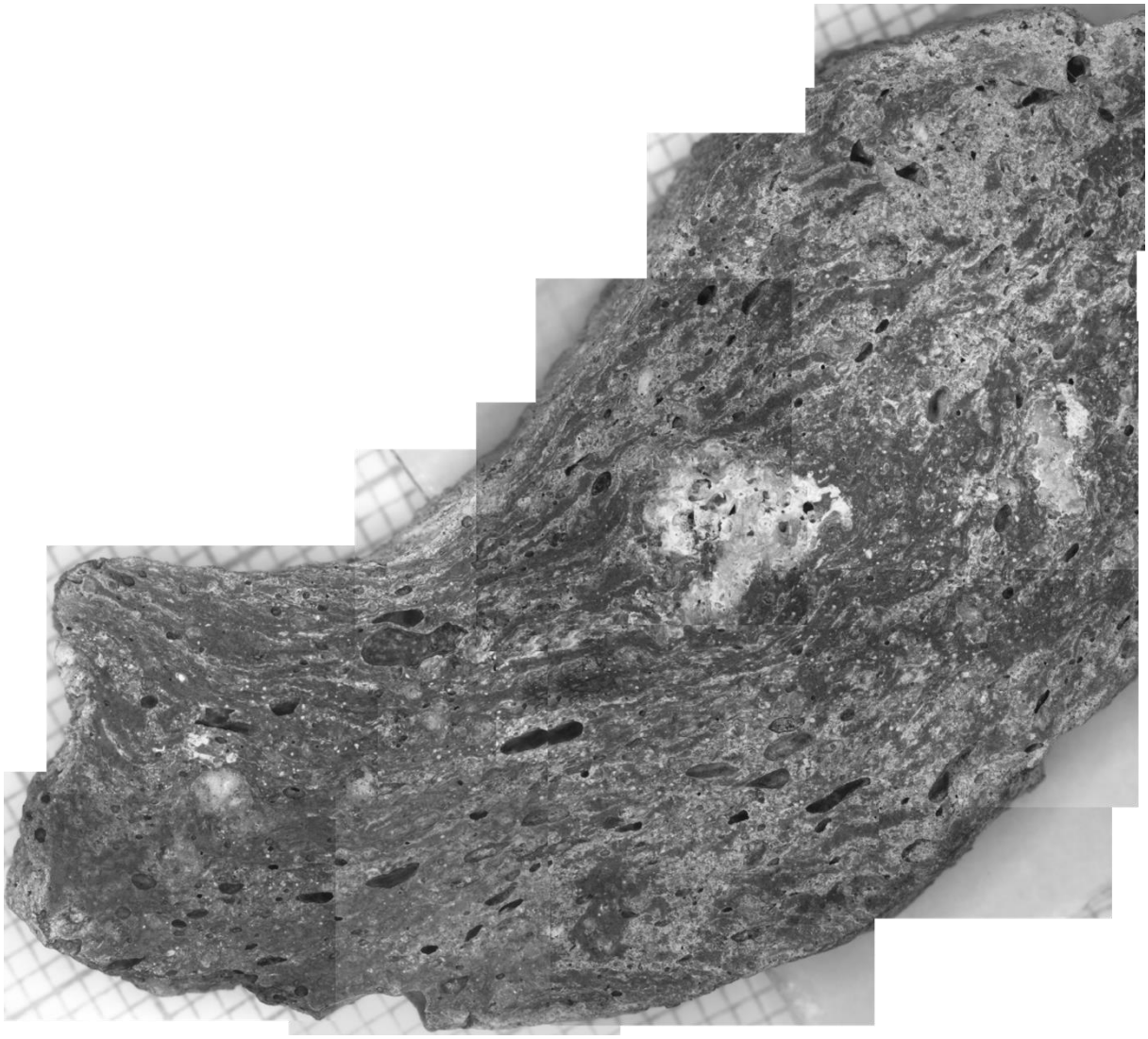

A polished slice of suevite (glass bomb) shows the flow lines and the elongated vesicles, along with inclusion of heterogeneous fragments, and glassy pockets (darker spots).

Flow lines; glass pocket; elongated micro and macro bubbles;

Polished interior section of suevite “glass bomb” showing large (mostly elongate) vesicles that follow the flow lines.

REFERENCES

Aboud, T. (2009). Libyan Desert Glass: has the enigma of its origin been resolved? *Physics Procedia*, **2**(3), 1425–1432.

Alvarez, L. W., Alvarez, W., Asaro, F., & Michel, H. V. (1980). Extraterrestrial Cause for the Cretaceous-Tertiary Extinction. *Science*, **208**(4448), 1095–1108.

Anderson, A. E. (1925). SAND FULGURITES FROM NEBRASKA THEIR STRUCTURE AND FORMATIVE FACTORS. *THE NEBRASKA STATE MUSEUM BULLETIN BULLETIN*, **7**(1).

Artemieva, N. (2002). Numerical modeling of tektite origin in oblique impacts : Implication to Ries-Moldavites strewn field. *Bulletin of the Czech Geological Survey*, **77**(4), 303–311.

Artemieva, N. A., Wünnemann, K., Krien, F., … Summerson, I. A. T. (2013). Ries crater and suevite revisited-Observations and modeling Part I: Observations. *Meteoritics & Planetary Science*, **48**(4), 590–627.

Atkatz, D., & Bragg, C. (1995). Determining the yield of the Trinity nuclear device via gamma-ray spectroscopy. *American Journal of Physics*, **63**(5), 411–413.

Baker, G., & Baker, A. A. (1964). *Hay–silica glass from Gnarkeet, Western Victoria*. *Memoirs of the National Museum of Victoria*, Vol. 26, National Museum of Victoria. doi:10.24199/j.mmv.1964.26.03

Barnes, V. E. (1958). Origin of Tektites. *Nature*, **181**(4621), 1457–1457.

Barrat, J.-A. J. A., Jahn, B. M. M., Amossé, J., … Diemer, E. (1997). Geochemistry and origin of Libyan Desert glasses. *Geochimica et Cosmochimica Acta*, **61**(9), 1953–1959.

Bates, R. L., & Jackson, J. A. (1987). Glossary of geology.

Bellot-Gurlet, L., Bourdonnec, F.-X. Le, Poupeau, G., & Dubernet, S. (2004). Raman micro-spectroscopy of western Mediterranean obsidian glass: one step towards provenance studies? *Journal of Raman Spectroscopy*, **35**(89), 671–677.

Bellucci, J. J., Simonetti, A., Koeman, E. C., Wallace, C., & Burns, P. C. (2014). A detailed geochemical investigation of post-nuclear detonation trinitite glass at high spatial resolution: Delineating anthropogenic vs. natural components. *Chemical Geology*, **365**, 69–86.

Bentor, Y. K. (1984). Combustion-metamorphic glasses. *Journal of Non-Crystalline Solids*. doi:10.1016/0022-3093(84)90168-6

Bentor, Y. K., Kastner, M., Perlman, I., & Yellin, Y. (1981). Combustion metamorphism of bituminous sediments and the formation of melts of granitic and sedimentary composition. *Geochimica et Cosmochimica Acta*. doi:10.1016/0016-7037(81)90074-0

Beran, A., & Koeberl, C. (1997). Water in tektites and impact glasses by fourier-transformed infrared spectrometry. *Meteoritics & Planetary Science*, **32**(2), 211–216.

Bigazzi, G., & Michele, V. (1996). New fission-track age determinations on impact glasses. *Meteoritics & Planetary Science*, **31**(2), 234–236.

Bohor, B. F. (1990). Shock-induced microdeformations in quartz and other mineralogical indications of an impact event at the Cretaceous-Tertiary boundary. *Tectonophysics*, **171**(1–4), 359–372.

Borucki, W. J., & Chameides, W. L. (1984). Lightning: Estimates of the rates of energy dissipation and nitrogen fixation. *Reviews of Geophysics*, **22**(4), 363.

Bouška, V. (1994). Terrestrial and Lunar , Volcanic and Impact Glasses , Tektites , and Fulgurites. In *Advanced Mineralogy*, Berlin, Heidelberg: Springer Berlin Heidelberg, pp. 258–265.

Bouška, V., & Povondra, P. (1964). Correlation of some physical and chemical properties of moldavites. *Geochimica et Cosmochimica Acta*, **28**(6), 783–791.

Brachaniec, T., Szopa, K., & Karwowski, Ł. (2014). Discovery of the most distal Ries tektites found in Lower Silesia, southwestern Poland. *Meteoritics & Planetary Science*, **49**(8), 1315–1322.

Brauns, R. (1912). Die chemische Zusammensetzung granatfuhrender kristalliner Schiefer, Cordieritgesteine und Sanidinite aus dem Laacher Seegebiet. *N. Jahrb. f. Min. Beilage-Bd*, **34**, 85.

Bridgman, P. W., & Šimon, I. (1953). Effects of Very High Pressures on Glass. *Journal of Applied Physics*, **24**(4), 405–413.

Bryant, D. E., Greenfield, D., Walshaw, R. D., … Kee, T. P. (2009). Electrochemical studies of iron meteorites: phosphorus redox chemistry on the early Earth. *International Journal of Astrobiology*, **8**(1), 27–36.

Bunch, T. E., Hermes, R. E., Moore, A. M. T., … Kennett, J. P. (2012). Very high-temperature impact melt products as evidence for cosmic airbursts and impacts 12,900 years ago. *Proceedings of the National Academy of Sciences*, **109**(28), E1903–E1912.

Calas, G., & Petiau, J. (1983). Coordination of iron in oxide glasses through high-resolution K-edge spectra: Information from the pre-edge. *Solid State Communications*, **48**(7), 625–629.

Callegari, E., & Pertsev, N. (2007). Contact metamorphic and associated rocks. In D. J. Fettes & J. Desmons, eds., *Metamorphic rocks: a classification and glossary of terms*, Cambridge University Press, pp. 69–81.

Canil, D., Mihalynuk, M., & Lacourse, T. (2018). Discovery of modern (post-1850 CE) lavas in south-central British Columbia, Canada: Origin from coal fires or intraplate volcanism? *Lithos*, **296**–**299**, 471–481.

Capitanio, F. (2005). Comment on: The Ricetto and Colle Fabbri wollastonite and melilite-bearing rocks of the central Apennines, Italy. *American Mineralogist*, **90**(11–12), 1934–1939.

Capitanio, F., Larocca, F., & Improta, S. (2004). High-temperature rapid pyrometamorphism induced by a charcoal pit burning: The case of Ricetto, central Italy. *International Journal of Earth Sciences*, **93**(1), 107–118.

Carmichael, I. S. E. (1979). Glass and the glassy rocks. In *The evolution of the igneous rocks*, pp. 233–244.

Carter, E. A., Pasek, M. A., Smith, T., Kee, T. P., Hines, P., & Edwards, H. G. M. (2010). Rapid Raman mapping of a fulgurite. In *Analytical and Bioanalytical Chemistry*, Vol. 397, pp. 2647–2658.

Castro, J., Manga, M., & Cashman, K. (2002). Dynamics of obsidian flows inferred from microstructures: Insights from microlite preferred orientations. *Earth and Planetary Science Letters*, **199**(1–2), 211–226.

Cavosie, A. J., & Koeberl, C. (2019). Overestimation of threat from 100 Mt–class airbursts? High-pressure evidence from zircon in Libyan Desert Glass. *Geology*, **47**(7), 609–612.

Champagnon, B., Panczer, G., & Chemarin, C. (1997). Differentiation of natural silica glasses using Raman microspectrometry. *Chemie Der Erde-Geochemistry*, **57**(2–3), 290–296.

Chapman, N., McKinley, I., & Smellie, J. (1984). *The potential of natural analogues in assessing systems for deep disposal of high-level radioactive waste*. *skb.se*.

Chen, J., Elmi, C., Goldsby, D., & Gieré, R. (2017). Generation of shock lamellae and melting in rocks by lightning-induced shock waves and electrical heating. *Geophysical Research Letters*, **44**(17), 8757–8768.

Cicconi, M. R., Giuli, G., Ertel-Ingrisch, W., Paris, E., & Dingwell, D. B. (2015). The effect of the [Na/(Na+K)] ratio on Fe speciation in phonolitic glasses. *American Mineralogist*, **100**(7), 1610–1619.

Cicconi, M. R., Le Losq, C., Moretti, R., & Neuville, D. R. (2020). Magma, the largest repository and carrier of Earth's redox processes. *Elements*, **16**(3).

Cicconi, M. R., & Neuville, D. R. (2019). Natural Glasses. In J. D. Musgraves, J. Hu, & L. Calvez, eds., *Springer Handbook of Glass*, Springer International Publishing. doi:10.1007/978-3-319-93728-1

Clayton, P. A. (1934). Silica-Glass from the Libyan Desert. *Mineralogical Magazine*, **23**(144), 501–508.

Cohen, H. M., & Roy, R. (1961). Effects of Ultra high Pressures on Glass. *Journal of the American Ceramic Society*, **44**(10), 523–524.

Cohen, H. M., & Roy, R. (1965). Densification of glass at very high pressure. *Physics and Chemistry of Glasses*, **6**(5), 149–155.

Cosca, M. A., Essene, E. J., Geissman, J. W., Simmons, W. B., & Coates, D. A. (1989). Pyrometamorphic rocks associated with naturally burned coal beds, Powder River Basin, Wyoming. *American Mineralogist*, **74**(1–2), 85–100.

Cuttitta, F., Carron, M. ., & Annell, C. . (1972). New data on selected Ivory Coast tektites. *Geochimica et Cosmochimica Acta*, **36**(11), 1297–1309.

De Blasio, F. V., & Medici, L. (2017). Microscopic model of rock melting beneath landslides calibrated on the mineralogical analysis of the Köfels frictionite. *Landslides*, **14**(1), 337–350.

de Boer, C. B., Dekkers, M. J., & van Hoof, T. A. . (2001). Rock-magnetic properties of TRM carrying baked and molten rocks straddling burnt coal seams. *Physics of the Earth and Planetary Interiors*, **126**(1–2), 93–108.

Deschamps, T., Kassir-Bodon, A., Sonneville, C., … Champagnon, B. (2013). Permanent densification of compressed silica glass: a Raman-density calibration curve. *Journal of Physics: Condensed Matter*, **25**(2), 025402.

Deutsch, A., Ostermann, M., & Masaitis, V. L. (1997). Geochemistry and neodymium-strontium isotope signature of tektite-like objects from Siberia (urengoites, South-Ural glass). *Meteoritics & Planetary Science*, **32**(5), 679–686.

Devouard, B., Rochette, P., Gattacceca, J., … Warner, M. (2014). A new Tektite Strewnfield in Atacama. In *77th Annual Meteoritical Society Meeting*, p. #5394.

Di Toro, G., Pennacchioni, G., & Teza, G. (2005). Can pseudotachylytes be used to infer earthquake source parameters? An example of limitations in the study of exhumed faults. *Tectonophysics*, **402**(1), 3–20.

Dos Santos, E., Scorzelli, R. B., Rochette, P., … Cournède, C. (2015). A New Strewnfield of Splash-Form Impact Glasses in Atacama, Chile: A Mössbauer Study. In *78th Annual Meeting of the Meteoritical Society*, Vol. 1856, p. 5074.

Dunlap, R. A. (1997). An investigation of Fe oxidation states and site distributions in a Tibetan tektite. *Hyperfine Interactions*, **110**(3–4), 217–225.

Dunlap, R. A., Eelman, D. A., & MacKay, G. R. (1998). A Mössbauer effect investigation of correlated hyperfine parameters in natural glasses (tektites). *Journal of Non-Crystalline Solids*, **223**(1–2), 141–146.

Dunlap, R. A., & Sibley, A. D. E. (2004). A Mössbauer effect study of Fe-site occupancy in Australasian tektites. *Journal of Non-Crystalline Solids*, **337**(1), 36–41.

Earth Impact Database. (2019). Earth Impact Database. Retrieved from http://www.passc.net/EarthImpactDatabase/New website_05-2018/Index.html

Eby, N. G., Charnley, N., Pirrie, D., Hermes, R., Smoliga, J., & Rollinson, G. (2015). Trinitite redux: Mineralogy and petrology. *American Mineralogist*, **100**(2–3), 427–441.

Eby, N., Hermes, R., Charnley, N., & Smoliga, J. A. (2010). Trinitite-the atomic rock. *Geology Today*, **26**(5), 180–185.

Ende, M., Schorr, S., Kloess, G., Franz, A., & Tovar, M. (2012). Shocked quartz in Sahara fulgurite. *European Journal of Mineralogy*, **24**(3), 499–507.

Engelhardt, W. . (1967). Chemical composition of Ries glass bombs. *Geochimica et Cosmochimica Acta*, **31**(10), 1677–1689.

Engelhardt, W. ., Luft, E., Arndt, J., Schock, H., & Weiskirchner, W. (1987). Origin of moldavites. *Geochimica et Cosmochimica Acta*, **51**(6), 1425–1443.

Engelhardt, W. V. (1972). Shock produced rock glasses from the Ries crater. *Contributions to Mineralogy and Petrology*, **36**(4), 265–292.

Erismann, T., Heuberger, H., & Preuss, E. (1977). Der Bimsstein von Koefels (Tirol), ein Bergsturz-?Friktionit? *TMPM Tschermaks Mineralogische Und Petrographische Mitteilungen*, **24**(1–2), 67–119.

1839 Essene, E. J., & Fisher, D. C. (1986). Lightning strike fusion: extreme reduction and metal-silicate
1840 liquid immiscibility. *Science (New York, N.Y.)*, **234**(4773), 189–93.
1841 Etiope, G. (2015). Seeps in the Ancient World: Myths, Religions, and Social Development. In *Natural*
1842 *Gas Seepage*, Cham: Springer International Publishing, pp. 183–193.
1843 Evans, B. J., & Leung, L. K. (1979). Mössbauer Spectroscopy of Tektites and Other Natural Glasses.
1844 *Le Journal de Physique Colloques*, **40**(C2), C2-489-C2-490.
1845 Ewing, R. (1979). Natural Glasses: Analogues for Radioactive Waste Forms. *Scientific Basis for*
1846 *Nuclear Waste Management*, 56–78.
1847 Fahey, A. J., Zeissler, C. J., Newbury, D. E., Davis, J., & Lindstrom, R. M. (2010). Postdetonation
1848 nuclear debris for attribution. *Proceedings of the National Academy of Sciences of the United*
1849 *States of America*, **107**(47), 20207–12.
1850 Feng, T., Lang, C., & Pasek, M. A. (2019). The origin of blue coloration in a fulgurite from
1851 Marquette, Michigan. *Lithos*, **342**–**343**, 288–294.
1852 Ferré, E. C., Zechmeister, M. S., Geissman, J. W., MathanaSekaran, N., & Kocak, K. (2005). The
1853 origin of high magnetic remanence in fault pseudotachylites: Theoretical considerations and
1854 implication for coseismic electrical currents. *Tectonophysics*, **402**(1-4 SPEC. ISS), 125–139.
1855 Ferrière, L., Barrat, J.-A., Giuli, G., … Wegner, W. (2017). A new tektite strewn field discovered in
1856 Uruguay. In *80th Annual Meeting of the Meteoritical Society*, p. #6195.
1857 Firestone, R. B., West, A., Kennett, J. P., … Wolbach, W. S. (2007). Evidence for an extraterrestrial
1858 impact 12,900 years ago that contributed to the megafaunal extinctions and the Younger Dryas
1859 cooling. *Proceedings of the National Academy of Sciences of the United States of America*,
1860 **104**(41), 16016–21.
1861 Folco, L., Bigazzi, G., D'Orazio, M., & Balestrieri, M. L. (2011). Fission track age of Transantarctic
1862 Mountain microtektites. *Geochimica et Cosmochimica Acta*, **75**(9), 2356–2360.
1863 Folco, L., D'Orazio, M., Gemelli, M., & Rochette, P. (2016). Stretching out the Australasian
1864 microtektite strewn field in Victoria Land Transantarctic Mountains. *Polar Science*, **10**, 147–159.
1865 Folco, L., D'Orazio, M., Tiepolo, M., … Glass, B. P. (2009). Transantarctic Mountain microtektites:
1866 Geochemical affinity with Australasian microtektites. *Geochimica et Cosmochimica Acta*,
1867 **73**(12), 3694–3722.
1868 Folco, L., Glass, B. P., D'Orazio, M., & Rochette, P. (2010). A common volatilization trend in
1869 Transantarctic Mountain and Australasian microtektites: Implications for their formation model
1870 and parent crater location. *Earth and Planetary Science Letters*, **293**(1–2), 135–139.
1871 Folco, L., Rochette, P., Perchiazzi, N., D'Orazio, M., Laurenzi, M. A. A., & Tiepolo, M. (2008).
1872 Microtektites from Victoria Land Transantarctic Mountains. *Geology*, **36**(4), 291–294.
1873 Ford, R. J. (1972). A possible impact crater associated with Darwin glass. *Earth and Planetary*
1874 *Science Letters*, **16**(2), 228–230.
1875 Fredriksson, K., Degasparis, A., & Ehmann, W. (1977). The Zhamanshin structure: chemical and
1876 physical properties of selected samples. *Meteoritics*, **12**, 229.
1877 French, B. M. (1998). *Traces of catastrophe: A handbook of shock-metamorphic effects in terrestrial*
1878 *meteorite impact structures*, Houston: Lunar and Planetary Institute.
1879 Frenzel, G., & Stahle, V. (1984). Uber Alumosilikatglas mit Lechatelierit-Einschlussen von einer
1880 Fulguritrohre des Hahnenstockes (Glarner Freiberg, Schweiz). *Chemie Der Erde - Geochemistry*,
1881 **43**(1), 17–26.
1882 Frey, F. A. (1977). Microtektites: a chemical comparison of bottle-green microtektites, normal
1883 microtektites and tektites. *Earth and Planetary Science Letters*, **35**(1), 43–48.
1884 Fudali, R. F. F., Dyar, M. D. D., Griscom, D. L., & Schreiber, H. D. (1987). The oxidation state of
1885 iron in tektite glass. *Geochimica et Cosmochimica Acta*, **51**(10), 2749–2756.
1886 Fudali, R. F., & Ford, R. J. (1979). Darwin Glass and Darwin Crater: a Progress Report. *Meteoritics*,
1887 **14**(3), 283–296.
1888 Galeener, F. L., Geissberger, A. E., & Weeks, R. A. (1984). On the thermal history of Libyan Desert

glass. *Journal of Non-Crystalline Solids*, **67**(1–3), 629–636.

Ganino, C., Libourel, G., Nakamura, A. M., Jacomet, S., Tottereau, O., & Michel, P. (2018). Impact-induced chemical fractionation as inferred from hypervelocity impact experiments with silicate projectiles and metallic targets. *Meteoritics & Planetary Science*, **53**(11), 2306–2326.

Gentner, von W., & Zähringer, J. (1959). Kalium-Argon-Alter einiger Tektite. *Zeitschrift Für Naturforschung A*, **14**(7), 686–687.

Gieré, R., Wimmenauer, W., Müller-Sigmund, H., Wirth, R., Lumpkin, G. R., & Smith, K. L. (2015). Lightning-induced shock lamellae in quartz. *American Mineralogist*, **100**(7), 1645–1648.

Giuli, G. (2017). Tektites and microtektites iron oxidation state and water content. *Rendiconti Lincei*, **28**(4), 615–621.

Giuli, G., Cicconi, M. R., Eeckhout, S. G., … Paris, E. (2013a). North American microtektites are more oxidized than tektites. *American Mineralogist*, **98**(11–12), 1930–1937.

Giuli, G., Cicconi, M. R., Eeckhout, S. G., Pratesi, G., Paris, E., & Folco, L. (2014a). Australasian microtektites from Antarctica: XAS determination of the Fe oxidation state. *Meteoritics and Planetary Science*, **49**(4), 696–705.

Giuli, G., Cicconi, M. R., & Paris, E. (2012). The [4]Fe3+-O distance in synthetic kimzeyite garnet, Ca3Zr2[Fe2SiO12]. *European Journal of Mineralogy*, **24**(5), 783–790.

Giuli, G., Cicconi, M. R., Stabile, P., … Koeberl, C. (2014b). New data on the Fe oxidation state and water content of Belize Tektites. In *45th Lunar and Planetary Science Conference*, p. #2322.

Giuli, G., Cicconi, M. R., Trapananti, A., … Koeberl, C. (2013b). Iron redox variations in Australasian Muong Nong-type tektites. *Meteoritics & Planetary Science*.

Giuli, G., Eeckhout, S. G., Cicconi, M. R., Koeberl, C., Pratesi, G., & Paris, E. Iron oxidation state and local structure in North American tektites, Large Meteorite Impacts and Planetary Evolution Iv (2010). doi:10.1130/2010.2465(31)

Giuli, G., Paris, E., Pratesi, G., Koeberl, C., & Cipriani, C. (2003). Iron oxidation state in the Fe-rich layer and silica matrix of Libyan Desert Glass: A high-resolution XANES study. *Meteoritics and Planetary Science*, **38**(8), 1181–1186.

Giuli, G., Pratesi, G., Cipriani, C., & Paris, E. (2002). Iron local structure in tektites and impact glasses by extended X-ray absorption fine structure and high-resolution X-ray absorption near-edge structure spectroscopy. *Geochimica et Cosmochimica Acta*, **66**(24), 4347–4353.

Giuli, G., Pratesi, G., Eeckhout, S. G., Koeberl, C., & Paris, E. (2010b). Iron reduction in silicate glass produced during the 1945 nuclear test at the Trinity site (Alamogordo, New Mexico, USA). In *Geological Society of America Special Papers*, Vol. 465, Geological Society of America, pp. 653–660.

Glass, B. (1967). Microtektites in deep-sea sediments. *Nature (London)*, **214**(5086), 372–374.

Glass, B. P. (1972). Bottle Green Microtektites. *Journal of Geophysical Research*, **77**(35), 7057–7064.

Glass, B. P. (1978). Australasian microtektites and the stratigraphic age of the australites. *Bulletin of the Geological Society of America*, **89**(10), 1455–1458.

Glass, B. P. (1990). Tektites and microtektites: key facts and inferences. *Tectonophysics*, **171**(1–4), 393–404.

Glass, B. P. (2016). Glass: The Geologic Connection. *International Journal of Applied Glass Science*, **7**(4), 435–445.

Glass, B. P., Huber, H., & Koeberl, C. (2004). Geochemistry of Cenozoic microtektites and clinopyroxene-bearing spherules. *Geochimica et Cosmochimica Acta*, **68**(19), 3971–4006.

Glass, B. P., & Pizzuto, J. E. (1994). Geographic variation in Australasian microtektite concentrations: Implications concerning the location and size of the source crater. *Journal of Geophysical Research*, **99**(E9), 19075.

Glass, B. P., Senftle, F. E., Muenow, D. W., Aggrey, K. E., & Thorpe, A. N. (1987). Atomic Bomb Glass Beads: Tektite and Microtektite Analogs. In *Second International Conference on Natural Glasses*, pp. 361--369.

Glass, B. P., & Simonson, B. M. (2013). *Distal Impact Ejecta Layers*, Berlin, Heidelberg: Springer Berlin Heidelberg. doi:10.1007/978-3-662-44185-5_100311

Glass, B. P., & Zwart, M. J. (1979). North American microtektites in Deep Sea Drilling Project cores from the Caribbean Sea and Gulf of Mexico. *Geological Society of America Bulletin*, **90**(6), 595.

Glindemann, D., de Graaf, R. M., & Schwartz, A. W. (1999). Chemical Reduction of Phosphate on the Primitive Earth. *Origins of Life and Evolution of the Biosphere*, **29**(6), 555–561.

Goderis, S., Paquay, F., & Claeys, P. (2012). Projectile Identification in Terrestrial Impact Structures and Ejecta Material. In *Impact Cratering*, Chichester, UK: John Wiley & Sons, Ltd, pp. 223–239.

Gomez-Nubla, L., Aramendia, J., Alonso-Olazabal, A., … Madariaga, J. M. (2015). Darwin impact glass study by Raman spectroscopy in combination with other spectroscopic techniques. *Journal of Raman Spectroscopy*, **46**(10), 913–919.

Gómez-Nubla, L., Aramendia, J., Fdez-Ortiz de Vallejuelo, S., Castro, K., & Madariaga, J. M. (2018). Detection of organic compounds in impact glasses formed by the collision of an extraterrestrial material with the Libyan Desert (Africa) and Tasmania (Australia). *Analytical and Bioanalytical Chemistry*, **410**(25), 6609–6617.

Gomez-Nubla, L., Aramendia, J., Fdez-Ortiz de Vallejuelo, S., … Madariaga, J. M. (2017). Multispectroscopic methodology to study Libyan desert glass and its formation conditions. *Analytical and Bioanalytical Chemistry*, **409**(14), 3597–3610.

Grapes, R. (2010). *Pyrometamorphism*, Berlin, Heidelberg: Springer Berlin Heidelberg. doi:10.1007/978-3-642-15588-8

Graup, G. (1999). Carbonate-silicate liquid immiscibility upon impact melting: Ries Crater, Germany. *Meteoritics & Planetary Science*, **34**(3), 425–438.

Greshake, A., Koeberl, C., Fritz, J., & Reimold, W. U. (2010). Brownish inclusions and dark streaks in Libyan Desert Glass: Evidence for high-temperature melting of the target rock. *Meteoritics & Planetary Science*, **45**(6), 973–989.

Greshake, A., Wirth, R., Fritz, J., Jakubowski, T., & Böttger, U. (2018). Mullite in Libyan Desert Glass: Evidence for high-temperature/low-pressure formation. *Meteoritics & Planetary Science*, **53**(3), 467–481.

Hamann, C., Fazio, A., Ebert, M., … Reimold, W. U. (2018). Silicate liquid immiscibility in impact melts. *Meteoritics & Planetary Science*, **53**(8), 1594–1632.

Hamann, C., Hecht, L., Ebert, M., & Wirth, R. (2013). Chemical projectile–target interaction and liquid immiscibility in impact glass from the Wabar craters, Saudi Arabia. *Geochimica et Cosmochimica Acta*, **121**, 291–310.

Heide, K., & Heide, G. (2011). Vitreous state in nature-Origin and properties. *Chemie Der Erde - Geochemistry*, **71**(4), 305–335.

Henderson, G. S., de Groot, F. M. F., & Moulton, B. J. A. (2014). X-ray Absorption Near-Edge Structure (XANES) Spectroscopy. In *Reviews in Mineralogy and Geochemistry*, Vol. 78, Mineralogical Society of America, pp. 75–138.

Hermes, R. E., & Strickfaden, W. B. (2005). A new look at trinitite. *Nuclear Weapons Journal*, **2**, 2–7.

Herring, J. R., & Modreski, P. J. (1986). *Unusual, high-temperature, iron-rich, mineral phases produced by natural burning of coal seams; analytical data*.

Hörz, F., See, T. H., Murali, A. V, & Blanchard, D. P. (1989). Heterogeneous dissemination of projectile materials in the impact melts from Wabar crater, Saudi Arabia. In *Lunar and Planetary Science Conference Proceedings*, Vol. 19, pp. 697–709.

Hosgormez, H., Etiope, G., & Yalçin, M. N. (2008). New evidence for a mixed inorganic and organic origin of the Olympic Chimaera fire (Turkey): a large onshore seepage of abiogenic gas. *Geofluids*, **8**(4), 263–273.

Howard, K. T. (2008). Geochemistry of Darwin glass and target rocks from Darwin Crater, Tasmania, Australia. *Meteoritics and Planetary Science*, **43**(3), 1–21.

Howard, K. T. (2009). Physical distribution trends in Darwin glass. *Meteoritics & Planetary Science*, **44**(1), 115–129.

Howard, K. T. (2011). Volatile enhanced dispersal of high velocity impact melts and the origin of tektites. *Proceedings of the Geologists' Association*, **122**(3), 363–382.

Howard, K. T., Bailey, M. J., Berhanu, D., … Verchovsky, S. (2013). Biomass preservation in impact melt ejecta. *Nature Geoscience*, **6**(12), 1018–1022.

Howard, K. T., & Haines, P. W. (2007). The geology of Darwin Crater, western Tasmania, Australia. *Earth and Planetary Science Letters*, **260**(1–2), 328–339.

Hu, Q. H., Rose, T. P., Zavarin, M., Smith, D. K., Moran, J. E., & Zhao, P. H. (2008). Assessing field-scale migration of radionuclides at the Nevada Test Site: "mobile" species. *Journal of Environmental Radioactivity*, **99**(10), 1617–1630.

Hudon, P., & Baker, D. R. (2002). The nature of phase separation in binary oxide melts and glasses. I. Silicate systems. *Journal of Non-Crystalline Solids*, **303**(3), 299–345.

Hudon, P., Jung, I., & Baker, D. R. (2004). Effect of pressure on liquid-liquid miscibility gaps: A case study of the systems $CaO\text{-}SiO_2$, $MgO\text{-}SiO_2$, and $CaMgSi_2O_6\text{-}SiO_2$. *Journal of Geophysical Research*, **109**(B3), B03207.

Izett, G. A. (1987). Authigenic ' spherules' in K-T boundary sediments at Caravaca, Spain, and Raton Basin, Colorado and New Mexico, may not be impact derived. *Geological Society of America Bulletin*, **99**(1), 78–86.

Jakes, P., Sen, S., Matsuishi, K., Reid, A. M., King, E. A., & Casanova, I. (1992). Silicate Melts at Super Liquidus Temperatures: Reduction and Volatilization. *Lunar and Planetary Science Conference*, **23**, 599.

Jessberger, E., & Gentner, W. (1972). Mass spectrometric analysis of gas inclusions in Muong Nong glass and Libyan Desert glass. *Earth and Planetary Science Letters*, **14**(2), 221–225.

Johnson, B. C., & Melosh, H. J. (2012). Formation of spherules in impact produced vapor plumes. *Icarus*, **217**(1), 416–430.

Johnson, B. C., & Melosh, H. J. (2014). Formation of melt droplets, melt fragments, and accretionary impact lapilli during a hypervelocity impact. *Icarus*, **228**, 347–363.

Jones, B. E., Jones, K. S., Rambo, K. J., Rakov, V. A., Jerald, J., & Uman, M. A. (2005). Oxide reduction during triggered-lightning fulgurite formation. *Journal of Atmospheric and Solar-Terrestrial Physics*, **67**(4), 423–428.

Kenkmann, T., Hornemann, U., & Stöffler, D. (2000). Experimental generation of shock-induced pseudotachylites along lithological interfaces. *Meteoritics & Planetary Science*, **35**(6), 1275–1290.

Khoury, H. N., Sokol, E. V., & Clark, I. D. (2015). Calcium uranium oxide minerals from Central Jordan: assemblages, chemistry, and alteration products. *The Canadian Mineralogist*, **53**, 61–82.

Killick, A. M. (2003). Fault Rock Classification: An aid to structural interpretation in mine and exploration geology. *South African Journal of Geology*, **106**(4), 395–402.

Koeber, C., & Fredriksson, K. (1986). Impact glasses from Zhamanshin crater (U.S.S.R.): chemical composition and discussion of origin. *Earth and Planetary Science Letters*, **78**(1), 80–88.

Koeberl, C. (1988). Blue glass: A new impactite variety from Zhamanshin crater, U.S.S.R. *Geochimica et Cosmochimica Acta*, **52**(3), 779–784.

Koeberl, C. (1992a). Geochemistry and origin of Muong Nong-type tektites. *Geochimica et Cosmochimica Acta*, **56**(3), 1033–1064.

Koeberl, C. (1992b). Water content of glasses from the K/T boundary, Haiti: An indication of impact origin. *Geochimica et Cosmochimica Acta*, **56**(12), 4329–4332.

Koeberl, C. (1994). Tektite origin by hypervelocity asteroidal or cometary impact. *Large Meteorite Impacts and Planetary Evolution*, p. 133.

Koeberl, C. (1997). Libyan Desert Glass: geochemical composition and origin. In *Proceedings of the Silica ´96 Meeting*, pp. 121–131.

2039 Koeberl, C. (2013). The Geochemistry and Cosmochemistry of Impacts. In *Treatise on Geochemistry:*
2040 *Second Edition*, Vol. 2, pp. 73–118.
2041 Koeberl, C., Brandstätter, F., Glass, B. P., Hecht, L., Mader, D., & Reimold, W. U. (2007). Uppermost
2042 impact fallback layer in the Bosumtwi crater (Ghana): Mineralogy, geochemistry, and
2043 comparison with Ivory Coast tektites. *Meteoritics & Planetary Science*, **42**(4–5), 709–729.
2044 Koeberl, C., Crósta, A. P., & Schulz, T. (2019). Geochemical Investigation of the Atacamaites, a New
2045 Impact Glass Occurrence in South America. In *50th Lunar and Planetary Science Conference*
2046 *2019*, p. #2132.
2047 Koeberl, C., & Ferrière, L. (2019). Libyan Desert Glass area in western Egypt: Shocked quartz in
2048 bedrock points to a possible deeply eroded impact structure in the region. *Meteoritics &*
2049 *Planetary Science*. doi:10.1111/maps.13250
2050 Koeberl, C., & Sigurdsson, H. (1992). Geochemistry of impact glasses from the K/T boundary in
2051 Haiti: Relation to smectites and a new type of glass. *Geochimica et Cosmochimica Acta*, **56**(5),
2052 2113–2129.
2053 Kokh, S., Dekterev, A., Sokol, E., & Potapov, S. (2016). Numerical simulation of an oil–gas fire: A
2054 case study of a technological accident at Tengiz oilfield, Kazakhstan (June 1985–July 1986).
2055 *Energy Exploration & Exploitation*, **34**(1), 77–98.
2056 Krider, E. P., Dawson, G. A., & Uman, M. A. (1968). Peak power and energy dissipation in a single-
2057 stroke lightning flash. *Journal of Geophysical Research*, **73**(10), 3335–3339.
2058 Kuenzer, C., & Stracher, G. B. (2012). Geomorphology of coal seam fires. *Geomorphology*, **138**(1),
2059 209–222.
2060 Lee, M.-Y., & Wei, K.-Y. (2000). Australasian microtektites in the South China Sea and the West
2061 Philippine Sea: Implications for age, size, and location of the impact crater. *Meteoritics &*
2062 *Planetary Science*, **35**(6), 1151–1155.
2063 Legros, F., Cantagrel, J., & Devouard, B. (2000). Pseudotachylyte (Frictionite) at the Base of the
2064 Arequipa Volcanic Landslide Deposit (Peru): Implications for Emplacement Mechanisms. *The*
2065 *Journal of Geology*, **108**(5), 601–611.
2066 Lin, A., & Shimamoto, T. (1998). Selective melting processes as inferred from experimentally
2067 generated pseudotachylytes. *Journal of Asian Earth Sciences*, **16**(5–6), 533–545.
2068 Lo, C.-H., Howard, K. T., Chung, S.-L., & Meffre, S. (2002). Laser fusion argon-40/argon-39 ages of
2069 Darwin impact glass. *Meteoritics & Planetary Science*, **37**(11), 1555–1562.
2070 Lukanin, O. A., & Kadik, A. A. (2007). Decompression mechanism of ferric iron reduction in tektite
2071 melts during their formation in the impact process. *Geochemistry International*, **45**(9), 857–881.
2072 Ma, P., Aggrey, K., Tonzola, C., … Klein, J. (2004). Beryllium-10 in Australasian tektites:
2073 Constraints on the location of the source crater. *Geochimica et Cosmochimica Acta*, **68**(19),
2074 3883–3896.
2075 Maddock, R. H. (1992). Effects of lithology, cataclasis and melting on the composition of fault-
2076 generated pseudotachylytes in Lewisian gneiss, Scotland. *Tectonophysics*, **204**(3–4), 261–278.
2077 Martin Crespo, T., Lozano Fernandez, R. P., & Gonzalez Laguna, R. (2009). The fulgurite of Torre de
2078 Moncorvo (Portugal): description and analysis of the glass. *European Journal of Mineralogy*,
2079 **21**(4), 783–794.
2080 Masch, L., & Preuss, E. (1977). Das Vorkommen des Hyalomylonits von Langtang, Himalaya
2081 (Nepal). *N. Jahrb. Min., Abh*, **129**(3), 292–311.
2082 Mathews, W. H., & Bustin, R. M. (1984). Why do the Smoking Hills smoke? *Canadian Journal of*
2083 *Earth Sciences*, **21**(7), 737–742.
2084 Matsubara, K., & Matsuda, J. (1991). Anomalous Ne enrichments in tektites. *Meteoritics*, **26**, 217–
2085 220.
2086 Matsuda, J., Maruoka, T., Pinti, D. L., & Koeberl, C. (1996). Noble gas study of a philippinite with an
2087 unusually large bubble. *Meteoritics & Planetary Science*, **31**(2), 273–277.
2088 McCloy, J. S. (2019). Frontiers in natural and un-natural glasses: An interdisciplinary dialogue and

review. *Journal of Non-Crystalline Solids*, **4**, 119401.

McMillan, P., Wolf, G., & Lambert, P. (1992). A Raman spectroscopic study of shocked single crystalline quartz. *Physics and Chemistry of Minerals*, **19**(2), 71–79.

McPherson, D., Pye, L. D., Fréchette, V. D., & Tong, S. (1984). Microstructure of natural glasses. *Journal of Non-Crystalline Solids*, **67**(1–3), 61–79.

Meisel, T., Koeberl, C., & Ford, R. J. (1990). Geochemistry of Darwin impact glass and target rocks. *Geochimica et Cosmochimica Acta*, **54**(5), 1463–1474.

Melluso, L., Conticelli, S., D'Antonio, M., Mirco, N. P., & Saccani, E. (2004). Petrology and mineralogy of wollastonite- and melilite-bearing paralavas from the Central Apennines, Italy. *American Mineralogist*, **88**(8–9), 1287–1299.

Melosh, H. J. (1989). *Impact cratering: A geologic process*. *Oxford Monographs on Geology and Geophysics*, Vol. 11, New York, NY: Oxford University Press.

Melosh, H. J. (2011). Impact cratering. In *Planetary Surface Processes*, Cambridge: Cambridge University Press, pp. 222–275.

Melosh, H. J. (2013). The contact and compression stage of impact cratering. In G. R. Osinski & E. Pierazzo, eds., *Impact Cratering: processes and products*, Chichester, UK: John Wiley & Sons, Ltd. doi:10.1002/9781118447307

Melosh, H. J. (2017). Impact geologists, beware! *Geophysical Research Letters*, **44**(17), 8873–8874.

Melosh, H. J., & Artemieva, N. (2004). How does tektite glass lose its water? In *Lunar and Planetary Science XXXV*, p. 1723.

Melson, W. G., & Potts, R. (2002). Origin of Reddened and Melted Zones in Pleistocene Sediments of the Olorgesailie Basin, Southern Kenya Rift. *Journal of Archaeological Science*, **29**(3), 307–316.

Mizera, J., Řanda, Z., & Kameník, J. (2016). On a possible parent crater for Australasian tektites: Geochemical, isotopic, geographical and other constraints. *Earth-Science Reviews*, **154**, 123–137.

Molgaard, J. J., Auxier, J. D., Giminaro, A. V., … Hall, H. L. (2015). Development of synthetic nuclear melt glass for forensic analysis. *Journal of Radioanalytical and Nuclear Chemistry*, **304**(3), 1293–1301.

Montanari, A., & Koeber, C. (2000). Distal ejecta and tektites. In *Impact Stratigraphy*, Berlin/Heidelberg: Springer-Verlag, pp. 57–99.

Montanari, A., & Koeberl, C. (2000). *Impact Stratigraphy*, Vol. 93, Berlin/Heidelberg: Springer-Verlag. doi:10.1007/BFb0010313

Morgan, J., Lana, C., Kearsley, A., … Neumann, V. (2006). Analyses of shocked quartz at the global K-P boundary indicate an origin from a single, high-angle, oblique impact at Chicxulub. *Earth and Planetary Science Letters*, **251**(3–4), 264–279.

Mottana, A. (2004). X-ray absorption spectroscopy in mineralogy: Theory and experiment in the XANES region. In A. Beran & E. Libowitzky, eds., *Spectroscopic methods in mineralogy*, Germany: Mineralogical Society of Great Britain and Ireland, pp. 465–552.

Müller, O., & Gentner, W. (1968). Gas content in bubbles of tektites and other natural glasses. *Earth and Planetary Science Letters*, **4**(5), 406–410.

Nestola, F., Mittempergher, S., Di Toro, G., Zorzi, F., & Pedron, D. (2010). Evidence of dmisteinbergite (hexagonal form of CaAl2Si2O8) in pseudotachylyte: A tool to constrain the thermal history of a seismic event. *American Mineralogist*, **95**(2–3), 405–409.

Neuville, D. R., de Ligny, D., & Henderson, G. S. (2014). *Advances in Raman Spectroscopy Applied to Earth and Material Sciences*. *Reviews in Mineralogy and Geochemistry*, Vol. 78. doi:10.2138/rmg.2013.78.13

O'Keefe, J. A. (1994). Origin of tektites. *Meteoritics*, **29**(1), 73–78.

O'Keefe, J. A., & Barnes, V. E. (1958). Origin of Tektites. *Nature*, **181**(4603), 1457–1457.

O'Keefe, J. A., Lowman, P. D., & Dunning, K. L. (1962). Gases in Tektite Bubbles. *Science (New York, N.Y.)*, **137**(3525), 228.

2139 Oberdorfer, R. (1905). Die vulkanischen Tuffe des Ries bei Nördlingen. *Jahreshefte Verein Für*
2140 *Vaterändische Naturkunde Württemberg*, **61**, 1–40.

2141 Okuno, M., Reynard, B., Shimada, Y., Syono, Y., & Willaime, C. (1999). A Raman spectroscopic
2142 study of shock-wave densification of vitreous silica. *Physics and Chemistry of Minerals*, **26**(4),
2143 304–311.

2144 Osinski, G. R., Grieve, R. A. F., & Tornabene, L. L. (2012). Excavation and Impact Ejecta
2145 Emplacement. In *Impact Cratering*, Chichester, UK: John Wiley & Sons, Ltd, pp. 43–59.

2146 Osinski, G. R., Haldemann, A. F. C., Schwarcz, H. P., … Churcher, C. S. (2007). Impact Glass at the
2147 Dakhleh Oasis, Egypt: Evidence for a Cratering Event or Large Aerial Burst? In *Lunar and*
2148 *Planetary Science Conference*, Vol. 38, p. 1346.

2149 Osinski, G. R., & Pierazzo, E. (2012). *Impact cratering : processes and products*.

2150 Ottemann, J. (1966). Zusammensetzung und Herkunft der Tektite und Impaktite. In *Kosmochemie*,
2151 Berlin/Heidelberg: Springer-Verlag, pp. 409–444.

2152 Pacold, J. I., Lukens, W. W., Booth, C. H., … Holliday, K. S. (2016). Chemical speciation of U, Fe,
2153 and Pu in melt glass from nuclear weapons testing. *Journal of Applied Physics*, **119**(19).
2154 doi:10.1063/1.4948942

2155 Paquay, F. S., Goderis, S., Ravizza, G., … Claeys, P. (2009). Absence of geochemical evidence for an
2156 impact event at the Bølling-Allerød/Younger Dryas transition. *Proceedings of the National*
2157 *Academy of Sciences of the United States of America*, **106**(51), 21505–10.

2158 Parekh, P., Semkow, T., Torres, M., & Haines, D. (2006). Radioactivity in trinitite six decades later.
2159 *Journal of Environmental Radioactivity*, **85**(1), 103–120.

2160 Pasek, M. A. (2008). Rethinking early Earth phosphorus geochemistry. *Proceedings of the National*
2161 *Academy of Sciences of the United States of America*, **105**(3), 853–8.

2162 Pasek, M. A. (2017). Schreibersite on the early Earth: Scenarios for prebiotic phosphorylation.
2163 *Geoscience Frontiers*, **8**(2), 329–335.

2164 Pasek, M. A., Block, K., & Pasek, V. (2012). Fulgurite morphology: A classification scheme and clues
2165 to formation. *Contributions to Mineralogy and Petrology*, **164**(3), 477–492.

2166 Pasek, M. A., & Pasek, V. D. (2018). The forensics of fulgurite formation. *Mineralogy and Petrology*,
2167 **112**(2), 185–198.

2168 Pasek, M., & Block, K. (2009). Lightning-induced reduction of phosphorus oxidation state. *Nature*
2169 *Geoscience*, **2**(8), 553–556.

2170 Peretyazhko, I. S., Savina, E. A., Khromova, E. A., Karmanov, N. S., & Ivanov, A. V. (2018). Unique
2171 Clinkers and Paralavas from a New Nyalga Combustion Metamorphic Complex in Central
2172 Mongolia: Mineralogy, Geochemistry, and Genesis. *Petrology*, **26**(2), 181–211.

2173 Pierazzo, E., Kring, D. A., & Melosh, H. J. (1998). Hydrocode simulation of the Chicxulub impact
2174 event and the production of climatically active gases. *Journal of Geophysical Research: Planets*,
2175 **103**(E12), 28607–28625.

2176 Pierazzo, E., & Melosh, H. J. (2012). Environmental Effects of Impact Events. In *Impact Cratering*,
2177 Chichester, UK: John Wiley & Sons, Ltd, pp. 146–156.

2178 Pinter, N., Scott, A. C., Daulton, T. L., … Ishman, S. E. (2011). The Younger Dryas impact
2179 hypothesis: A requiem. *Earth-Science Reviews*, pp. 247–264.

2180 Potuzak, M., Nichols, A. R. L., Dingwell, D. B., & Clague, D. A. (2008). Hyperquenched volcanic
2181 glass from Loihi Seamount, Hawaii. *Earth and Planetary Science Letters*, **270**(1–2), 54–62.

2182 Povenmire, H., & Cornec, J. (2015). The 2014 Report on the Belize Tektite Strewn Field. In *46th*
2183 *Lunar and Planetary Science Conference*, p. #1132.

2184 Povenmire, H., Harris, R., & Cornec, J. (2011). The new Central American tektite strewn field. In
2185 *42nd Lunar and Planetary Science Conference*, p. #1224.

2186 Pratesi, G. (2009). Impact diamonds: Formation, mineralogical features and cathodoluminescence
2187 properties. In *Cathodoluminescence and its Application in the Planetary Sciences*.
2188 doi:10.1007/978-3-540-87529-1_4

Pratesi, G., Viti, C., Cipriani, C., & Mellini, M. (2002). Silicate-silicate liquid immiscibility and graphite ribbons in Libyan desert glass. *Geochimica et Cosmochimica Acta*, **66**(5), 903–911.

Rakov, V. A., & Uman, M. A. (2003). *Lightning : physics and effects*.

Reimold, W. U., & Gibson, R. L. (2005). "Pseudotachylites" in Large Impact Structures. In *Impact Tectonics*, Berlin/Heidelberg: Springer-Verlag, pp. 1–53.

Reimold, W. U., & Jourdan, F. (2012). IMPACT! – BOLIDES, CRATERS, AND CATASTROPHES. *Elements*, **8**(1), 19–24.

Reimold, W. U., & Koeberl, C. (2014). Impact structures in Africa: A review. *Journal of African Earth Sciences*. doi:10.1016/j.jafrearsci.2014.01.008

Rietmeijer, F. J. M., Karner, J. M., Nuth, J. A., & Wasilewski, P. J. (1999). Nanoscale phase equilibrium in a triggered lightning-strike experiment. *European Journal of Mineralogy*, **11**(1), 181–186.

Rocchia, R., Robin, E., Fröhlich, F., Meon, H., Froget, L., & Diemer, E. (1996). L'origine des verres du désert libyque: Un impact météoritique. *Comptes Rendus de l'Académie Des Sciences. Série 2. Sciences de La Terre et Des Planètes*, **322**(10), 839–845.

Roedder, E. (1978). Silicate liquid immiscibility in magmas and in the system K2O-FeO-AI2O3-SiO2: an example of serendipity. *Geochimica et Cosmochimica Acta*, **42**(11), 1597–1617.

Roedder, E. (1992). Fluid inclusion evidence for immiscibility in magmatic differentiation. *Geochimica et Cosmochimica Acta*, **56**(1), 5–20.

Rogers, G. S. (1918). *Baked shale and slag formed by the burning of coal beds*, US Government Printing Office.

Ron, H., & Kolodny, Y. (1992). Paleomagnetic and rock magnetic study of combustion metamorphic rocks in Israel. *Journal of Geophysical Research*, **97**(B5), 6927.

Roperch, P., Gattacceca, J., Valenzuela, M., … Beck, P. (2017). Surface vitrification caused by natural fires in Late Pleistocene wetlands of the Atacama Desert. *Earth and Planetary Science Letters*, **469**, 15–26.

Ross, C. S. (1948). Optical properties of glass from Alamogordo, New Mexico. *American Mineralogist*, **33**, 360–362.

Rossano, S., Balan, E., Morin, G., Bauer, J.-P., Calas, G., & Brouder, C. (1999). 57 Fe Mössbauer spectroscopy of tektites. *Physics and Chemistry of Minerals*, **26**(6), 530–538.

Rost, R. (1964). Surfaces of and inclusions in moldavites. *Geochimica et Cosmochimica Acta*, **28**(6), 931–936.

Rowan, L. R., & Ahrens, T. J. (1994). Observations of impact-induced molten metal-silicate partitioning. *Earth and Planetary Science Letters*, **122**(1–2), 71–88.

Schmieder, M., Kennedy, T., Jourdan, F., Buchner, E., & Reimold, W. U. (2018). A high-precision 40Ar/39Ar age for the Nördlinger Ries impact crater, Germany, and implications for the accurate dating of terrestrial impact events. *Geochimica et Cosmochimica Acta*, **220**, 146–157.

Schnetzler, C. ., & Pinson, W. . (1964). A report on some recent major element analyses of tektites. *Geochimica et Cosmochimica Acta*, **28**(6), 793–806.

Schnetzler, C. ~C. (1970). The lunar origin of tektites: R.I.P. *Meteoritics*, **5**, 221–222.

Schreiber, H. D., Minnix, L. M., & Balazs, G. B. B. (1984). The redox state of iron in tektites. *Journal of Non-Crystalline Solids*, **67**(1–3), 349–359.

See, T. H., Wagstaff, J., Yang, V., Hörz, F., & McKay, G. A. (1998). Compositional variation and mixing of impact melts on microscopic scales. *Meteoritics & Planetary Science*, **33**(4), 937–948.

Seebaugh, W. R., & Strauss, A. M. (1984). A cometary impact model for the source of Libyan Desert glass. *Journal of Non-Crystalline Solids*, **67**(1–3), 511–519.

Senftle, F. E., Thorpe, A. N., Grant, J. R., … May, L. (2000). Magnetic measurements of glass from Tikal, Guatemala: Possible tektites. *Journal of Geophysical Research: Solid Earth*, **105**(B8), 18921–18925.

Shoemaker, E. M., & Chao, E. C. T. (1961). New evidence for the impact origin of the Ries Basin, Bavaria, Germany. *Journal of Geophysical Research*, **66**(10), 3371–3378.

Sigurdsson, H., D'Hondt, S., Arthur, M. a., … Channel, J. E. T. (1991). Glass from the Cretaceous/Tertiary boundary in Haiti. *Nature*, **349**(6309), 482–487.

Skinner, H. C. W., & Jahren, A. H. (2003). Biomineralization. In *Treatise on Geochemistry*, Vol. 8–9, pp. 1–69.

Smit, J., & Klaver, G. (1981). Sanidine spherules at the Cretaceous-Tertiary boundary indicate a large impact event. *Nature*, pp. 47–49.

Sokol, E., Novikov, I., Zateeva, S., Vapnik, Y., Shagam, R., & Kozmenko, O. (2010). Combustion metamorphism in the Nabi Musa dome: new implications for a mud volcanic origin of the Mottled Zone, Dead Sea area. *Basin Research*, **22**(4), 414–438.

Sokol, E., Volkova, N., & Lepezin, G. (1998). Mineralogy of pyrometamorphic rocks associated with naturally burned coal-bearing spoil-heaps of the Chelyabinsk coal basin, Russia. *European Journal of Mineralogy*, **10**(5), 1003–1014.

Sokol, E. V., Kokh, S. N., Vapnik, Y., Thiery, V., & Korzhova, S. A. (2014). Natural analogs of belite sulfoaluminate cement clinkers from Negev Desert, Israel. *American Mineralogist*, **99**(7), 1471–1487.

Spray, J. G. (1987). Artificial generation of pseudotachylyte using friction welding apparatus: simulation of melting on a fault plane. *Journal of Structural Geology*, **9**(1), 49–60.

Spray, J. G. (1992). A physical basis for the frictional melting of some rock-forming minerals. *Tectonophysics*, **204**(3–4), 205–221.

Spray, J. G. (2010). Frictional Melting Processes in Planetary Materials: From Hypervelocity Impact to Earthquakes. *Annual Review of Earth and Planetary Sciences*, **38**(1), 221–254.

Stöffler, D. (1971). Progressive metamorphism and classification of shocked and brecciated crystalline rocks at impact craters. *Journal of Geophysical Research*, **76**(23), 5541–5551.

Stöffler, D., Artemieva, N. a., & Pierazzo, E. (2002). Modeling the Ries-Steinheim impact event and the formation of the moldavite strewn field. *Meteoritics & Planetary Science*, **37**(12), 1893–1907.

Stöffler, D., & Grieve, R. A. F. (2007). Impactites. In D. J. Fettes & J. Desmons, eds., *Metamorphic rocks: a classification and glossary of terms*, Cambridge University Press, pp. 82–92.

Stöffler, D., Hamann, C., & Metzler, K. (2018). Shock metamorphism of planetary silicate rocks and sediments: Proposal for an updated classification system. *Meteoritics & Planetary Science*, **53**(1), 5–49.

Stöffler, D., & Langenhorst, F. (1994). Shock metamorphism of quartz in nature and experiment: I. Basic observation and theory*. *Meteoritics*, **29**(2), 155–181.

Stoppa, F., Rosatelli, G., Cundari, A., Castorina, F., & Woolley, A. R. (2005). Comment on Melluso et al. (2003): Reported data and interpretation of some wollastonite- and melilite-bearing rocks from the Central Apennines of Italy. *American Mineralogist*, **90**(11–12), 1919–1925.

Storzer, D., & Koeberl, C. (1991). Uranium and Zirconium Enrichments in Libyan Desert Glass: Zircon Baddeleyite, and High Temperature History of the Glass. *Lunar and Planetary Science*, **22**, 1345.

Storzer, D., & Wagner, G. A. (1977). Fission track dating of meteorite impacts. *Meteoritics*, **12**, 368–369.

Sugiura, H., Ikeda, R., Kondo, K., & Yamadaya, T. (1997). Densified silica glass after shock compression. *Journal of Applied Physics*, **81**(4), 1651–1655.

Susman, S., Volin, K. J., Price, D. L., … Liebermann, R. C. (1991). Intermediate-range order in permanently densified vitreous SiO2: A neutron-diffraction and molecular-dynamics study. *Physical Review B*, **43**(1), 1194–1197.

Svensen, H., Dysthe, D. K., Bandlien, E. H., Sacko, S., Coulibaly, H., & Planke, S. (2003). Subsurface combustion in Mali: Refutation of the active volcanism hypothesis in West Africa. *Geology*,

31(7), 581.

Swaenen, M., Stefaniak, E. A., Frost, R., Worobiec, A., & Van Grieken, R. (2010). Investigation of inclusions trapped inside Libyan desert glass by Raman microscopy. *Analytical and Bioanalytical Chemistry*, **397**(7), 2659–2665.

Switzer, G., & Melson, W. G. (1972). Origin and composition of rock fulgurite glass. *Smithsonian Contributions to the Earth Sciences*, **9**, 47.

Tancredi, G., Ishitsuka, J., Schultz, P. H., … Dalmau, A. (2009). A meteorite crater on Earth formed on September 15, 2007: The Carancas hypervelocity impact. *Meteoritics & Planetary Science*, **44**(12), 1967–1984.

Thorpe, A. N., Senftle, F. E., & Cuttitta, F. (1963). Magnetic and Chemical Investigations of Iron in Tektites. *Nature*, **197**(4870), 836–840.

Thy, P., Segobye, A. K., & Ming, D. W. (1995). Implications of prehistoric glassy biomass slag from east-central Botswana. *Journal of Archaeological Science*, **22**(5), 629–637.

Tompson, A. F. B., Bruton, C. J., Pawloski, G. A., … Maxwell, R. M. (2002). On the evaluation of groundwater contamination from underground nuclear tests. *Environmental Geology*, **42**(2–3), 235–247.

Tompson, A. F. B., Hudson, G. B., Smith, D. K., & Hunt, J. R. (2006). Analysis of radionuclide migration through a 200-m Vadose zone following a 16-year infiltration event. *Advances in Water Resources*, **29**(2), 281–292.

Uman, M. A. (1964). The peak temperature of lightning. *Journal of Atmospheric and Terrestrial Physics*, **26**(1), 123–128.

Uman, M. A., & Krider, E. P. (1989). Natural and artificially initiated lightning. *Science (New York, N.Y.)*, **246**(4929), 457–64.

Urey, H. C. (1955). On the origin of tektites. *Proceedings of the National Academy of Sciences of the United States of America*, **41**(1), 27–31.

Urey, H. C. (1963). Cometary Collisions and Tektites. *Nature*, **197**(4864), 228–230.

Van Hoesel, A., Hoek, W. Z., Pennock, G. M., & Drury, M. R. (2014). The younger dryas impact hypothesis: A critical review. *Quaternary Science Reviews*, **83**, 95–114.

Veksler, I. V. (2004). Liquid immiscibility and its role at the magmatic–hydrothermal transition: a summary of experimental studies. *Chemical Geology*, **210**(1–4), 7–31.

Vogel, W. (1994). *Glass Chemistry*, Springer Berlin Heidelberg.

Volovetsky, M. V., Rusakov, V. S., Chistyakova, N. I., & Lukanin, O. A. (2008). Mössbauer study of tektites. *Hyperfine Interactions*, **186**(1–3), 83–88.

Wallace, C., Bellucci, J. J., Simonetti, A., Hainley, T., Koeman, E. C., & Burns, P. C. (2013). A multi-method approach for determination of radionuclide distribution in trinitite. *Journal of Radioanalytical and Nuclear Chemistry*, **298**(2), 993–1003.

Wasserman, A., & Melosh, H. (2001). Chemical reduction of impact processed materials. *Lunar and Planetary Institute …*.

Weeks, R. A. A., Underwood, J. R., & Giegengack, R. (1984). Libyan Desert glass: A review. *Journal of Non-Crystalline Solids*, **67**(1–3), 593–619.

Weidinger, J. T., Korup, O., Munack, H., … Lottermoser, W. (2014). Giant rockslides from the inside. *Earth and Planetary Science Letters*, **389**, 62–73.

Wilding, M., Webb, S., Dingwell, D., Ablay, G., & Marti, J. (1996a). Cooling rate variation in natural volcanic glasses from Tenerife, Canary Islands. *Contributions to Mineralogy and Petrology*, **125**(2–3), 151–160.

Wilding, M., Webb, S., & Dingwell, D. B. (1996b). Tektite cooling rates: Calorimetric relaxation geospeedometry applied to a natural glass. *Geochimica et Cosmochimica Acta*, **60**(6), 1099–1103.

Wilke, M., Farges, F., Partzsch, G. M., Schmidt, C., & Behrens, H. (2007). Speciation of Fe in silicate glasses and melts by in-situ XANES spectroscopy. *American Mineralogist*, **92**(1), 44–56.

Wilke, M., Farges, F., Petit, P.-E., Brown, G. E., & Martin, F. (2001). Oxidation state and coordination of Fe in minerals: An Fe *K*- XANES spectroscopic study. *American Mineralogist*, **86**(5–6), 714–730.

Wilke, M., Partzsch, G. M., Bernhardt, R., & Lattard, D. (2004). Determination of the iron oxidation state in basaltic glasses using XANES at the K-edge. *Chemical Geology*, **213**(1–3), 71–87.

Wittke, J. H., Weaver, J. C., Bunch, T. E., … Firestone, R. B. (2013). Evidence for deposition of 10 million tonnes of impact spherules across four continents 12,800 y ago. *Proceedings of the National Academy of Sciences*, **110**(23), E2088–E2097.

Zähringer, J., & Gentner, W. (1963). Radiogenic and atmospheric argon content of tektites. *Nature*, **199**(4893), 583.

Žák, K., Skála, R., Řanda, Z., & Mizera, J. (2012). A review of volatile compounds in tektites, and carbon content and isotopic composition of moldavite glass. *Meteoritics and Planetary Science*, pp. 1010–1028.

Zolensky, M. E., & Koeberl, C. (1991). Why are blue zhamanshinites blue? Liquid immiscibility in an impact melt. *Geochimica et Cosmochimica Acta*, **55**(5), 1483–1486.